FABRICATION OF HYDROPHILIC MAGNETIC NANOPARTICLES

by

Canan Odaman

B.S., Chemistry, Boğaziçi University, 2010

Submitted to the Institute for Graduate Studies in
Science and Engineering in partial fulfillment of
the requirements for the degree of
Master of Science

Graduate Program in Chemistry

Boğaziçi University

2013

FABRICATION OF HYDROPHILIC MAGNETIC NANOPARTICLES

APPROVED BY:

Prof. Naz Zeynep Atay .....
(Thesis Supervisor)

Assoc. Prof. Seyda Bucak Malta .....

Assoc. Prof. Amitav Sanyal .....

DATE OF APPROVAL: 11.02.2013

ACKNOWLEDGEMENTS

This work is completed with the immense encouragement, support and guidance of Prof. N. Zeynep Atay. I am sincerely grateful and forever in debt to her for that.

I would like to express my genuine gratitude to Assoc. Prof. Seyda Bucak Malta for all the guidance and attention she has shown that made this research possible. I am also very thankful to Assoc. Prof. Amitav Sanyal for his invaluable insights that he never denied me of throughout my research.

I would like to thank all the members of Chemistry Department who always made everything easier with their kindness and positive spirits. I also specially thank to members of Sanyal Group that extended their help to me.

I am always appreciative for all my friends, but I would like to thank to Melis Çağdaş especially for supporting me whenever I needed and whatever I needed it for, and mostly just by being there, making my day.

To Aslı Yıldırım and Merve Akdemir, I am very much thankful for all the hours of studying and sometimes just talking that made me got through these last two years.

I am grateful for my family for never second guessing my decisions and always standing beside me.

This research was supported by Boğaziçi University Research Fund, with Project No: 5569, which is very much appreciated.

ABSTRACT

FABRICATION OF HYDROPHILIC MAGNETIC NANOPARTICLES

Magnetic properties of nanoparticles (NPs) enable them to be oriented and self-assembled into nanostructures. Magnetic nanoparticles (MNPs) used in this study are magnetite (Fe_3O_4) NPs. These particles have great application potential in various fields including bioapplications. However, magnetites by their nature, have hydrophobic surfaces, hence cannot be used in aqueous media as bare particles. In order magnetites to be biocompatible, they need surface modifications. The surface modification this project aims involves coating them with SiO_2. Silica-coating (Si-coating) can be achieved with two methods; “in situ” coating of magnetite NPs where both magnetite synthesis and Si-coating occur in the same reaction mixture, and coating of pre-prepared magnetite NPs where solid NPs are first dispersed, then coated with SiO_2. In both methods the reaction takes place in aqueous cores of water-in-oil (w/o) microemulsion (ME). AOT is the surfactant used in all reactions, where n-heptane is the oil phase. The NP size is controlled by controlling the nanodroplet size within the ME. It has been observed that “in situ” method resulted in NPs where coating was more successful when compared with the “pre-prepared particles” method in AOT-stabilized reverse ME. The particles obtained were more polydispersed compared to the pre-prepared reaction.

ÖZET

HİDROFİLİK YÜZEYLİ MANYETİK NANOPARÇACIK ÜRETİMİ

Nanoparçacıkların (NPlerin) manyetik özellikleri onların yönlendirilebilen ve kendi kendine sıralanabilen nano boyutlu yapılar oluşturulmalarını sağlar. Bu çalışmada kullanılan manyetik NP olarak magnetit (Fe_3O_4) NPler kullanılmıştır. Bu parçacıklar, biyolojik uygulamalar da dahil olmak üzere birçok farklı alanda önemli uygulama potansiyeline sahiptirler. Ancak magnetit NPler yapıları gereği hidrofobik yüzeye sahiptirler, bu yüzden sulu ortamlarda yalın halleriyle bulunamazlar. Biyolojik uygulamalarda kullanıma uygun olabilmeleri için yüzeyleri modifiye edilmelidir. Bu projede amaçlanan yüzey modifikasyonu yüzeyin SiO_2 ile kaplanmasıdır. Silis kaplama (Si-kaplama) iki yöntemle gerçekleştirilebilir; "in situ" kaplama yöntemiyle, hem magnetit sentezinin hem de Si-kaplamanın aynı tepkime karışımı içinde yapılması ve "önceden hazırlanmış magnetit NP" yöntemiyle de, bu magnetitlerin katı haldeyken önce mikroemülsiyon (ME) içinde dağılımlarının sağlanması, sonra da SiO_2 ile kaplanması bu iki yöntemi özetler. Tepkimeler iki yöntemde de ters (yağ-içinde-su) ME içinde gerçekleşir. Tüm tepkimelerde yüzey-aktif-madde olarak AOT, yağ fazı olarak da n-heptan kullanılmıştır. NPlerin boyut kontrolü, içerisinde sentezlendikleri nano boyutlu damlacıkların boyutları kontrol edilerek sağlanır. AOT ile hazırlanmış ME'larda "in situ" yöntemiyle sentezlenen NPlerde yüzey kaplamasının "önceden hazırlanmış magnetit NP" yöntemiyle sentezlenen parçacıklara kıyasla daha başarılı oldukları gözlenmiştir. Bu parçacıklar "önceden hazırlanmış magnetit NP" yöntemiyle sentezlenenlere kıyasla daha geniş bir çap aralığına sahiptirler.

TABLE OF CONTENTS

ACKNOWLEDGEMENTS 3
ABSTRACT 4
ÖZET 5
LIST OF FIGURES 9
LIST OF TABLES 13
LIST OF SYMBOLS 14
LIST OF ACRONYMS/ABBREVIATIONS 15
1. INTRODUCTION 16
2. THEORY 17
2.1. Magnetic Nanoparticles 17
2.1.1. Iron (II, III) Oxide (Fe_3O_4) Nanoparticles 18
2.1.2. Methods for Synthesizing Iron Oxide Nanoparticles 19
2.2. Microemulsion Systems 21
2.2.1. Surfactants 23
2.2.2. Droplet Size 23
2.2.3. Occupancy Number 24
2.3. Silica Nanoparticles 25
2.3.1. Methods for Synthesizing Silica Nanoparticles 26
2.3.2. Reverse Microemulsion Systems 27
2.3.3. Mechanism for Silica Nanoparticle Synthesis Reaction 28
2.4. Silica-coated Magnetite (Fe_3O_4) Nanoparticles 29
2.4.1. Methods for Formation of Si-coated Magnetite Nanoparticles 31
2.4.1.1. “In situ” Synthesis Method 31
2.4.1.2. Coating of Pre-prepared Magnetite Nanoparticles 32
3. MATERIALS AND METHODS 33
3.1. Reagents 33
3.1.1. Surfactants 33
3.1.2. Solvents 33
3.1.3. Ammonia Solution 33

3.1.4. Tetraethyl Orthosilicate (TEOS) 34
3.1.5. Iron Salts 34
3.1.6. Bio-Beads SM-2 Adsorbent 34
3.2. Instruments 35
3.2.1. Analytical Balance 35
3.2.2. Centrifuge 35
3.2.3. Sonicator 35
3.3. Instrumental Techniques 35
3.3.1. Particle Size Measurements 35
3.3.2. Electron Microscopy Techniques 36
3.3.3. XRD Technique 38
4. EXPERIMENTAL METHODS 39
4.1. Preparation of AOT/Oil Stock Solution 39
4.2. Prepation of Fe^{+2} and Fe^{+3} Stock Solutions 39
4.3. Synthesis of Silica Nanoparticles in Reverse Microemulsion 39
4.3.1. AOT-stabilized Reverse Microemulsion with Silica Nanoparticles 40
4.4. Synthesis of Magnetite Nanoparticles in Reverse Microemulsion 40
4.4.1. AOT-stabilized Reverse Microemulsion Systems with Magnetite Nanoparticles 41
4.5. Synthesis of Si-coated Magnetite Nanoparticles in Reverse Microemulsion 42
4.5.1. “In situ” Synthesis Method 42
4.5.2. Coating of Pre-prepared Magnetite Nanoparticles 43
4.6. Bio-Beads SM-2 Adsorbent Treatment 44
5. RESULTS AND DISCUSSION 45
5.1. General Observations 45
5.2. Particle Size Analysis 46
5.3. XRD Analysis 54
5.4. SEM Analysis 55
5.5 Occupancy Number 62
6. CONCLUSIONS 64
7. SUGGESTIONS FOR FUTURE WORK 65
APPENDIX A: DLS ANALYSIS RESULTS 67
APPENDIX B: SEM IMAGES AND MEASUREMENTS 109

APPENDIX C: LIST OF SAMPLES 128
REFERENCES 130

LIST OF FIGURES

Figure 2.1. Schematic representation of the inverse spinel structure of (Fe_3O_4). 18

Figure 2.2. Schematic representation of (a) o/w ME, (b) a nanodroplet in reverse (w/o) ME. 22

Figure 2.3. Growth of a droplet upon addition of water. 23

Figure 2.4. Ammonia catalyzed TEOS hydrolysis in a system of reverse ME. 27

Figure 2.5. Molecular structure of anionic AOT surfactant. 27

Figure 2.6. Molecular structure of nonionic Igepal® CO-520. 28

Figure 2.7. Molecular structure of nonionic Triton X-100 surfactant. 28

Figure 3.1. Molecular structure of TEOS. 34

Figure 3.2. Schematic representation of a DLS instrument. 36

Figure 3.3. An example of a TEM image of core-shell magnetite/mesoporous silica nanoparticles. 37

Figure 3.4. An example of a SEM image for Si-coated magnetite NPs. 37

Figure 3.5. Schematic representation of a XRD. 38

Figure 4.1. Schematic representation of the silica NP reaction. 40

Figure 4.2. Schematic representation of the magnetite synthesis reaction. 41

Figure 4.3. Schematic representation of the “in situ” coating reaction. 43

Figure 4.4. Schematic representation of the pre-prepared coating reactions. 44

Figure 5.1. XRD analysis of Sample 60. 54

Figure 5.2. XRD analysis of Sample 61. 55

Figure A.1. DLS analysis of Sample 3. 68

Figure A.2. DLS analysis of Sample 4. 69

Figure A.3. DLS analysis of Sample 5. 70

Figure A.4. DLS analysis of Sample 6. 71

Figure A.5. DLS analysis of Sample 8. 72

Figure A.6. DLS analysis of Sample 9. 73

Figure A.7. DLS analysis of Sample 10. 74

Figure A.8. DLS analysis of Sample 16. 75

Figure A.9. DLS analysis of Sample 18. 76

Figure A.10. DLS analysis of Sample 19. 77

Figure A.11. DLS analysis of Sample 20. 78
Figure A.12. DLS analysis of Sample 22. 79
Figure A.13. DLS analysis of Sample 23. 80
Figure A.14. DLS analysis of Sample 24. 81
Figure A.15. DLS analysis of Sample 25. 82
Figure A.16. DLS analysis of Sample 26. 83
Figure A.17. DLS analysis of Sample 28. 84
Figure A.18. DLS analysis of Sample 29. 85
Figure A.19. DLS analysis of Sample 30. 86
Figure A.20. DLS analysis of Sample 31. 87
Figure A.21. DLS analysis of Sample 32. 88
Figure A.25. DLS analysis of Sample 1. 89
Figure A.26. DLS analysis of Sample 1 suspended in water. 90
Figure A.27. DLS analysis of Sample 2. 91
Figure A.28. DLS analysis of Sample 2 suspended in ethanol. 92
Figure A.29. DLS analysis of Sample 2 suspended in water. 93
Figure A.30. DLS analysis of Sample 27. 94
Figure A.31. DLS analysis of Sample 27 suspended in ethanol. 95
Figure A.32. DLS analysis of Sample 33 suspended in ethanol. 96
Figure A.33. DLS analysis of Sample 33 suspended in water. 97
Figure A.34. DLS analysis of Sample 34. 98
Figure A.35. DLS analysis of Sample 35. 99
Figure A.36. DLS analysis of Sample 36. 100
Figure A.37. DLS analysis of Sample 37. 101
Figure A.38. DLS analysis of Sample 38. 102
Figure A.39. DLS analysis of Sample 39. 103
Figure A.40. DLS analysis of Sample 40. 104
Figure A.41. DLS analysis of Sample 41. 105
Figure A.42. DLS analysis of Sample 42. 106
Figure A.43. DLS analysis of Sample 43. 107
Figure A.44. DLS analysis of Sample 44. 108
Figure B.1. SEM image of Sample 41. 110
Figure B.2. SEM image of Sample 42. 110

Figure B.3. SEM image of Sample 43. 111
Figure B.4. SEM image of Sample 44 with measurements. 111
Figure B.5. SEM image of Sample 44 from another part. 112
Figure B.6. SEM image of Sample 38. 112
Figure B.7. SEM image of Sample 40. 113
Figure B.8. SEM image of Sample 40 from another part. 113
Figure B.9. SEM image of Sample 39. 114
Figure B.10. SEM image of Sample 39 from another part, with measurements. 114
Figure B.11. SEM image of Sample 47. 115
Figure B.12 SEM image of Sample 47 from another part. 115
Figure B.13. SEM image of Sample 47 from another part, with measurements. 116
Figure B.14. SEM image of Sample 47 from another part of the sample, with measurements. 116
Figure B.15. SEM image of Sample 48. 117
Figure B.16. SEM image of Sample 53. 117
Figure B.17. SEM image of Sample 53 from another part. 118
Figure B.18. SEM image of Sample 54. 118
Figure B.19. SEM image of Sample 54 from another part. 119
Figure B.20. SEM image of Sample 56. 119
Figure B.21. SEM image of Sample 56 from another part. 120
Figure B.22. SEM image of Sample 57. 120
Figure B.23. SEM image of Sample 57 from another part. 121
Figure B.24. SEM image of Sample 58. 121
Figure B.25. SEM image of Sample 58 from another part with measurements. 122
Figure B.26. SEM image of Sample 59. 122
Figure B.27. SEM image of Sample 59 from another part with measurements. 123
Figure B.28. SEM image of Sample 60. 123
Figure B.29. SEM image of Sample 60 from another part. 124
Figure B.30. SEM image of Sample 60 taken from another part. 124
Figure B.31. SEM image of Sample 60 taken from somewhere else within the sample. 125
Figure B.32. SEM image of Sample 60 with measurements. 125
Figure B.33. SEM image of Sample 62. 126

Figure B.34. SEM image of Sample 63. 126
Figure B.35. SEM image of Sample 63 from another part. 127
Figure B.36. SEM image of Sample 64. 127

LIST OF TABLES

Table 5.1. Refractive index and viscosity values of solvents. 46
Table 5.2. Sample list of silica NPs at different R values with particle size analysis results. 47
Table 5.3 Particle size analysis results of w/o ME samples at different R values. 48
Table 5.4. Sample list of silica NPs suspended in different solvents with particle size analysis results. 49
Table 5.5. Sample list of pre-prepared coating reaction products with particle size analysis results. 51
Table 5.6. Sample list of magnetite in ME reaction products with particle size analysis results. 53
Table 5.7. Samples of magnetite in reverse ME reaction products with SEM images. 57
Table 5.8. EDS analysis of samples of magnetite in reverse ME reaction products. ... 57
Table 5.9. Samples of pre-prepared Si-coating reaction products with SEM images. . 59
Table 5.10. EDS analysis of samples of pre-prepared Si-coating reaction products. 59
Table 5.11. Samples of “in situ” Si-coating reaction products with SEM images. 61
Table 5.12. EDS analysis of samples of “in situ” Si-coating reaction products. 61
Table 5.13. Samples of Bio-Beads treated products. 62
Table 5.14. EDS analysis of samples of Bio-Beads treated products. 62
Table C.1. List of all samples and the reaction conditions they were synthesized in. 131

LIST OF SYMBOLS

a_0	Area of the surfactant head group
C	Concentration of the droplets in microemulsion
h	Water-to-TEOS molar ratio
n	Occupancy number
r_H	Hydrodynamic radius
r_{core}	Radius of the core
R	Water-to-surfactant molar ratio
V	Volume
V_m	Molar Volume
$\downarrow$	Precipitate
Φ	Volume fraction

LIST OF ACRONYMS/ABBREVIATIONS

AOT	Aerosol Orange T
DLS	Dynamic Light Scattering
EDS	Energy-Dispersive Spectroscopy
FSP	Flame Spray Pyrolysis
ME	Microemulsion
MNP	Magnetic Nanoparticle
MRI	Magnetic Resonance Imaging
NP	Nanoparticle
o/w	Oil-in-water
SEM	Scanning Electron Microscopy
Si-coated	Silica-coated
SPION	Superparamagnetic Iron Oxide Nanoparticle
TEM	Transmission Electron Microscopy
TEOS	Tetraethyl orthosilicate
w/o	Water-in-oil
XRD	X-Ray Diffraction

1. INTRODUCTION

Nanoscience is the science of spherical nanoparticle (NP) materials, since the particles more readily form in spherical shape [1]. In modern science, nanoscience has become one of the most significant research and development areas [2]. NPs are remarkably different from their bulk materials because of the great properties they exhibit [3]. Magnetic nanoparticles (MNPs) are a good example in this respect. They have some unusual properties such as superparamagnetism and quantum tunneling of magnetization. These magnetic properties are mainly dependent on the crystal size and the distribution of particle sizes. Therefore to control these parameters, several methods for synthesis have been developed [4].

There exists a variety of superparamagnetic NPs, i.e., particles which are attracted to an applied magnetic field, but have no residual magnetism once the field is removed [1]. Fe_3O_4 NP is one of these particles, and it is of special interest due to its unique magnetic properties and feasibility of preparation [5]. A NP which has high magnetic susceptibility, a narrow range of particle size (6-15 nm), and tailored surface chemistry can be effective since it is very likely to be used for specific bio-applications [6]. Both in powder or colloid form, MNPs tend to agglomerate and form larger entities in time, which results in lowering of their magnetic characteristics [3]. To our benefit, nanofabricated Fe_3O_4 NPs can be easily engineered into many forms of composite materials [7]. Using this, one can maintain the NPs as un-agglomerated by coating the metal oxide NPs to form core-shell NPs.

The aim of this work is to synthesize silica-coated Fe_3O_4 NPs in the aqueous nanodroplets of water-in-oil (w/o) microemulsion (ME), while silica serves both as a protective layer and provides biocompatibility to the core particle, Fe_3O_4, the metal oxide which is also called a magnetite.

2. THEORY

2.1. Magnetic Nanoparticles

MNPs are a class of NPs that can be guided with applied magnetic field. They can be oriented into nanoscale structures, where dipole-dipole interactions between adjacent particles elicit them to couple. Over the years, fabrication of various nanostructures has been studied, and yet most of the attention is focused on the structures with magnetic nanoparticulate components. Full comprehension of their magnetic behavior due to new possible surfaces, interparticle, and exchange interactions, in both magnetic and nonmagnetic matrix is aimed [8]. These MNPs possess a strong potential for research for their applications in various fields of biomedicine and bioengineering, and in technological frontiers. Drug delivery systems, cancer therapy and magnetic resonance imaging (MRI) can be given as examples of applications in biomedical and bioengineering areas [9]. Also, technologically, these MNPs can be used as magnetic recording media and as magnetic fluids [10]. For biomedical applications, properties like blood circulation time and bioavailability are of utmost importance, which are directly related with the characteristics of the NPs used; such as the size, charge, and surface chemistry [11].

Recently MNPs have been shown to orient and self-assemble into micro-scale structures under the influence of a magnetic field, using magnetic nanobeads to magnify the field's effects [12, 13].

Traits of MNPs are highly dependent on their method of synthesis and the chemical composition. Several types of MNPs with different compositions and phases can be synthesized. Pure metallic NPs, such as Fe or Co, spinel-type ferromagnets, such as $MgFe_2O_4$, $MnFe_2O_4$, and $CoFe_2O_4$, alloys, such as $CoPt_3$ and FePt and iron oxides can be given as examples of MNPs [14]. Iron oxides, such as Fe_3O_4 (magnetite), α-Fe_2O_3 (hematite) and γ-Fe_2O_3 (maghemite), are especially important. Magnetites have cubic inverse spinel structure with oxygen forming an fcc closed packing and Fe cations occupy interstitial tetrahedral and octahedral sites [15] as can be seen in Figure 2.1 [16]. The

electrical and magnetic properties this compound exhibit is due to the electron transfer between Fe^{+2} and Fe^{+3} in the octahedral sites [17]. Magnetite has high saturation magnetization and it is an efficient CO dissociation catalyst [18].

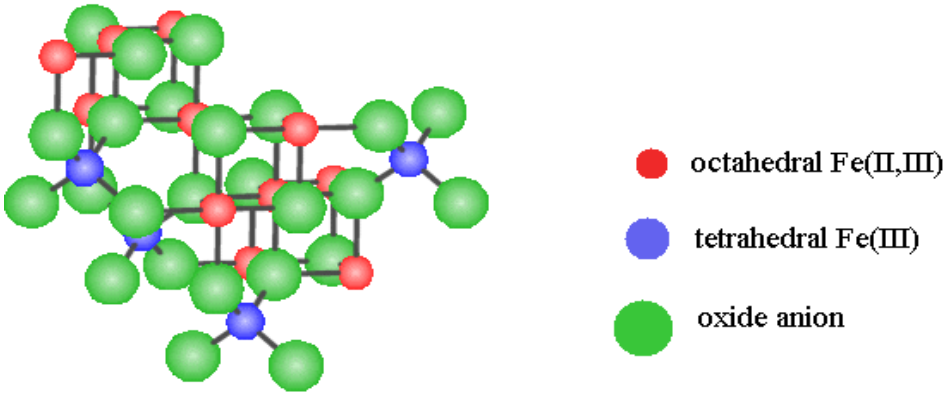


Figure 2.1. Schematic representation of the inverse spinel structure of (Fe_3O_4) [16].

2.1.1. Iron (II, III) Oxide (Fe_3O_4) Nanoparticles

Superparamagnetism of iron oxide NPs is what makes them so popular among researchers. And this property can be explained as responding to a magnetic field and possessing the ability of disowning any magnetism once the magnetic field is removed [7]. Superparamagnetic iron oxide NPs (SPIONs) have several applications such as MRI contrast enhancement, tissue repair, immunoassay, detoxification of biological fluids, hyperthermia, drug delivery and cell separation [6].

When SPIONs are coated with a proper coating material on the surface, they can be dispersed into some types of solvents [19, 20]. These dispersions of single domain magnetic particles are called ferrofluids [21] which have anisotropic magnetic dipolar attractions within particles. MRI for medical diagnosis can utilize ferrofluids by applying an external magnetic field to dispersion that guides the dispersed to a specific area, which provides enhancement to imaging. Ferrofluids can also facilitate AC magnetic field-

assisted cancer therapy [22].

The synthesized Fe_3O_4 NPs should have some specific properties so that they can be used in biomedical and bioengineering applications. High magnetization, small size (<100 nm), narrow size distribution, nontoxicity, biocompatibility, chemical stability, water solubility, being well-dispersed in dispersant of interest, and ease of surface modification are of great significance [6, 23].

Since dispersibility in media is the most basic property concerning the applications in medical fields, coating the surface of NPs is a frequently studied topic. Coating the surface of NPs warrants them both dispersibility and stability [24]. Another reason for coating NPs is to avoid agglomeration. Due to large surface area to volume ratio MNPs tend to aggregate together which prompts them to no longer retain the distinct properties associated with their nanostructures [11, 23]. Also, Fe_3O_4 is extremely susceptible to oxidation, which can be avoided by coating. Exposure to atmosphere of bare magnetite NPs result in poor stoichiometry, bad stability and higher crystallite size [23].

2.1.2. Methods for Synthesizing Iron Oxide Nanoparticles

It has been a challenge to control the size and shape of the iron oxide NPs. Different methods of synthesis were employed, but not all of them were successful of overcoming the issue of size control. The physical methods were proven to be less capable in this respect, compared to wet chemical methods. Gas phase deposition and electron beam lithography are some examples for physical procedures [6] that lack particle size control. These methods may even result in with particles which are not in the nanometer size range.

On the other hand, wet chemical routes are easier to manipulate when size is concerned. Further, these procedures enable control over the composition and even the shape of NPs to some extent [11, 25, 26]. Some examples for these routes can be given as; coprecipitation method (Si et al.) [17], hydrothermal reaction of Fe^{+3} in the presence of a

weak reducing agent and sonochemical decomposition of hydrolyzed Fe^{+2} salt, each forming Fe_3O_4 (Fried and Sun) [27, 28], γ-irradiation-induced chemical change from β-FeOOH to Fe_3O_4 (Wang and Xin) [29], organic solution phase decomposition routes, and sol-gel methods [30].

Coprecipitation is the most widely used synthesis method for iron oxide NPs which can either yield Fe_3O_4 (magnetite) or γ-Fe_2O_3 (maghemite). It is the coprecipitation of Fe^{+2} and Fe^{+3} aqueous salt solutions by addition of a base [31]. The type of salt used is very important, and chlorides, sulfates and nitrates can be some of the choices. Along with this, there are other criteria that can highly affect the size, shape and composition of NPs, which are Fe^{+2}:Fe^{+3} ratio and the ionic strength of the media .These are the factors that define the properties of iron oxide NPs for the coprecipitation method [32, 33].

In the coprecipitation method, magnetite (Fe_3O_4) is prepared with a 1:2 ferrous to ferric molar ratio, and the overall chemical reaction for this precipitation is [6]:

$$Fe^{+2} + 2Fe^{+3} + 8OH^- \rightarrow Fe_3O_4\downarrow + 4H_2O \qquad (2.1)$$

The precipitate is black in color for magnetite.

As thermodynamics is concerned, the reaction should take place at pH between 9 and 14 in order to have a complete precipitation [6]. Also, the eagerness for oxidation of iron species should be considered for this reaction, if the reaction kinetics is to be controlled. The synthesis must be done in non-oxidizing oxygen free environment by bubbling N_2 gas through the solution. Otherwise, Fe_3O_4 would be critically oxidized as:

$$Fe_3O_4 + \frac{1}{4}O_2 + \frac{9}{2}H_2O \rightarrow 3Fe(OH)_3 \qquad (2.2)$$

Furthermore, it has been reported that passing N_2 reduces the particle size compared to cases when the reaction took place in the presence of O_2 [6, 26, 27].

Lastly, there is a more recently discovered method which is the synthesis of iron oxide NPs in the water cores of w/o MEs. This provides even easier control over the particle size compared to the coprecipitation method [34].

2.2. Microemulsion Systems

MEs are an important focus of research throughout the world since they can be utilized in various technological applications. Chemical synthesis of NPs in MEs is what most of the focus is concentrated on [35]. It had been the common knowledge that water and oil are immiscible with each other. This concept has been somewhat modified since it was observed that if some energy is added into the system of oil and water (by stirring them for example), a dispersion of one into the other can be formed. However this dispersion is not stable enough, and the system returns to its original state in time. The reason that the dispersion can exist upon addition of the energy is due to the increase in the interfacial area. Bearing this thermodynamic principle in mind; a third component can be added into the system, and if it is a surface-active-agent (i.e., surfactant) with an amphiphilic behavior [36, 37], the surface tension would be decreased by the interfacial film formed between the oil and water. The presence of the surfactant would provide a stable dispersion [38].

Schulman and Hoar [39] were the ones to discover that emulsions (i.e., macrodispersions with dimensions between 0.2-10μm) can turn into solutions with much smaller particles (~10 nm). This can be achieved by addition of short chain alkanols (like butanol, pentanol, hexanol etc.) to the system, which are referred as cosurfactants. These types of solutions are called MEs and their formation does not require any additional input of energy. Though, some surfactants, such as AOT can form MEs without the cosurfactant [40].

MEs are homogeneous, optically isotropic, low viscous and thermodynamically stable dispersions. Such preparations can either be oil-in-water (o/w) (Figure 2.2a) or w/o dispersions (Figure 2.2b) depending on the proportion of the components [35]. In w/o MEs (without a cosurfactant), aqueous phase is dispersed as nanosized droplets which are surrounded by a layer of surfactant molecules [41, 42]. These nanodroplets existing in the bulk oil phase have several advantages. First of all, they are nanoreactors where synthesis of NPs can take place. The water pool has a spherical shape, therefore the particles formed would be spherical as well [43]. Another advantage is that they prevent aggregation of NPs because the surfactants adsorb on the surface of the particles when they reach the size of the nanodroplets they are in, acting as protective layers. Therefore, the particles obtained are usually very fine and monodispersed [35, 44, 45]. W/o ME systems enable easily controllable processes and yield a narrow particle size distribution [46].

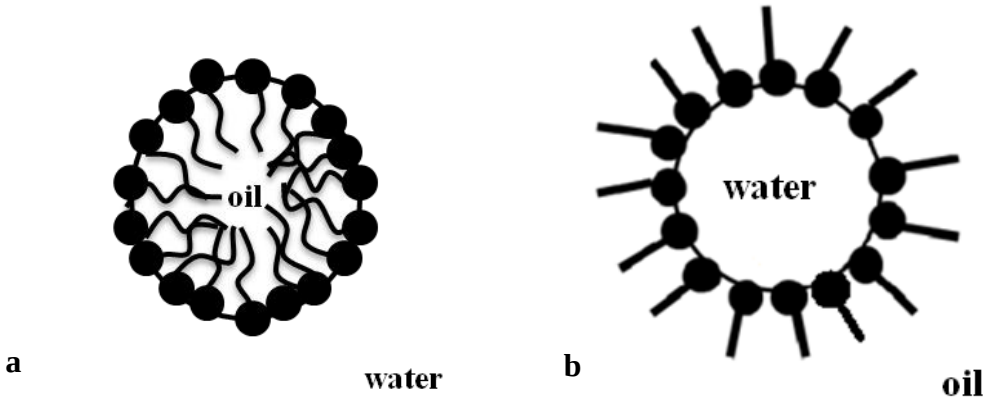


Figure 2.2. Schematic representations of a) an o/w ME, and b) a nanodroplet in reverse (w/o) ME.

When two reactants of a reaction are dissolved in two separate but identical w/o MEs, and mixed afterwards, they will form the precipitate as the product. Then, the surfactant can be washed off from the surface of the precipitated particles. Regarding the terminology, w/o MEs are sometimes called as reverse micelle solutions. The two terms are not interchangeable, though a reverse micelle solution can be called as w/o ME if the dispersion is in a continuous nonpolar organic phase [47].

Magnetite is one of the NP types that can be synthesized via w/o ME method. The main idea of the synthesis is the alkalization of a solution of iron salts and hydrolysis, which can be thought as coprecipitation technique in MEs.

2.2.1. Surfactants

The surfactants are compounds that lower the surface tension of a liquid, or the interfacial tension between two liquids, increasing the contact between them. There are many types of manufactured surfactants for various purposes; such as detergents, wetting agents, foamers, lubricants, etc. The term surface active agent refers to the fact that surfactant interacts with the surface of the liquid and change its properties by the process of adsorption.

2.2.2. Droplet Size

In w/o ME systems, a "droplet" is the water nanopool circumscribed by the surfactant molecules within the oil medium. The droplet size increases with increased amount of the dispersed phase (Figure 2.3). The size of this pool greatly affects the size of the synthesized NP.

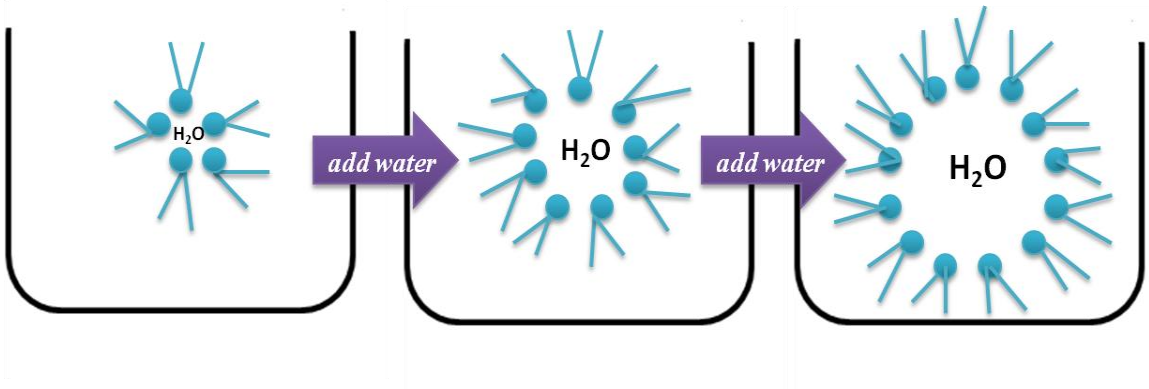


Figure 2.3. Growth of a droplet upon addition of water.

Hydrodynamic radius, r_H, is the radius of the droplet including the surfactant molecules around it. Hence,

$$r_H = r_{core} + chain\ length \tag{2.3}$$

The measure of the water pool is defined as the radius of the core, r_{core}, which is directly related to the *R* value, the water-to-surfactant molar ratio.

$$r_{core} = \frac{3V_m}{a_0} \frac{[H_2O]}{[Surfactant]} \tag{2.4}$$

where

$$\frac{[H_2O]}{[Surfactant]} = R \tag{2.5}$$

and $\left({V_m}/{a_0}\right)$ is a constant value for any particular surfactant. As expected, the size of the NP increases with the increasing *R* value in general, which provides the opportunity of tuning the size of the NP [43].

Within the droplets, the NPs are being synthesized and then start to grow. When their diameter reaches that of the ME droplet, the surfactant molecules adsorb on the surfaces of the particles. This limits the further growth of them which indicates the significance of the composition of ME solutions; i.e., the choice of the surfactant [44] (since the size of the droplets depend on the type of the surfactant).

2.2.3. Occupancy Number

Occupancy number is the number of species solubilized within the core of the dispersed phase of a ME. Assuming the amount of magnetite NPs in the solution is also the magnetite concentration in the water phase, the average occupancy number of magnetite in

a droplet can be calculated [48].

$$C\ (mol.dm^{-3}) = {[Surfactant] \times a_0}\Big/{4\pi r_H^2} \quad (2.6)$$

C is the concentration of the droplets in ME, and a_0 is the area of surfactant head group.

$$[magnetite]_{ME} = [magnetite]_{water} \times \Phi_{water} \quad (2.7)$$

Φ_{water} is the volume fraction of water .

$$n_{magnetite} = \left({[magnetite]_{ME}}\Big/{C}\right) \quad (2.8)$$

$n_{magnetite}$ is the average occupancy number of a droplet.

2.3. Silica Nanoparticles

Nanosized silica, SiO_2 production is valued for several applications. It has been widely used as filler in engineering composite [49] and in bioanalysis applications such as labeling and DNA detection. The naturally found crystalline silica (mineral silica – quartz, tridymite, cristobalite) can be reduced into nanosized particles by physical techniques with a top-down approach. However, these extracted silica particles contain metal impurities, which makes them not suitable for bioapplications. Therefore the production of synthetic silica (colloidal silica, silica gels, pyrogenic silica, and precipitated silica) is of great interest [49].

Chemical synthesis of silica NPs yields pure, mostly amorphous powder forms [50]. The synthesized particles may display aggregation and non-specific binding but this

can be eliminated or at least reduced by surface modification of the NPs. The surface of the silica NPs can be functionalized by additional coating with various alkoxysilanes, such as carboxyethylsilanetriol for introduction of carboxylic acid groups (-COOH), 3-aminopropyltriethoxysilane for amino groups ($-NH_2$), or 3-mercaptopropyl trimethoxysilane for thiol groups [51, 52].

2.3.1. Methods for Synthesizing Silica Nanoparticles

Some of the commonly used methods to synthesize silica NPs are sol-gel process, flame synthesis and reverse ME [49]. Sol-gel process is hydrolysis and condensation of metal alkoxides ($Si(OR)_4$) such as tetraethyl orthosilicate (TEOS, $Si(OC_2H_5)_4$) or inorganic salts (such as sodium silicate) in the presence of mineral acid or base as catalyst [49]. Stöber et al. [53] had reported a pioneer work on the synthesis of silica NPs of which the silica particles are formed from aqueous alcohol solutions of silica alkoxides in presence of ammonia catalyst. Many contemporary researches are evolved from the Stöber method [49].

Flame synthesis is utilized mostly to form silica NPs from TEOS. Flame spray pyrolysis (FSP) is one of the popular routes of the thermal decomposition methods. Understanding the final product properties is aimed with this method, therefore the rates of gas phase reactions leading to particle formation is an important aim of these studies [50].

Reverse ME method employs the synthesis of silica NPs in the nanodroplets of reverse ME formed by the ternary system of surfactant/water/oil in the presence of a base catalyst (Figure 2.4).

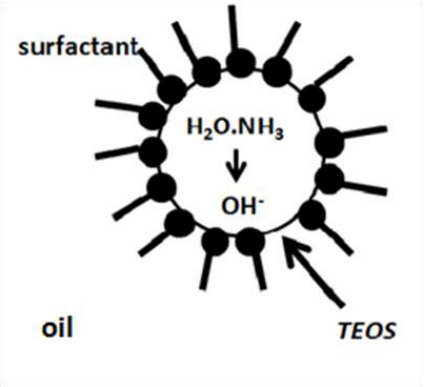


Figure 2.4. Ammonia catalyzed TEOS hydrolysis in a system of reverse ME.

2.3.2. Reverse Microemulsion Systems

Reverse ME is a widely used method to synthesize silica NPs. There is variety of surfactants used to obtain these systems such as AOT [54, 55] (Figure 2.5), Igepal® CO-520 (or NP-5) [56-58, 43] (Figure 2.6), and Triton X-100 [59, 43] (Figure 2.7) combined with different types of oil and catalysts.

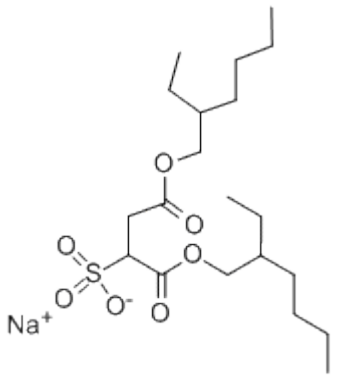


Figure 2.5. Molecular structure of anionic AOT surfactant [60].

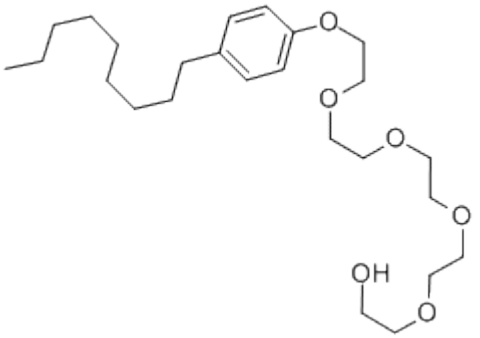


Figure 2.6. Molecular structure of nonionic Igepal® CO-520 surfactant [61].

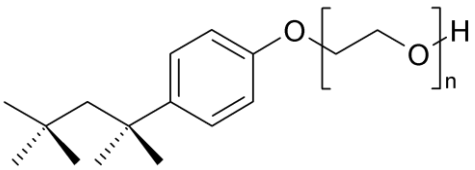


Figure 2.7. Molecular structure of nonionic Triton X-100 surfactant [62].

Among them, AOT is the most frequently used one. AOT (or aerosol orange T) is the compound sodium bis (2-ethylhexyl) sulfosuccinate also named as dioctyl sodium sulfosuccinate. It is anionic and doubly-chained, and it has low solubility in water [47].

2.3.3. Mechanism for Silica Nanoparticle Synthesis Reaction

In the aqueous nanodroplets of reverse MEs, synthesis of silica (SiO_2) NPs is carried out from TEOS as mentioned before. Chang and Fogler [63] have proposed a mechanism for the reactions that take place in the formation of silica NPs in a w/o ME medium. These reactions are; hydrolysis of TEOS and condensation of the hydrolyzed species forming SiO_2 in the presence of a base catalyst. The proposed mechanism is given in below, for R being C_2H_5:

Hydrolysis:

$$Si(OR)_4 + H_2O \rightleftharpoons (RO)_3Si - OH + ROH \quad (2.9)$$

Alcohol Condensation:

$$Si(OR)_4 + (RO)_3Si - OH \rightleftharpoons (RO)_3Si - O - Si(OR)_3 + ROH \quad (2.10)$$

Water Condensation:

$$(RO)_3Si - OH + (RO)_3Si - OH \rightleftharpoons (RO)_3Si - O - Si(OR)_3 + H_2O \quad (2.11)$$

Overall Reaction:

$$Si(OR)_4 + 2H_2O \xrightarrow{OH^-} SiO_2\downarrow + 4ROH \quad (2.12)$$

Once the silanol ($(RO)_3Si - OH$) is formed by hydrolysis, it can either react with another silanol (2.11) or a silicate ($Si(OR)_4$) (2.10) molecule, resulting in either with water or alcohol respectively.

2.4. Silica-coated Magnetite (Fe_3O_4) Nanoparticles

MNPs can easily be aggregated due to their hydrophobic characteristics. To stabilize them, most commonly a surface modification is introduced, which does not only stabilize them, but enables additional derivatization with new functional groups [64]. Where the main reason of bare magnetic particles not being desirable is their eagerness to aggregate, there are other limitations that cause them to be not so useful in practical applications. One of them is their instability, which may lead a change in their original structure. A structure change in MNPs can easily alter their magnetic properties. Another reason is biodegradation, which may occur when they are used in biological systems. These limitations further imply the necessity of a coating layer [6].

Coating can be done by modifying the surface with creation of a few atomic layers of organic polymer or inorganic metallic (e.g. gold) or oxide (e.g. silica, alumina) surfaces [65]. Among the coating materials, silica is a very popular one. Encapsulation of MNPs in

silica is an important step in full realization of the MNP behavior in both bioapplications and technological frontiers. As Philipse *et al.* [66] have explained the "spherical MNPs with well-defined magnetic interactions", they have emphasized the interest Si-coated MNPs draw because of both a magnetic dipole and a nonmagnetic silica shell which serves the purpose of screening.

There are various reasons for the commonness and practicality of the silica layer. First of all, silica-coated (Si-coated) particles can react with alcohols and various silane coupling agents to produce dispersions which are stable in non-aqueous solvents due to the presence of silane groups. Also, silica enriched surfaces enable hydrogen bonding/covalent bonding of specific ligands or groups. Moreover, a silica surface provides high chemical stability against aggregation, biodegradation, pH and electrolyte concentration changes, inertness and biocompatibility in biological systems. It acts as a protective layer and helps to improve dispersibility. When magnetite NPs are coated with silica, their hydrophilicity is greatly improved and they have strong magnetic susceptibility and minimal residual magnetism when the magnetic field is removed [23].

There are two main methods to obtain Si-coated magnetite NPs and two different ways of achieving it. The first way is to use pre-prepared magnetite particles and coating them. And the second way is to synthesize magnetite and coat them "in situ". One of the methods to obtain these particles is Stöber method which is only applicable for pre-existing magnetite NPs. Similar to what was discussed before, Stöber method is mixing of magnetite NPs, aqueous solution and alkoxysilane (TEOS) in alcohol where TEOS is hydrolyzed and condensed. It is a sol-gel reaction which is easy and takes place in several hours maximum. As a result a silica shell layer is formed around magnetite NPs. However, the control over the thickness of the shell layer and the shape of the particles is limited. Though it can be optimized through solvent components and volume of alkoxysilane, it is not fully controlled. Also the particles are mostly formed as aggregates [24].

The other method to serve purpose of coating is reverse ME method which may be carried out "in situ". The core-shell NPs formed have controlled shape of a sphere which is achieved with the spherical media that the droplets in the core of the micelles provide. By

using different surfactants to form the ME, and having different water-to-surfactant molar ratio (R), different sizes of the particles can be obtained. The amount of alkoxysilane used would determine the thickness of the shell, so this means it needs to be measured strictly. This reaction is more time consuming and more expensive compared to Stöber method, but it has much more control over the morphology of the particles [24].

The general purpose to synthesize silica-coated MNPs is to utilize them in magnetoelectronic applications in which these NPs are used to form ordered arrays with interparticle magnetic couplings controlled through the silica shell thickness [67]. Magnetically guided drug delivery, tumor targeting and magnetically assisted chemical separation of cells and/or proteins demonstrate the practical usage of these particles [68-70]. A pioneer work in magnetic separation is done by Robinson et al. [71] in 1973. They used silica-coated magnetic iron oxide and cellulose-coated magnetic iron oxide to immobilize the enzymes α-chymotrypsin and β-galactosidase in bioreactors, hence separated the enzymes from cells. This was the first time magnetic separation was used in bioapplications, and it became very prominent afterwards.

2.4.1. Methods for Formation of Si-coated Magnetite Nanoparticles

Si-coated magnetite NPs can be obtained either by Stöber method or reverse ME method. As to focus on the mechanism of the reverse ME method, these two approaches should be considered; "in situ" synthesis and coating of pre-prepared particles.

2.4.1.1. "In situ" Synthesis Method. The first step is to synthesize magnetite NPs in the aqueous cores of reverse micelles by the coprecipitation of ferric and ferrous iron salts with an organic base. Since the reaction mixture already contains excess base, upon the direct addition of TEOS leads to hydrolysis and polymerization reaction. The polymerization reaction takes place much slower in the core of the water droplets of the ME than in an aqueous solution (as it is in Stöber method which is much faster), therefore a layer of uniform silica coating is expected to be formed around each NP [43]. This is a simple, one-pot process that utilizes reverse ME.

2.4.1.2. Coating of Pre-Prepared Magnetite Nanoparticles. The pre-prepared magnetite NPs are dispersed in the reverse ME initially. Then again; in the presence of a strong base, TEOS is added into the reaction mixture and the layer of silica coating is assumed to be formed.

3. MATERIALS AND METHODS

3.1. Reagents

3.1.1. Surfactants

The doubly chained anionic surfactant dioctyl sodium sulfosuccinate (AOT) is obtained from Sigma-Aldrich, and used with no further purification to form reverse ME systems. Similarly, Triton X-100 was obtained from Merck and experimented to form reverse ME systems to synthesize silica NPs. However the first experiments have failed to yield silica NPs, so this surfactant was not used anymore.

3.1.2. Solvents

Solvents used as the oil-continuous phase of w/o ME systems were n-heptane and n-decane which were obtained from Merck, and used without further purification.

3.1.3. Ammonia Solution

The ammonia solution used in this research is from Merck with 29 weight %. The ammonia solution acts as a pH buffer, providing the system with OH^- ions in the magnetite NP synthesis reaction, and acts as catalyst in magnetite NP synthesis, silica NP synthesis and silica layer coating reactions. It also provides the water needed to form the reverse micelles.

3.1.4. Tetraethyl Orthosilicate (TEOS)

TEOS is the metal alkoxide used as the precursor to silicon dioxide in the silica NP synthesis and silica-coating synthesis reactions. It was provided from Merck and its molecular structure can be seen in Figure 3.1.

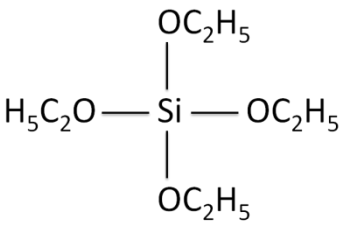


Figure 3.1. Molecular structure of TEOS.

3.1.5. Iron Salts

In the experiments Fe^{+3} salt was always used in 2:1 stoichiometric ratio to Fe^{+2} salt. Iron salts used in the synthesis of magnetite NPs were iron (II) sulfate heptahydrate ($FeSO_4.7H_2O$) from Sigma-Aldrich, iron (II) chloride tetrahydrate ($FeCl_2.4H_2O$) from J. T. Baker, and iron (III) chloride ($FeCl_3$) from Merck .

3.1.6. Bio-Beads SM-2 Adsorbent

Bio-Beads SM-2 Adsorbent is polystyrene-divinyl-benzene which particularly well-adsorbs nonpolar substances or surfactants from aqueous solutions. It is neutral, macroporous, polymeric, and Analytical Grade adsorbent of high surface area and it is composed of a large number of highly cross-linked microspheres [72]. It is used to remove AOT from synthesized NPs by a batch protocol, where prewashed (ethanol) adsorbent is added into the mixture which contains the NPs. It is obtained from Bio-Rad Laboratories.

3.2. Instruments

3.2.1. Analytical Balance

The analytical balance used in this research is AND GR-200.

3.2.2. Centrifuge

Hettich Rotofix 32 centrifuge is used to recover the solid NPs which are broken out of the reverse micelles they were synthesized in.

3.2.3. Sonicator

It is used in the preparation of AOT/n-heptane stock solution and dispersing the magnetite NPs in ME. The model is Bandelin Sonorex.

3.3. Instrumental Techniques

Silica NPs, Si-coated magnetite NPs and magnetite NPs were characterized through their particle size and shape. For the magnetite containing NPs, it was necessary to check the type of iron oxide present; i.e., to prove that the NPs were indeed magnetite, but not maghemite or hematite, which are other types of iron oxides.

3.3.1. Particle Size Measurements

For particle size analysis of the colloids Dynamic Light Scattering (DLS) is a commonly used instrument. A size distribution profile can be obtained and the polydispersity of the system can be investigated. If the system is monodisperse, the determination of the mean effective diameter can be achieved. For ME systems, DLS does not measure the direct particle size, but it measures the diameter of the dispersed phase, i.e,

r_H (hydrodynamic radius) [73]. Since the particles are assumed to be reaching to the size of the micelles as the reaction proceeds then ends, the hydrodynamic radius can be assumed to be in proxy with the particle size of the NPs.

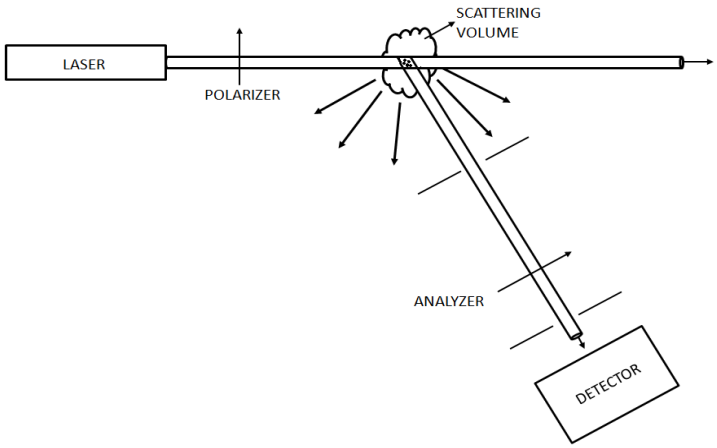


Figure 3.2. Schematic representation of a DLS instrument [74].

Particle Size Measurements were done with Brookhaven Instruments 90 Plus Particle Size/Zeta Analyzer. 2.5 mL of samples were placed in sample holders, and then into the instrument. The scattering angle of the instrument was 90°. The measurements yield with effective diameter sizes of the reverse micelles. Also polydispersity and size distribution (lognormal and multimodal) of the MEs were determined. The data regarding these measurements can be found in Appendix A, and the results are discussed in Chapter 5.

3.3.2. Electron Microscopy Techniques

Microscopic techniques can be used to determine both the size and the shape of the NPs. TEM (Transmission Electron Microscopy) and SEM (Scanning Electron Microscopy) are widely used for these purposes. Electron microscopy is the method used in both of the instruments which enables the high resolution visualization of small (micrometer-nanometer) or subatomic particles (depending on the resolution of the instrument used).

The method used in SEM is based on scattered electrons (or secondary electrons), where the microscope collects and counts the scattered electrons to produce the image. Whereas TEM uses a beam of electrons transmitted through the sample and form the image.

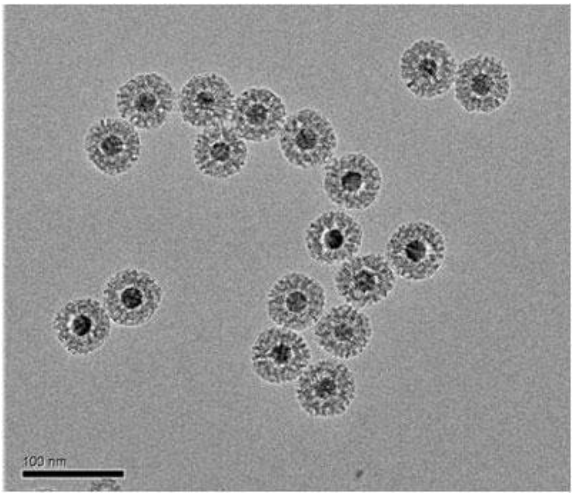


Figure 3.3. An example of a TEM image of core-shell magnetite/mesoporous silica nanoparticles [75] (from the work of Dr. Hyeon from Seoul National University).

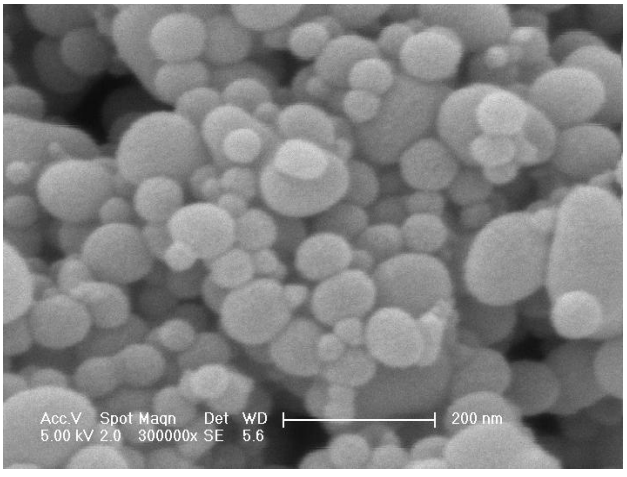


Figure 3.4. An example of a SEM image for Si-coated magnetite NPs.

Philips XL30 ESEM-FEG/EDAX instrument was used to visualize the particles and samples were coated with gold before analysis. Voltage and spot diameter values vary for the sample. Magnification is limited by resolution of the instrument, so 300,000 is a maximum. For most of the samples 200,000 times magnified images were obtained. Also less magnified (10,000x) version images of samples were taken where clusters of the NPs can be seen. Energy-Dispersive X-Ray Spectroscopy (EDS) technique was used to determine the presence of elements in % ratios. The images and the related EDS analyses can be found in Appendix B and Section 5.4, respectively.

3.3.3. XRD Technique

X-Ray Diffraction (XRD) technique can be used for identification purposes of NPs. It generally gives information about the crystal structure and chemical composition of the materials. This method is based on the measurement of the scattered intensity of an X-ray after it hits the sample. The magnetite for example, has specific peaks that can be matched through databases in XRD analysis, so that it can be differentiated from other iron oxides.

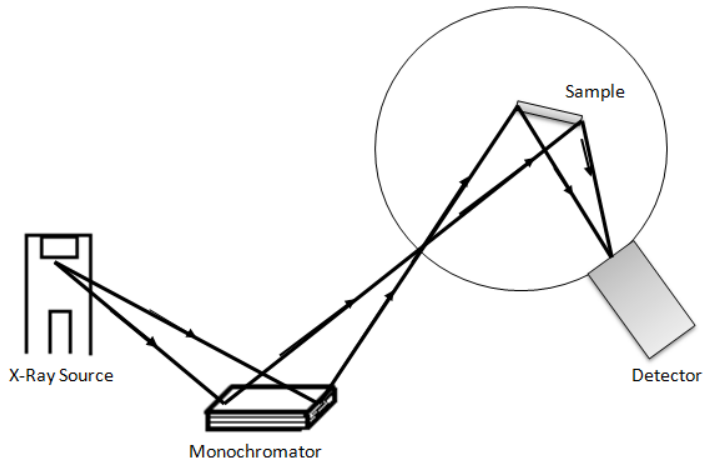


Figure 3.5. Schematic representation of a XRD instrument [76].

XRD analyses were carried out with Rigaku D/MAX-Ultima+/PC X-Ray Diffraction instrument. Solid samples in powder form were used.

4. EXPERIMENTAL METHODS

4.1. Preparation of AOT/Oil Stock Solution

In all synthesis reactions, an AOT/oil/ammonia reverse ME was used where oil was either n-heptane or n-decane. AOT needs to be introduced into the system from a stock solution of AOT in oil. In preliminary silica NP synthesis reactions [AOT] is kept at 0.1 M. In most of the other reactions 0.75 M AOT was used. The concentration was raised to 1 M in two experiments; however this required preparation of 2 M stock solutions of the surfactant in oil which proved to be a very difficult task, since AOT does not dissolve easily in oil at very high concentrations. Due to experimental difficulties, the stock solution was kept at 1 M concentration, and the samples were diluted to 0.1 M or 0.75 M as indicated in the thesis.

4.2. Prepation of Fe^{+2} and Fe^{+3} Stock Solutions

Since the amounts of iron salts used were very low and they possess a hygroscopic nature, it was mostly not practical to weigh them and add them to the system. It was therefore preferred to prepare stock solution of $FeCl_3$ and $FeCl_2.4H_2O$ salts and add them as solutions to the mixture. Since $FeSO_4.7H_2O$ is not very hygroscopic so it could be used as solid. 0.075 M aqueous $FeCl_3$ stock solution was prepared with deionized water and the appropriate amount of it was used so that $[Fe^{+3}]$: $[Fe^{+2}]$ was 1:2 in the reaction mixture.

4.3. Synthesis of Silica Nanoparticles in Reverse Microemulsion

Silica NPs were prepared in AOT-stabilized reverse ME systems, and [AOT] was kept at 0.1 M in all of the reactions.

4.3.1. AOT-stabilized Reverse Microemulsion with Silica Nanoparticle

AOT-stabilized reverse MEs were prepared with two different oil-continuous phases (n-heptane and n-decane), and at three different R values; 5, 7.5 and 10. The variable h, $\left(\frac{[H_2O]}{[TEOS]}\right)$, was 18.5 for all of the reverse ME systems. The reactions were carried out under N_2 gas.

A sealed round bottom flask with a magnet inside was de-aired by running N_2 gas through. Then a $N_{2\ (g)}$ filled balloon was attached to the flask. Ammonia and AOT solutions were added into the flask and the mixture was magnetically stirred until a transparent ME was obtained. After the addition of TEOS, the reaction was carried out for 24 hours. In the end, ethanol was added to break the micelles and free the silica NPs. The mixture was then transferred into a centrifuge tube and centrifuged for 20 minutes at 4000 rpm. Washing with ethanol, then centrifuging steps were repeated for two more times, and the particles were dried in oven at 100°C overnight.

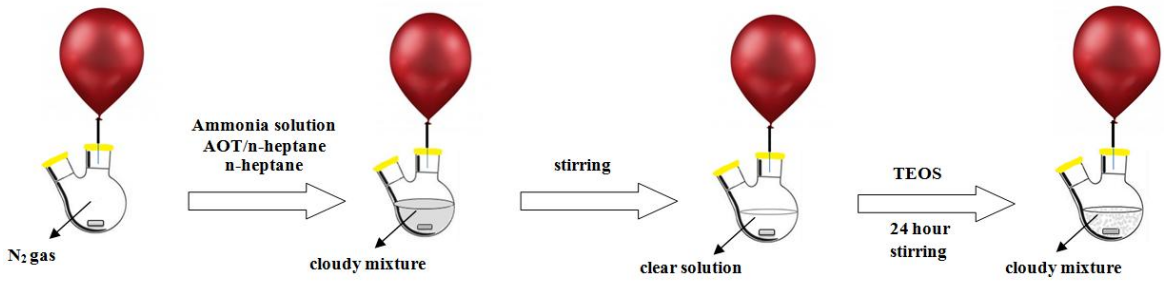


Figure 4.1. Schematic representation of the silica NP synthesis reaction.

4.4. Synthesis of Magnetite Nanoparticles in Reverse Microemulsion

Magnetite NPs were prepared in an AOT-stabilized reverse ME. The reaction mixtures had a total volume of 50 mL with R value of 5. [AOT] was kept at 0.75 M and the variable h was kept at a value of 18.5 in all of the reactions.

4.4.1. AOT-stabilized Reverse Microemulsion Systems with Magnetite Nanoparticles

AOT-stabilized reverse MEs containing magnetite NPs were only prepared with the oil n-heptane. Unlike the silica NP synthesis reactions where the only source of water was ammonia, for these reactions the aqueous phase consisted of both ammonia and the iron salt solutions.

Required amounts of $FeSO_4.7H_2O_{(s)}$ and $FeCl_{3\,(aq)}$ were added into a round bottom flask with AOT and n-heptane. The mixture was then sonicated until a clear yellow-orange colored ME was obtained. A magnet was added and the flask was sealed. The mixture was purged under $N_{2\,(g)}$ for 10 minutes while being stirred. A measured amount of ammonia solution was added that changed the color of the reaction mixture to black, and the reaction was kept going for 30 minutes, under N_2 gas, while still being stirred. Ethanol was then added and the mixture was centrifuged. The collected precipitate was washed with n-heptane, centrifuged, washed with ethanol once more and centrifuged again. The precipitate was dried in a 100°C oven overnight.

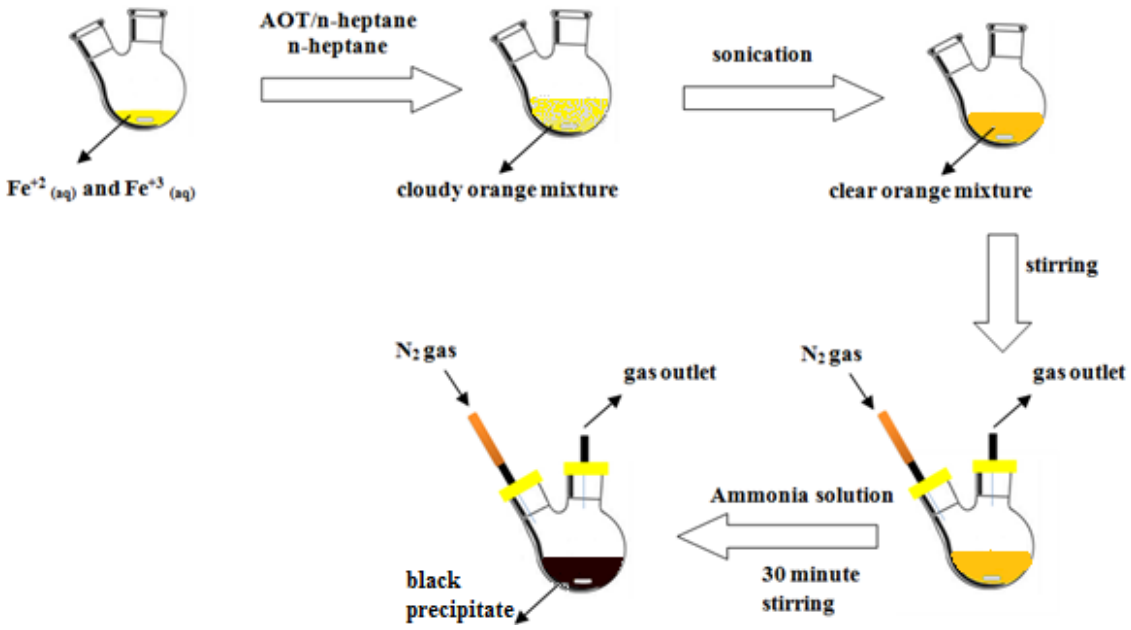


Figure 4.2. Schematic representation of the magnetite synthesis reaction.

4.5. Synthesis of Si-coated Magnetite Nanoparticles in Reverse Microemulsion

Two different approaches for synthesis of Si-coated magnetite NPs were employed. Both were carried out with the same ternary system; AOT/n-heptane/water. The R value was 5 and h was 18.5, in all the reactions.

4.5.1. "In Situ" Synthesis Method

This method aims for "one-pot synthesis" of Si-coated magnetite NPs from the initial Fe^{+2} and Fe^{+3} salts**.** The [AOT] used in these reactions were; 1 M and 0.75 M. For practicality reasons, 0.75 M AOT concentration was preferred. The aqueous phase consisted of both ammonia and aqueous iron salt again.

The initial stage of the reaction procedure was the same with the magnetite NP synthesis, but in this case the constant flow of N_2 gas was stopped after 30 minutes since magnetite synthesis reaction was assumed to be over. A $N_{2\ (g)}$ filled balloon was attached to the flask containing the reverse ME with magnetite NPs, and TEOS was added into this reaction mixture as a precursor to Si-coating reaction.

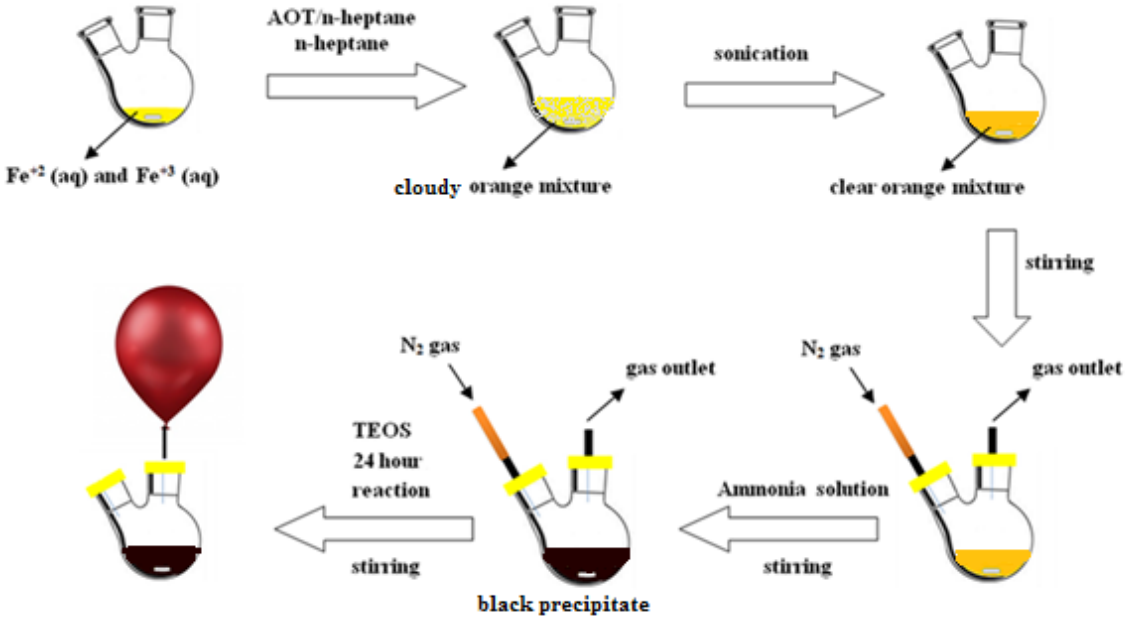


Figure 4.3. Schematic representation of the "in situ" coating reaction.

4.5.2. Coating of Pre-prepared Magnetite Nanoparticles

The magnetites used in these reactions were provided by Yeditepe University Chemical Engineering Department, and used without further treatment. The magnetites were products of either co-precipitation or partial oxidation reaction. They were dispersed either in $NH_{3\,(aq)}$ or in AOT solution before being added into the reaction flask.

The reverse ME used here has aqueous ammonia as the only source of water. Ammonia solution was the first choice to disperse magnetite NPs in, and this was achieved by sonication. The mixture was then de-aired for 10 minutes while being stirred, followed by addition of AOT and n-heptane. The reaction mixture was stirred for a further 30 minutes with a magnet, while N_2 gas was run through it (Figure 4.4). The second choice as dispersion phase was the AOT solution. Dispersion was again done by sonicating the particles in the solution. The next step was to add n-heptane and ammonia. The reaction mixture was constantly subjected to N_2 gas for 30 minutes, while being stirred.

TEOS was then added in to the mixture (same procedure for both NH_3 and AOT/n-heptane dispersed systems), and for 24 hours it was only stirred, but was not disturbed otherwise, with an attached N_2 filled balloon on the flask. When the reaction was over, ethanol was added and the mixture was centrifuged. The precipitate was washed with n-heptane, and then with ethanol once more, and dried overnight in the oven at 100°C.

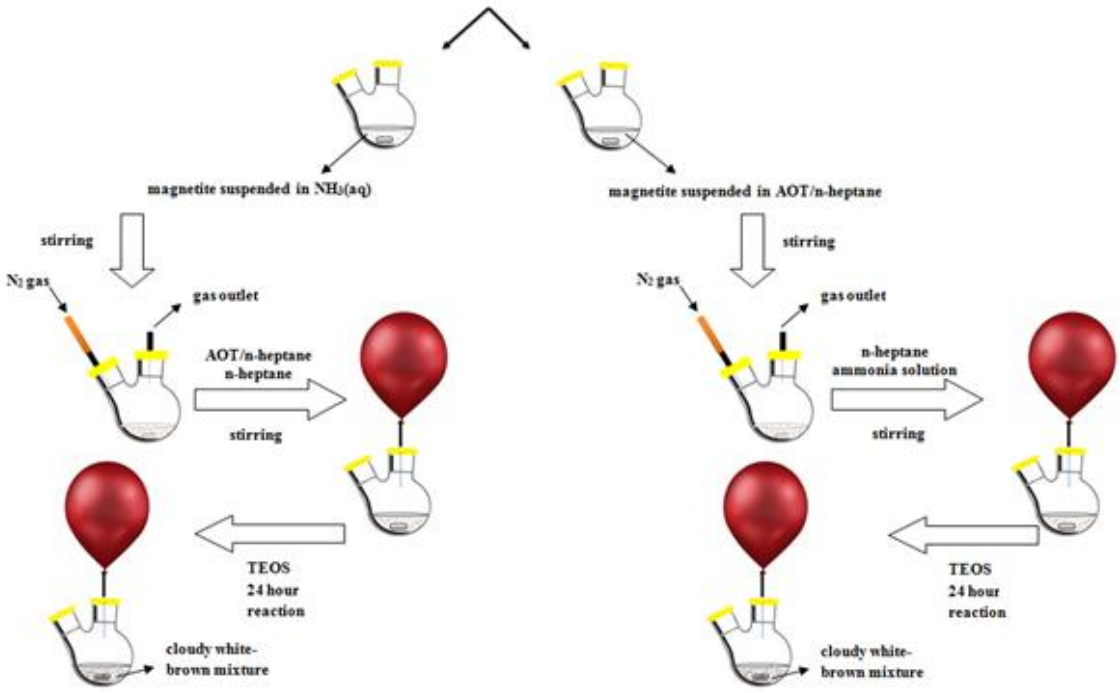


Figure 4.4. Schematic representation of the pre-prepared coating reactions.

4.6. Bio-Beads SM-2 Adsorbent Treatment

The solid NP samples were dispersed in deionized water using a sonicator for one hour. Five grams of slurried (in ethanol) Bio-Beads SM-2 Adsorbent is weighed (for approximately 25 mL of suspension), and added to the suspension. The mixture was then stirred for 30 minutes with a magnet. When Bio-Beads particles were settled at the bottom, the solution on the top was transferred into a tube and centrifuged. The precipitate was collected, dried and used for measurements.

5. RESULTS AND DISCUSSION

5.1 General Observations

During the silica NP synthesis reaction, the formation of the particles could be observed through color change when TEOS was introduced into the system. Initially colorless and clear reaction mixture became turbid when TEOS was added. When the system has n-decane instead of n-heptane, the mixture became even milkier. A similar visual change was observed in both of the methods for coating when TEOS was added. For the pre-prepared method a brownish mixture became an orange-brown color upon the addition of TEOS. And the “in situ” reaction, the clear brown color before the addition of TEOS, got cloudy after the addition. The yellow-orange magnetite NP synthesis reaction mixture turned black-brown in color when NH_3 was introduced into the system.

Silica NPs were formed as white powder-like precipitates. The magnetite NPs were dark brown in color, and low in amount. The pre-prepared coating reactions resulted in white, powder-like precipitates with brown spots on them. “In situ” coating reactions on the other hand yielded three different types of precipitates. One of them was orange-white and powdery and another one was light yellow and powder-like and the last one was formed as brown and sticky precipitate.

The pre-prepared magnetite NPs that were obtained from Yeditepe University were responsive to a magnet. Whereas, neither magnetite NPs synthesized in reverse MEs nor Si-coating reaction products showed any response to a magnetic field. These products were also dispersed in water to check their magnetic response, but again there was none.

5.2. Particle Size Analysis

The particle size analyses were done with the DLS instrument where the instrument was set with appropriate refractive index [77] and viscosity [78] values for each solvent. Table 5.1 lists the solvents that are used, and some of the related properties at 25 °C.

Table 5.1. Refractive index and viscosity values of solvents.

Oil phase /Solvent	Refractive Index	Viscosity (cP)
n-Heptane	1.388	0.39
n-Decane	1.408	0.92
Ethanol	1.361	1.07
Water	1.333	0.89

Particle size analysis was first done for the silica NPs. These silica NPs were synthesized either in AOT/n-heptane/ammonia or AOT/n-decane/ammonia ternary systems. The effective diameter and polydispersity values at different R values can be found in Table 5.2.

Table 5.2. Sample list of silica NPs at different *R* values with particle size analysis results.

Sample no	Oil Phase	*R*	Effective Diameter (nm)	Average Effective Diameter (nm)	Polydispersity	DLS analysis
3	n-heptane	5	38.7	45.6 (± 5.6)	0.070	Figure A.1
4			39.7		0.148	Figure A.2
5			39.9		0.135	Figure A.3
6			49.5		0.150	Figure A.4
8			47.6		0.124	Figure A.5
9			51.4		0.081	Figure A.6
10			52.1		0.105	Figure A.7
16	n-heptane	7.5	81.9	80.8 (± 4.5)	0.073	Figure A.8
18			75.1		0.048	Figure A.9
19			80.4		0.038	Figure A.10
20			85.9		0.066	Figure A.11
22	n-heptane	10	92.5	102.2 (± 9.3)	0.042	Figure A.12
23			111.1		0.060	Figure A.13
24			102.9		0.053	Figure A.14
25	n-decane	5	120.3	115.8 (± 23.6)	0.116	Figure A.15
26			136.8		0.306	Figure A.16
28			90.2		0.205	Figure A.17
29	n-decane	7.5	205.0		0.243	Figure A.18
30			221.2		0.390	Figure A.19
31	n-decane	10	234.0		0.244	Figure A.20
32			131.3		0.325	Figure A.21

The preliminary experiments regarding silica NPs were done to have a better understanding of AOT-stabilized reverse MEs; i.e., the change in particle size when *R* value is changed, and the effect of the type of oil on the particle formation. The theory behind DLS suggests that what is measured is the radius of the dispersed nanodroplet which incorporates the surfactant molecules around the core, together with any oil solvent tightly bound to the surfactant.

The results on Table 5.2 suggest that the droplets including the silica NPs are in the 38-234 nm range, depending on the composition of the reverse ME. Three *R* values were used; 5, 7.5 and 10. It was observed that by increasing the *R* value, larger NPs could be obtained. This general trend is supported by the theory as well as it was explained in Section 2.1.3.2. With n-heptane, when *R* value was 5, NPs with diameters between 38-53

nm were synthesized. The diameters had greatly increased in size when n-decane was used. The range of the in-decane-synthesized NPs with $R = 5$ was 90-137 nm. A similar relation between n-heptane and n-decane used NPs was observed with $R = 7.5$ and $R = 10$.

It is safe to say that when n-heptane is used; smaller-sized particles with a narrower range can be obtained, compared to in-decane-synthesized NPs. Also, in-decane-synthesized NPs had higher polydispersities than in-heptane-synthesized NPs. However, it is aimed to have the NPs as monodisperse as possible. Therefore; the magnetite synthesis and Si-coating reactions all took place in n-heptane. Since it was also desired to synthesize the NPs as small as possible, all reactions were carried out at $R=5$.

In Table 5.3. DLS analyses of w/o ME samples can be found. The effective diameter values are the diameters of empty aqueous nanodroplets incorporated with surfactant molecules within the bulk oil phase, n-heptane.

Table 5.3. Particle size analysis results of w/o ME samples at different R values

R	Effective Diameter (nm)	Polydispersity	DLS analysis
5	8.8	0.185	Figure A.22
7.5	7.2	0.178	Figure A.23
10	8.0	0.177	Figure A.24

All silica NP samples were washed with ethanol to free the NPs from the dispersed phase, and then dried. Some of the samples were then suspended in either water or ethanol, or in both by sonicating for 2 hours. The particle size analysis results of these samples are shown in Table 5.4.

Table 5.4. Sample list of silica NPs suspended in different solvents with particle size analysis results.

	Droplet (containing NP) size measured in ME			**"Dried-then-suspended-in-water/ethanol" silica NP size**			
Sample no	**Effective Diameter (nm)**	**Polydispersity**	**DLS Analysis**	**Dispersion Phase**	**Effective Diameter (nm)**	**Polydispersity**	**DLS Analysis**
1	62.6	0.142	Figure A.25	Water	247.6	0.309	Figure A.26
2	63.5	0.163	Figure A.27	Ethanol	56.1	0.200	Figure A.28
				Water	325.9	0.293	Figure A.29
27	136.8	0.306	Figure A.30	Ethanol	731.8	0.321	Figure A.31
33				Ethanol	194.2	0.286	Figure A.32
				Water	280.5	0.326	Figure A.33

Since the reaction mixture was washed with ethanol and NPs were dried, and then suspended in water/ethanol, it is certain that ME no longer exists, hence nanodroplets no longer exists. According to the measurements at Table 5.4, we can say that DLS analysis of this type of samples was no longer suitable to predict the size of the NPs.

Results in Table 5.4 suggest that the effective diameters of the ME dispersions are in fact smaller than the "dried-then-suspended-in-water/ethanol" silica NPs. Further, polydispersity values of these silica NPs are considerably higher than those of the ME dispersions. This may be explained through agglomeration. Once the particles leave the nanodroplets, they tend to agglomerate and form clusters. This effect may have been minimized by sonicating the samples in the solvent for longer periods of time (longer than 2 hours).

The particle size analyses on pre-prepared Si-coating reaction products were also done. The samples were collected at the end of 24 hours and measurements were carried out without any further processing. The type of dispersion phase pre-prepared magnetite NPs were dispersed in when added into the reaction mixture are also indicated in Table 5.5. It should be noted that when samples were collected, the NPs were still dispersed in reverse ME. This should not be mistaken with the case in Table 5.4, where the silica NPs were suspended in water/ethanol after the AOT, i.e., the ME, was removed and the particles were dried.

Table 5.5. Sample list of pre-prepared coating reaction products with particle size analysis results.

Sample no	[AOT] (M)	Magnetite Suspension	Effective Diameter (nm)	SEM Measured Diameter (nm)	Polydispersity	DLS Analysis	SEM Image
34	0.1	in NH_3	219.9		0.376	Figure A.34	
35			353.5		0.395	Figure A.35	
36			162.5		0.322	Figure A.36	
37			267.3		0.380	Figure A.37	
38			562.6	21-28	0.214	Figure A.38	Figure B.6
39	0.75	in NH_3	1134.6	18-26	0.269	Figure A.39	Figure B.10
40		in AOT/n-heptane	1174.3	20-28	0.286	Figure A.40	Figure B.7

The SEM results that are also listed in Table 5.5 give a completely different story than the DLS results. The reason behind this could be the fact that the magnetite NPs were not properly dispersed in the ME to begin with. If they were dispersed as larger entities, like micro structures, due to the strong aggregation tendencies, this would explain why the effective diameter of the dispersed phase is so much larger than the diameter of the actual particles revealed by SEM for samples 38-40, hence explaining the inapplicability of DLS to these systems.

The effective diameters were noticeably increased when the [AOT] was increased from 0.1 M to 0.75 M (also the amount of pre-prepared magnetite NPs used was increased accordingly). The aim of increasing the concentration was to coat larger amount of NPs, not to end up with larger effective diameter of droplets.

Unfortunately these results would also suggest that there were no nanosized magnetites to coat with silica in the dispersed phase. So the 18-28 nm sized particles visualized by SEM could only be silica NPs. The pre-prepared coating method and its suspected success will be further discussed in the upcoming sections.

Before proceeding to the next coating method, it is important to mention another type of particle synthesis; only magnetite NP synthesis in w/o ME. These reactions were carried out to compare their products to the Si-coated magnetite NPs as a result of the “in situ” reaction. The analyses of magnetite NP samples directly taken from the ME at the end of the reaction were also done and the results are given in Table 5.6.

Table 5.6. Sample list of magnetite in ME reaction products with particle size analysis results.

Sample no	Effective Diameter (nm)	SEM Measured Diameter (nm)	Polydispersity	DLS Analysis	SEM Image
41	7032.5		0.442	Figure A.41	
42	562.1		0.406	Figure A.42	
43	1671.9		0.386	Figure A.43	
44	383.6	12-15	0.343	Figure A.44	Figure B.4

The measurements in Table 5.6 do not show any kind of consistency even though the samples 41-44 were all prepared at same conditions, where 41-42 and 43-44 were synthesized in batch. This suggests that either the attempts to synthesize only magnetite NPs in reverse ME are not successful or the nanodroplets somehow come together and form clusters so that they appear as larger.

The particles in dispersion have a constant, random Brownian motion and this causes the intensity of scattered light to fluctuate as a function of time. The DLS instrument generates a correlation function of that scattered intensity. Baseline index is a constant in this correlation function. Size is obtained from the correlation function by using algorithms and a plot of size distribution of the relative intensity of light scattered by particles in various sizes is given at the end [79]. The instrument used in this research makes ten runs of equal elapsed times and generates the plot. The theory suggests that baseline index value shows how well each run within one measurement of the instrument fits to the size distribution plot. It is a value between 0-10, and it is important the baseline index to be at least higher than 5 for a dependable measurement.

The measurements 41, 42 and 44 all have baseline index values equal to zero combined with the fact that they all have high polydispersities, which supports the latter theory of “nanodroplets somehow come together and form clusters so that they appear as larger”, because these measurements cannot be regarded as reliable.

With the SEM, diameter measurement of only the Sample 44 could be done but the rest of the samples also have SEM images, without the size measurement (Figures B.1-B.3). They most certainly prove the presence of NPs. However the type of iron oxide NP present is yet to be determined. The SEM results are also discussed further on in Section 5.4.

5.3. XRD Analysis

Generally XRD analysis requires a substantial amount of sample. Since our yields were insufficient it was only possible to carry out two measurements. The two samples were product of "in situ" Si-coating reactions. These measurements could be done since the original [AOT] was 1 M and a higher yield could be obtained. However due to experimental difficulties experienced in preparing high concentration stock solution of AOT (see Section 4.1) it was not possible to carry on with these conditions. Figure 5.1 and Figure 5.2 shows the results of these two analyses.

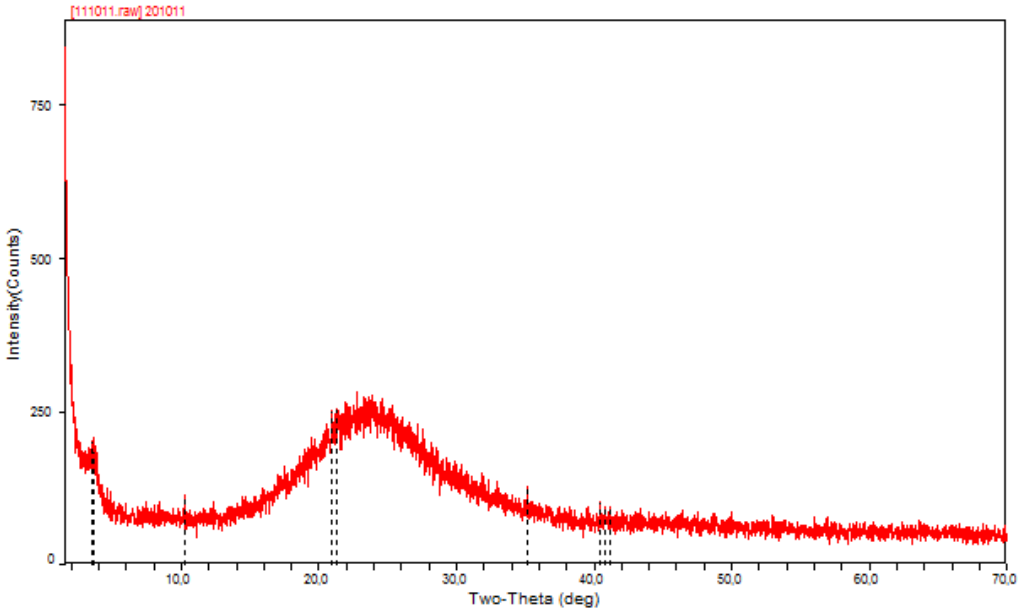


Figure 5.1. XRD analysis of Sample 60.

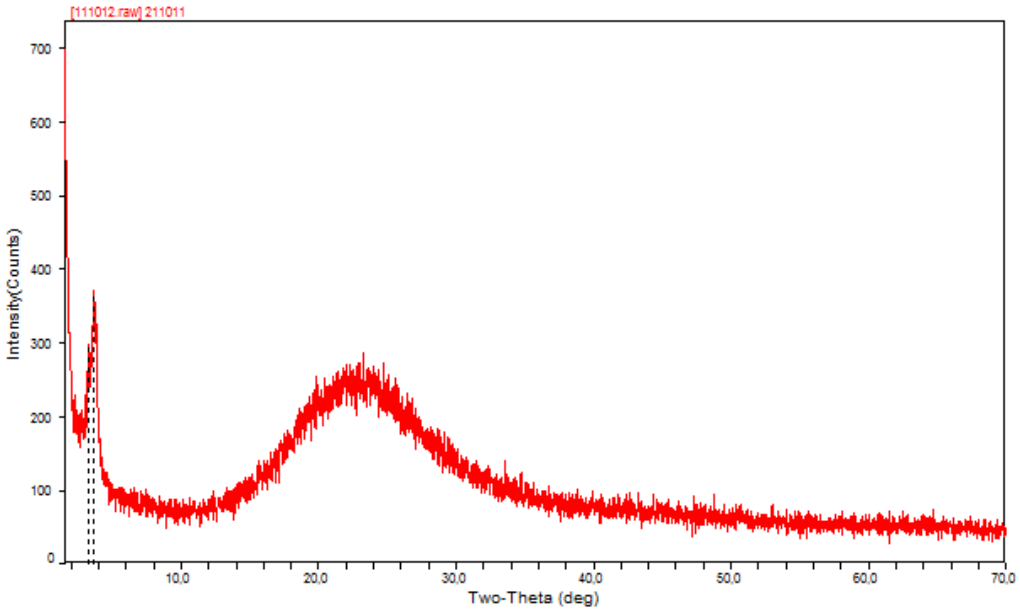


Figure 5.2. XRD analysis of Sample 61.

In XRD experiments, the characteristic broad peak of SiO_2 is expected at 22 degrees [80]. The pure magnetite has a peak with high intensity at around 36.5 degrees [81]. From the Figures 5.1 and 5.2, the peaks become intense between the region of 22-26 degrees. This certainly proves the presence of silica. However, since the silica peak is very broad, it dominates the whole region, so presence of any iron oxide peak is hidden under this peak.

5.4. SEM Analysis

SEM images of dried solid samples were taken. For the images where spherical particle formation could be observed, the particle sizes were measured. Also EDS analysis of some of the samples were carried out.

The magnetite NP synthesis in reverse ME reaction products are listed in Table 5.7 and the related EDS analysis measurements are given in Table 5.8. For some samples, only at one place EDS analysis was done, but for others at two or more places, the analyses were carried out.

In SEM images of samples 41-43 well-defined spherical NP formation cannot be observed. Instead, it looks like there are sphere-like structures covered by a sticky coating, which may suggest that the magnetite NPs are indeed present but the surfactant, AOT, could not be entirely washed off so the exact shapes of NPs could not be seen. This theory is supported by the EDS analysis as well. When we look at the % sulfur amount, it is seen that all four of the samples have values between 5-10; on the other hand it should have been at most a trace amount (<1%) or non-existent, if the samples were cleared off of AOT well.

The suggested high amounts of AOT concentration might be causing sticky interactions between particles, making them coagulate; hence they appear as much larger entities. This might be the case for sample 44 where diameters of some spherical-like particles were measured. However Figure B.4 is not a really good example of a spherical NP sample since there are some rod-like or even clustered structures there. For all we know, the 12-15 nm range might have been measured for entities that were formed as a result of the aggregation of much smaller magnetite NPs.

The samples 43 and 44 have especially higher AOT concentrations, and the sodium ion concentrations are also very high to this respect. In these samples silicon seems to be present too. However TEOS was never used, so there was no source of silicon in reaction mixtures. As an explanation for this contradiction, the following experimental error can be given. The flasks used for silica NP synthesis were always very hard to clean. When the reaction was over and the flask was emptied, there was always a thin layer of silica covering the bottom of the flasks and it was never entirely cleaned. So this residual silica might have been transferred to the reaction mixture, if those flasks were used in these reactions too, hence showing up at the EDS analysis.

Table 5.7. Samples of magnetite in reverse ME reaction products with SEM images.

Sample no	Diameter Range (nm)	SEM image(s)
41		Figure B.1
42		Figure B.2
43		Figure B.3
44	12-16	Figure B.4, Figure B.5

Table 5.8. EDS analysis of samples of magnetite in reverse ME reaction products.

Sample No	% Weight						
	C	O	Na	Si	S	Cl	Fe
41	36.64	19.47	5.22	-	6.86	0.73	31.09
	44.46	23.43	5.41	-	5.50	0.55	19.75
42	31.56	14.33	5.05	-	8.06	1.15	39.78
	51.02	24.56	6.00	-	5.38	0.35	12.65
43	15.38	21.96	18.29	1.26	9.34	-	33.76
44	19.33	20.14	15.87	0.63	8.48	-	35.55

Pre-prepared Si-coating reaction products were visualized with SEM as well. In Table 5.9, it is specified whether the pre-prepared magnetite NPs were suspended in ammonia or AOT/n-heptane, and the type of reaction magnetites were initially synthesized with. The EDS analysis results of these samples are listed in Table 5.10.

First of all, the choice between co-precipitation product magnetite and partial oxidation product magnetite was not difficult to make since most of the partial oxidation product used coating reactions yielded either not very well-defined, spherical-like particles, or no spherical particles at all. An example of the spherical-like sample (Sample 48) image can be found at Appendix B (Figure B9). The experimental trials with partial oxidation products were no longer continued since it was obvious that co-precipitation products have better chance of being coated.

The co-precipitation product used samples yielded NPs within a close range of diameters (17-28 nm), that using whether NH_3 or AOT solution as the suspension phase made no apparent difference.

The Sample 47 was unique of its own way because two different types of particles were observed when Figures B.11, B.13 and B.14 were compared with Figure B.12. We see the particles in Figure B.8b are much larger and they are not exactly spherical unlike the NPs seen in Figures B.11, B.13 and B14. An explanation for this can be provided as the particles in Figure B.12 might be only silica NPs and they do not contain magnetite NPs inside. And the magnetites are still there, uncoated. The silica NPs might have been formed in nanodroplets that were not occupied by magnetite NPs.

The increase of the AOT concentration from 0.1 M to 0.75 M had no effect on the NP size, and it only caused the yield of the reaction to be increased, which was the aim to begin with.

Table 5.9. Samples of pre-prepared Si-coating reaction products with SEM images.

Sample no	[AOT] (M)	Magnetite suspension	Type of reaction that synthesized in	Diameter Range (nm)	SEM image(s)
38	0.1	in NH_3	Co-precipitation	21-28	Figure B.6
40	0.75	in AOT/heptane	Co-precipitation	20-28	Figure B.7, Figure B.8
39	0.75	in NH_3	Co-precipitation	17-26	Figure B.9, Figure B.10
47	0.75	in NH_3	Co-precipitation	20-25	Figure B.11, Figure B.12, Figure B.13 Figure B.14
48	0.75	in NH_3	Partial-oxidation		Figure B.15

Table 5.10. EDS analysis of samples of pre-prepared Si-coating reaction products.

Sample No	% Weight						
	C	O	Na	Si	S	Cl	Fe
40	25.81	33.16	9.15	25.83	5.10	0.00	0.64
	36.38	31.43	8.30	17.75	5.71	0.00	0.28
39	35.27	24.56	6.48	24.57	8.00	0.00	0.73
	31.53	28.61	7.98	24.67	6.26	0.00	0.53
47	34.32	29.45	5.65	21.07	4.66	0.12	4.35
	25.11	22.73	4.81	31.10	4.60	0.70	10.61
	17.03	38.06	5.72	30.03	2.06	0.44	5.93
48	22.58	32.93	6.23	32.83	4.12	0.29	0.22
	28.25	28.63	6.17	30.69	5.78	0.00	0.21

SEM images of samples of “in situ” Si-coating reaction products are listed in Table 5.11 and the related EDS analysis data are given in Table 5.12.

The NP samples synthesized with “in situ” coating method were very different from each other. The visually “better” ones compared to the rest are Samples 56 and 60. What make them “better” than the rest are their well-defined spherical shapes and narrow size distributions. Whether or not there are magnetite NPs within the silica coating is not known at this stage, but for Sample 56, the lack of Fe in EDS analysis (because % weight is <1) indicates that it is only composed of silica NPs. For the rest of the samples, TEM analysis would reveal better explanation regarding presence of Si-coated magnetite NPs.

The samples 56 and 60 are actually quite different from each other; 56 was prepared with 0.75 M of AOT concentration, where 60 was prepared with 1 M. Since 60 is a better candidate for what we have aimed in the project, it can be assumed that an increase in concentration to 1 M yields with “better” NPs with higher amounts.

The samples 53, 54 and 57 are seemed to be covered with AOT, i.e., something sticky that NPs look to be buried in. They should be better washed off of AOT. The samples 12 and 14 are highly polydispersed; they have very wide ranges of diameter. Again an unusual behavior was observed with Sample 54, where it seems to have two different types of particles. One type is spherical and the other one type is randomly shaped which appears as larger. This might indicate that coating was not successful and the silica and magnetite NPs formed separately. However, this theory was contradicted by the fact that “if magnetite NPs were formed without coating of silica, they would not be in the range of 50-110, but they’d be much smaller, like it was observed in magnetite NP synthesis in ME reactions, where NPs were in between 10-20 nm.

Since the EDS results for samples 54 and 57 prove the presence of Fe, the possibility of a successful coating cannot be eliminated for all the samples except 56. Though, it could not be proved in this research whether the coating have actually taken place on “magnetite” NPs.

Table 5.11. Samples of “in situ” Si-coating reaction products with SEM images.

Sample no	[AOT] (M)	Diameter Range (nm)	SEM image(s)
53	0.75		Figure B.16, Figure B.17
54	0.75		Figure B.18, Figure B.19
56	0.75		Figure B.20, Figure B.21
57	0.75		Figure B.22, Figure B.23
58	0.75	50-110	Figure B.24, Figure B.25
59	0.75	44-115	Figure B.26, Figure B.27
60	1.0	40-48	Figure B.28, Figure B.29, Figure B.30, Figure B.31, Figure B.32

Table 5.12. EDS analysis of samples of “in situ” Si-coating reaction products.

Sample No	% Weight						
	C	O	Na	Si	S	Cl	Fe
54	45.22	22.26	4.39	16.38	6.06	0.32	5.37
	47.48	27.39	5.59	12.82	2.00	0.81	3.91
	58.76	17.92	6.22	4.78	6.85	3.53	1.94
	61.79	18.28	5.79	3.90	7.43	1.39	1.41
56	24.61	20.69	6.29	37.81	9.57	0.14	0.90
	55.53	25.10	6.55	7.92	4.76	0.00	0.33
	25.83	26.47	7.62	32.38	7.26	0.09	0.34
57	29.08	28.23	6.82	24.39	4.99	1.73	4.76
	40.98	21.04	5.17	19.90	7.50	0.00	5.41

Some of the samples were treated with Bio-Beads SM-2 Adsorbent and SEM analysis was done on the solid particles afterwards. Table 5.13 lists SEM images and Table 5.14 lists the EDS anaylsis results of Bio-Beads treated samples that were products of different types of reactions.

Table 5.13. Samples of Bio-Beads treated products.

Sample no	**Reaction Type**	**SEM image(s)**
62	Pre-prepared magnetite coating	Figure B.33
63	Magnetite synthesis in ME	Figure B.34, Figure B.35
64	"In situ" coating	Figure B.36

Table 5.14. EDS analysis of samples of Bio-Beads treated products.

Sample No	**% Weight**						
	C	**O**	**Na**	**Si**	**S**	**Cl**	**Fe**
62	52.45	28.03	0.84	17.60	0.55	-	0.53
63	13.90	20.80	2.37	0.94	1.98	-	60.01
64	17.40	25.89	0.79	41.27	0.32	-	14.33

All the samples mentioned in Chapter 5 can be found as listed at Appendix C.

5.5. Occupancy Number

By using the relations 2.3, 2.4, and 2.6-8 the occupancy number of an AOT-stabilized reverse ME system where $[AOT] = 0.75\,M$ and $R = 5$ was calculated. This calculation is applicable for both Si-coated pre-prepared magnetite NPs and "in situ" Si-coated magnetite NPs, because the theoretical amount of Fe_3O_4 formed as a result of the "in situ" reaction was the amount of Fe_3O_4 added into the pre-prepared reaction mixture.

For the surfactant AOT, $\left(\frac{3V_m}{a_0}\right) = 0.175\,nm$ [82] and chain length is equal to $1.5\,nm$ [82]. r_H is calculated to be $2.375\,nm$. a_0, the area of surfactant head group is $0.51\,nm^2$ [83] for AOT. Therefore $C = 5.40\ \times 10^{-3} mol.dm^{-3}$.

Φ_{water} is volume fraction of water and calculated to be $1.11\ \times 10^{-1}$ for a system with V_{water} is equal to $5.53\ \times 10^{-3} L$ and $V_{Total} = 5\ \times 10^{-2} L$. For $[magnetite]_{water} = 7.14 \times 10^{-3}\ mol.dm^{-3}$, $[magnetite]_{ME}$ is found to be $7.90 \times 10^{-4}\ mol.dm^{-3}$.

As a result, for a w/o ME system with the properties mentioned as above, average occupancy number of magnetite in a droplet ($n_{magnetite}$) was calculated to be 0.146. Hence there seems to be less than one NP per droplet (from every ten droplets approximately one was occupied). For better results this number has to be increased. It is also possible that, the rest of the droplets which are unoccupied could be have been occupied by silica NPs when TEOS is introduced into the system. It further supports the theory of two types (both magnetite and silica) of NPs are present in the end.

6. CONCLUSIONS

(i) The aim of the project was to prepare Si-coated magnetite NPs. In order to carry out the coating under controlled environment, the reaction medium was chosen to be the aqueous dispersed phase of a w/o ME.

(ii) Initially, coating of the NPs was tried by inserting the pre-prepared magnetite NPs into the nanodroplets and then adding a precursor to initiate a reaction to coat them with SiO_2. Results have shown that this reaction does not proceed as expected, i.e., instead of the coating, inside the empty nanodroplets, silica NPs form.

(iii) Another trial for Si-coating was carried out as "in situ". In this one-pot reaction, first the magnetite NPs were formed inside the dispersed phase, and then these NPs were coated with SiO_2 upon the addition of silica reaction precursor into the same medium.

(iv) Magnetite NP synthesis within the nanodroplets of w/o ME was carried out. The reaction yielded much smaller (10-20 nm) NPs compared to the Si-coated ones (20-115 nm). The aim here was to compare the size of the NPs with Si-coated magnetite NP samples.

(v) The effects of changing the composition of the AOT-stabilized reverse MEs on the formation of silica NPs were studied. Increasing the R value of the ME yielded increased nanodroplet size, resulting in increased NP size. Also two different oil phases were tried, among them n-heptane was proved to be more suitable to our aim than n-decane, since the MEs having n-heptane yielded much smaller particles. These preliminary silica NP reactions were as guidance to the magnetite coating reactions where they were all carried out at $R = 5$ (the smallest R value possible for the given system), and with n-heptane as the oil.

7. SUGGESTIONS FOR FUTURE WORK

(i) The Bio-Beads treatment of the NPs, in order to remove the traces of the surfactant left around them, needs to be developed. First the best procedure to use this adsorbent should be determined, then the SEM and EDS analyses should be carried out on the samples of "before" and "after" Bio-Beads treatment and the results should be compared accordingly.

(ii) It was mentioned that occupancy number needs to be increased so that, most of the nanodroplets within the ME are occupied. This can be done by using more magnetite NPs in the pre-prepared reaction. However, it is not possible to suspend that much amount of magnetite NP in the aqueous phase. Simply using more water is not the solution, because it restricts the growth of the coating layer of NPs. Therefore, another method should be searched to use pre-prepared magnetite NPs.

(iii) Though in "in situ" reaction, the amounts of solid salts of irons can be increased without any change in water or AOT amount, and this would increase the occupancy number in the same ratio.

(iv) The NPs were dried in oven exposed to the air. Due to agglomeration problems, the drying should be carried out in a vacuum oven.

(v) TEM analyses of the better samples of "in situ" coating reactions should be done to confirm that there are really magnetite NPs within the silica shell. Also, the number of magnetite NPs residing within the silica shell should be known.

(vi) If the samples could be obtained with higher yields, it would allow having their XRD measurements to be done. This would give a better idea on the iron oxide NP content.

(vii) The types of reactions carried out in this research should be tried again by using another surfactant. A nonionic surfactant can be used instead of the anionic AOT. According to Santra *et al.* [43], Brij-97 as a surfactant yields the smallest Si-coated magnetite NPs that are aggregated in the most orderly fashion, whereas Igepal® CO-520 used particles are less agglomerated but form tubelike structures.

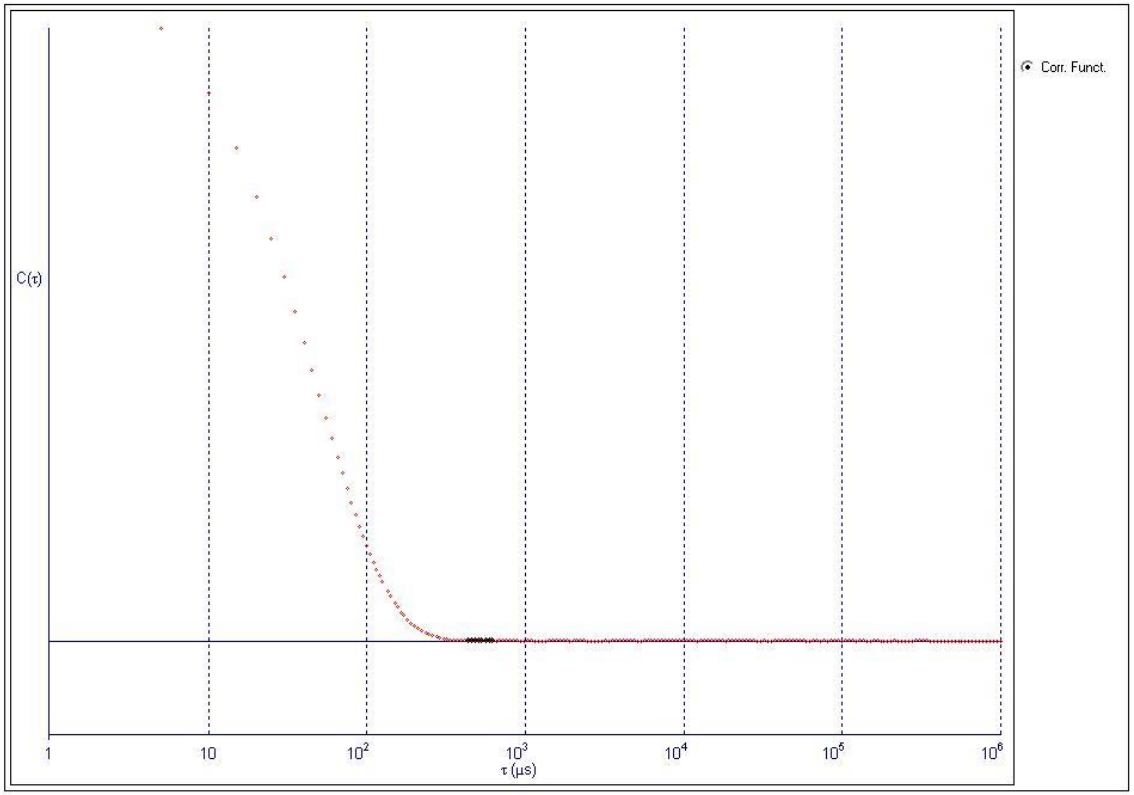
(viii) The fact that the aqueous iron salt solution used in the "in situ" systems was not deaired at the beginning, oxidation of the Fe^{2+} might have occurred, hence not resulting in the magnetite NPs desired. This can be avoided by using smaller flasks so that the complete deairation of the iron salt solution can be successfully done.

APPENDIX A: DLS ANALYSIS RESULTS

The following pages (68-108) show DLS analysis results of the samples mentioned in Section 5.2.

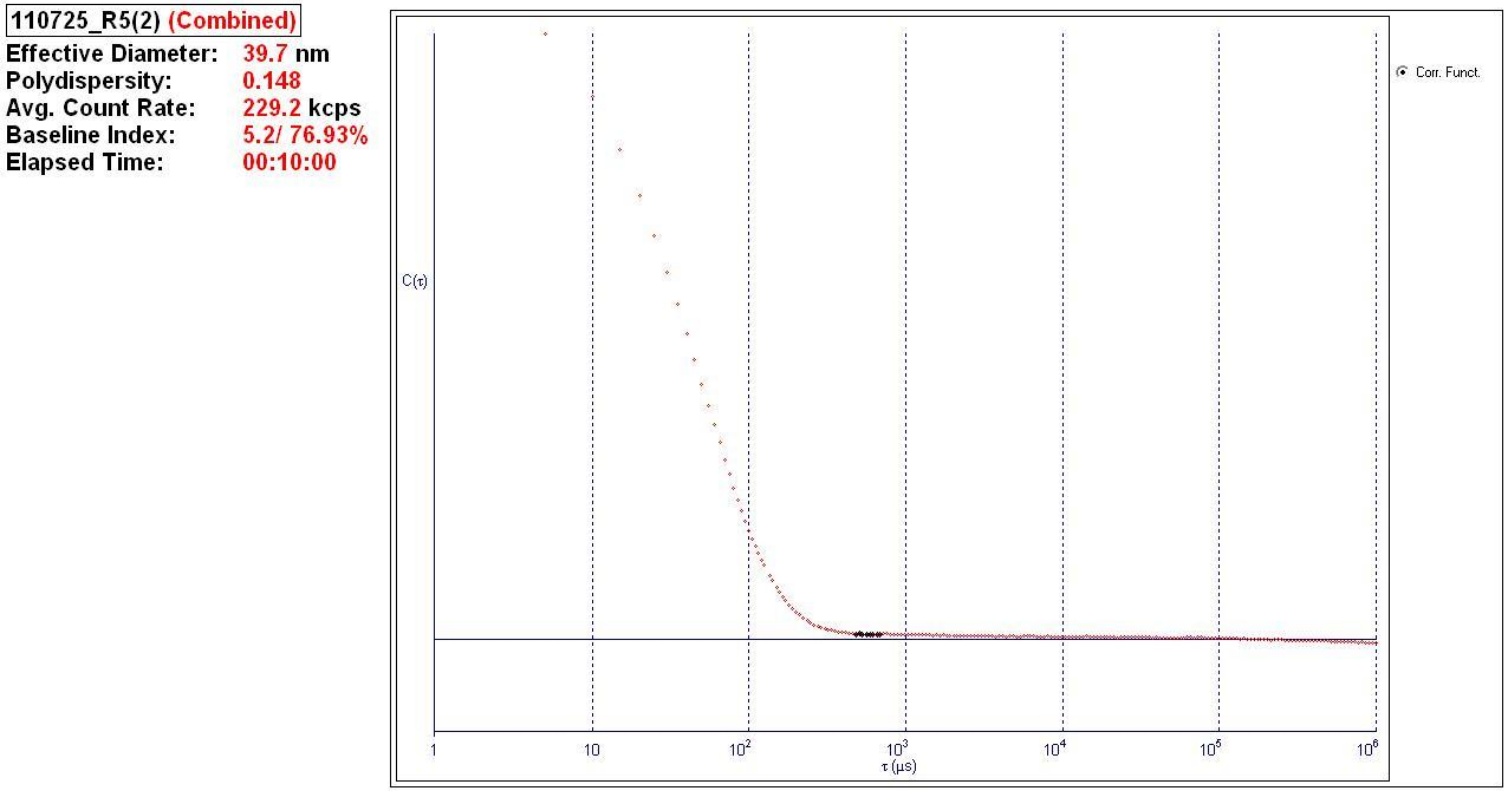
110725_R5(1) (Combined)

Effective Diameter:	**38.7 nm**
Polydispersity:	**0.070**
Avg. Count Rate:	**405.6 kcps**
Baseline Index:	**9.7/ 91.45%**
Elapsed Time:	**00:10:00**



Run	Eff. Diam. (nm)	Half Width (nm)	Polydispersity	Baseline Index
1	38.5	10.4	0.073	9.9/ 73.89%
2	38.1	10.5	0.076	9.1/100.00%
3	38.5	10.7	0.078	9.7/ 80.44%
4	38.9	9.2	0.056	8.5/ 95.58%
5	38.5	10.0	0.067	8.5/ 95.56%
6	38.9	11.9	0.094	9.5/ 86.73%
7	38.5	9.7	0.064	8.0/ 91.15%
8	38.7	7.5	0.038	9.7/100.00%
9	39.2	12.8	0.107	9.1/100.00%
10	38.7	10.2	0.069	9.9/ 91.15%
Mean	38.7	10.3	0.072	9.2/ 91.45%
Std. Error	0.1	0.5	0.006	0.2/ 2.80
Combined	38.7	10.3	0.070	9.7/ 91.45%

Figure A.1. DLS analysis of Sample 3.

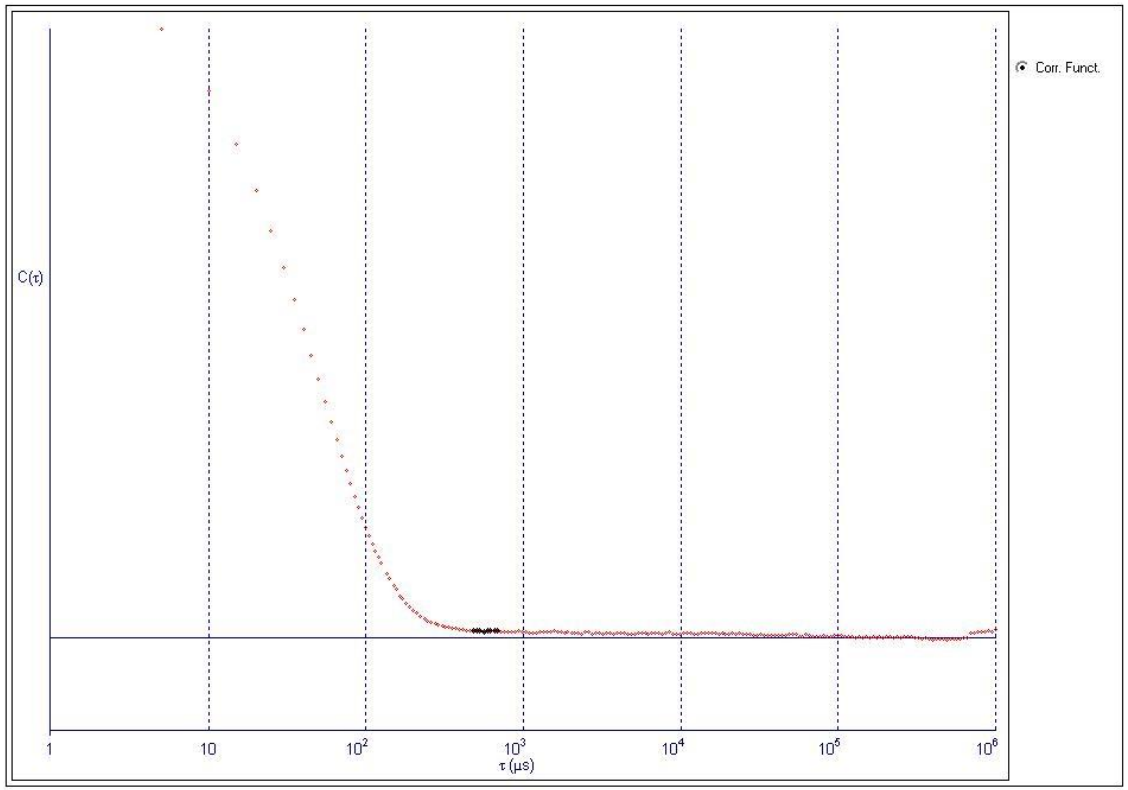


Run	Eff. Diam. (nm)	Half Width (nm)	Polydispersity	Baseline Index
1	40.0	15.1	0.142	3.6/ 76.00%
2	39.5	16.3	0.171	7.5/ 72.89%
3	39.1	15.2	0.150	7.0/ 64.89%
4	39.3	15.0	0.146	5.7/ 87.05%
5	39.6	14.8	0.139	6.4/ 80.00%
6	39.0	13.7	0.123	5.6/ 88.89%
7	39.8	16.9	0.180	3.0/ 57.78%
8	39.2	14.5	0.137	7.1/ 98.67%
9	42.1	17.6	0.176	0.0/ 52.00%
10	39.4	15.4	0.154	8.2/ 91.11%
Mean	39.7	15.4	0.152	5.4/ 76.93%
Std. Error	0.3	0.4	0.006	0.8/ 4.81
Combined	39.7	15.3	0.148	5.2/ 76.93%

Figure A.2. DLS analysis of Sample 4.

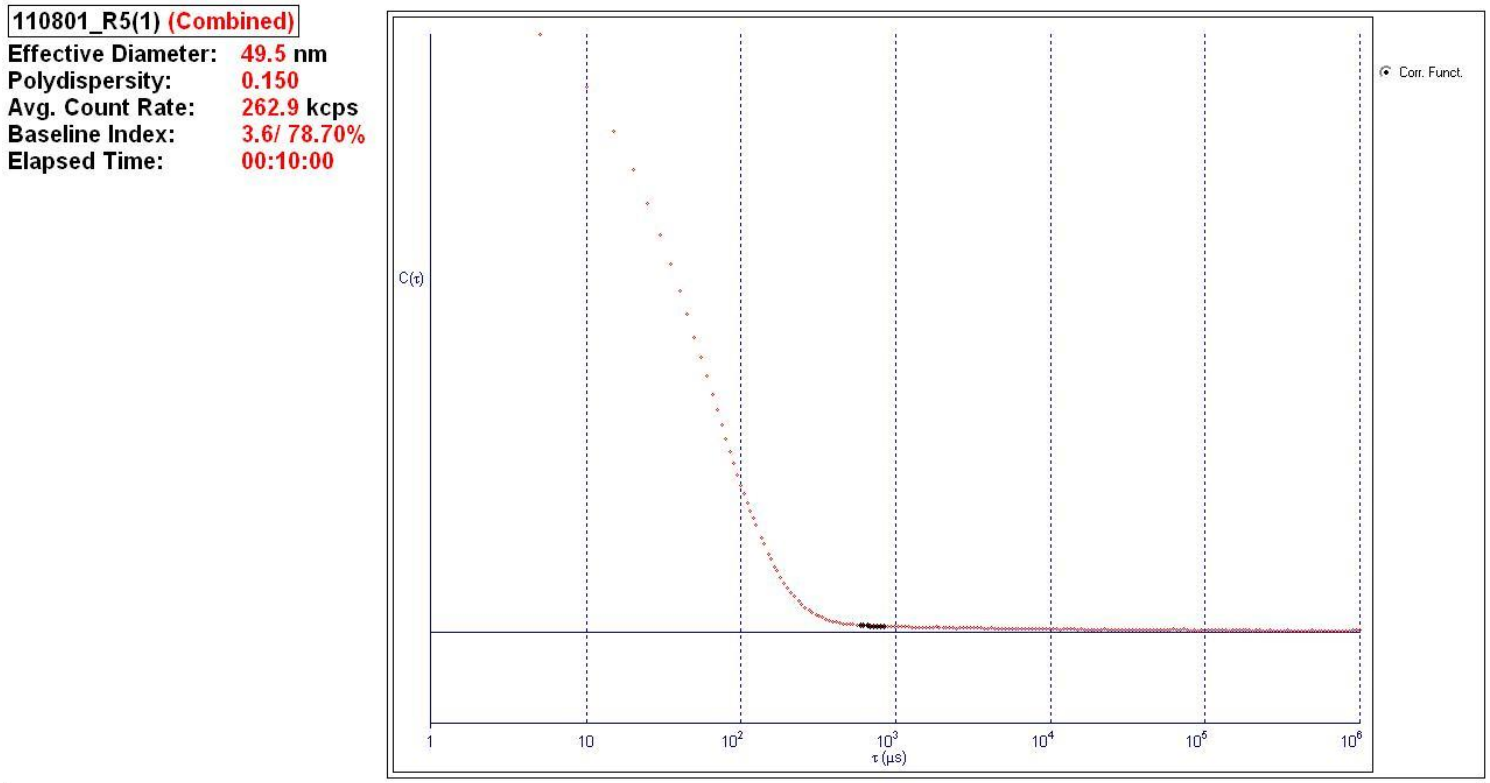
110725_R5(3) (Combined)

Effective Diameter: 39.9 nm
Polydispersity: 0.129
Avg. Count Rate: 713.5 kcps
Baseline Index: 4.9/ 31.28%
Elapsed Time: 00:10:00



Run	Eff. Diam. (nm)	Half Width (nm)	Polydispersity	Baseline Index
1	40.1	12.8	0.101	1.0/ 7.49%
2	40.5	17.8	0.194	2.7/ 25.55%
3	39.6	15.5	0.153	8.6/ 22.03%
4	39.1	13.2	0.114	6.8/ 29.07%
5	38.7	14.5	0.140	7.3/ 34.36%
6	40.6	16.2	0.159	4.7/ 31.28%
7	42.0	3.0	0.005	0.0/ 14.10%
8	39.0	12.4	0.102	9.9/ 60.79%
9	41.9	16.7	0.158	1.7/ 38.33%
10	38.7	14.1	0.132	5.0/ 49.78%
Mean	40.0	13.6	0.126	4.8/ 31.28%
Std. Error	0.4	1.3	0.016	1.1/ 5.01
Combined	39.9	14.4	0.129	4.9/ 31.28%

Figure A.3. DLS analysis of Sample 5.

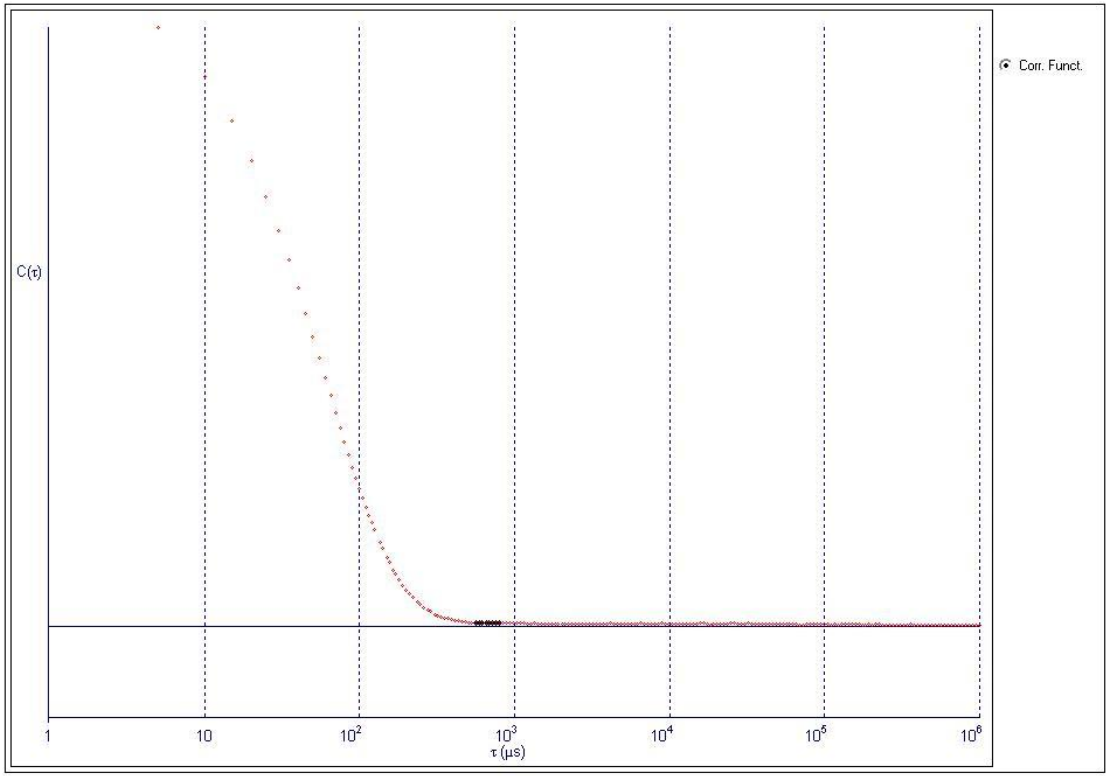


Run	Eff. Diam. (nm)	Half Width (nm)	Polydispersity	Baseline Index
1	49.8	19.2	0.149	1.2/ 68.44%
2	49.2	19.9	0.163	6.0/ 33.78%
3	49.2	20.6	0.175	4.4/ 76.99%
4	49.2	18.5	0.141	3.0/ 86.67%
5	49.9	18.2	0.132	4.9/ 91.56%
6	49.4	19.4	0.154	5.1/ 86.22%
7	49.2	19.2	0.152	7.3/ 82.67%
8	48.4	18.2	0.141	7.5/100.00%
9	50.7	20.2	0.159	1.2/ 91.56%
10	49.1	19.9	0.164	2.7/ 69.03%
Mean	49.4	19.3	0.153	4.3/ 78.69%
Std. Error	0.2	0.3	0.004	0.7/ 5.91
Combined	49.5	19.2	0.150	3.6/ 78.70%

Figure A.4. DLS analysis of Sample 6.

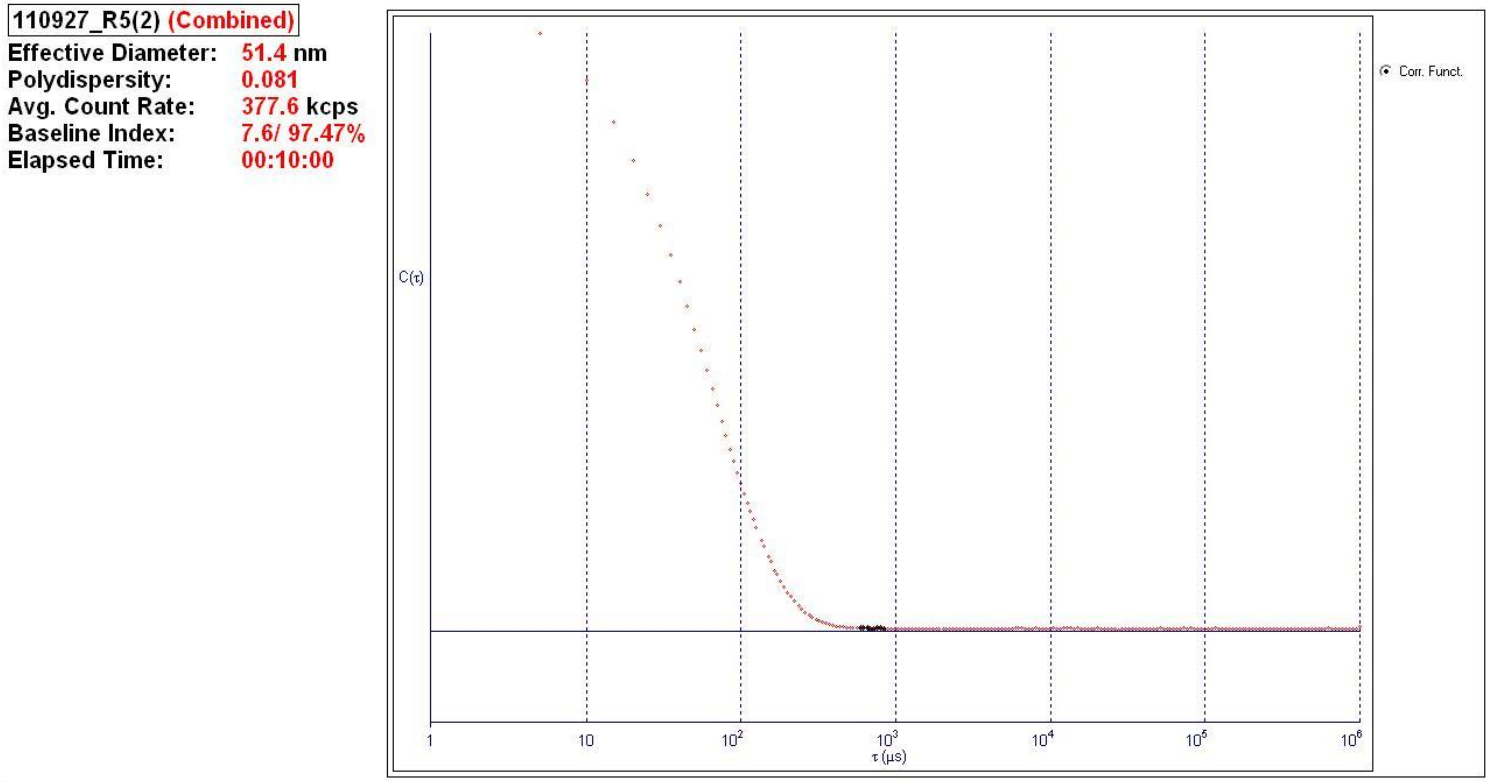
110927_R5(1) (Combined)

Effective Diameter: 47.6 nm
Polydispersity: 0.124
Avg. Count Rate: 373.5 kcps
Baseline Index: 7.0/ 87.61%
Elapsed Time: 00:10:00



Run	Eff. Diam. (nm)	Half Width (nm)	Polydispersity	Baseline Index
1	47.6	17.2	0.131	6.4/ 54.22%
2	48.4	14.9	0.095	6.5/ 77.33%
3	48.3	16.6	0.118	5.8/ 95.56%
4	47.4	18.9	0.160	8.7/ 91.11%
5	47.2	18.2	0.148	9.6/ 95.56%
6	47.4	16.1	0.115	7.5/ 93.33%
7	46.9	17.7	0.143	10.0/ 83.11%
8	47.5	16.6	0.123	7.9/ 95.56%
9	48.1	16.0	0.110	7.5/ 90.27%
10	47.6	15.7	0.108	8.1/100.00%
Mean	47.6	16.8	0.125	7.8/ 87.60%
Std. Error	0.2	0.4	0.006	0.4/ 4.26
Combined	47.6	16.8	0.124	7.0/ 87.61%

Figure A.5. DLS analysis of Sample 8.

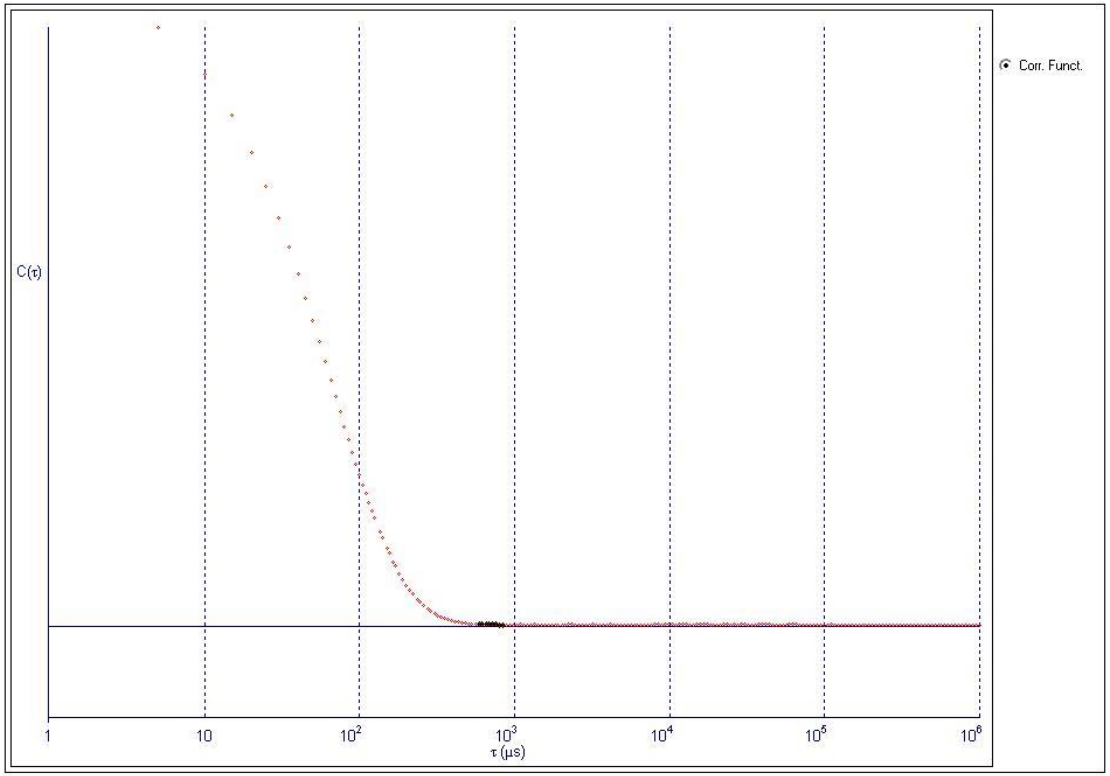


Run	Eff. Diam. (nm)	Half Width (nm)	Polydispersity	Baseline Index
1	52.1	17.1	0.107	9.9/ 92.04%
2	51.7	14.0	0.074	9.2/100.00%
3	51.6	13.8	0.072	9.1/100.00%
4	50.8	16.4	0.104	9.4/ 91.15%
5	51.6	13.0	0.064	8.9/100.00%
6	50.9	13.4	0.069	9.0/ 96.00%
7	51.0	15.1	0.087	9.8/100.00%
8	50.4	17.7	0.123	9.7/ 95.56%
9	51.6	13.8	0.071	9.8/100.00%
10	50.8	12.9	0.064	9.2/100.00%
Mean	51.3	14.7	0.084	9.4/ 97.47%
Std. Error	0.2	0.6	0.007	0.1/ 1.12
Combined	51.4	14.6	0.081	7.6/ 97.47%

Figure A.6. DLS analysis of Sample 9.

110927_R5(3) (Combined)

Effective Diameter: 52.1 nm
Polydispersity: 0.105
Avg. Count Rate: 426.0 kcps
Baseline Index: 8.3/ 96.90%
Elapsed Time: 00:10:00



Run	Eff. Diam. (nm)	Half Width (nm)	Polydispersity	Baseline Index
1	53.8	17.2	0.102	8.0/ 99.12%
2	52.2	17.5	0.112	8.8/ 91.15%
3	51.5	18.5	0.130	9.7/100.00%
4	51.9	17.6	0.115	9.7/100.00%
5	52.1	17.2	0.109	7.7/ 87.17%
6	51.5	16.9	0.107	9.6/100.00%
7	52.0	16.1	0.096	9.8/100.00%
8	51.7	17.8	0.119	9.1/100.00%
9	52.0	16.5	0.101	9.7/ 95.58%
10	52.0	15.6	0.090	8.4/ 96.02%
Mean	52.1	17.1	0.108	9.1/ 96.90%
Std. Error	0.2	0.3	0.004	0.2/ 1.43
Combined	52.1	16.9	0.105	8.3/ 96.90%

Figure A.7. DLS analysis of Sample 10.

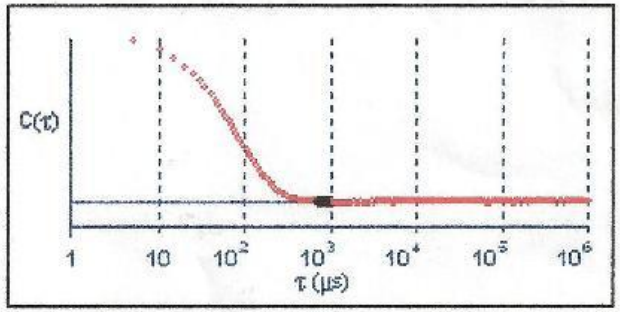
110504-R7.5 (Combined)

Effective Diameter: 81.9 nm

Polydispersity: 0.073

Baseline Index: 9.3/ 96.50%

Elapsed Time: 00:10:00



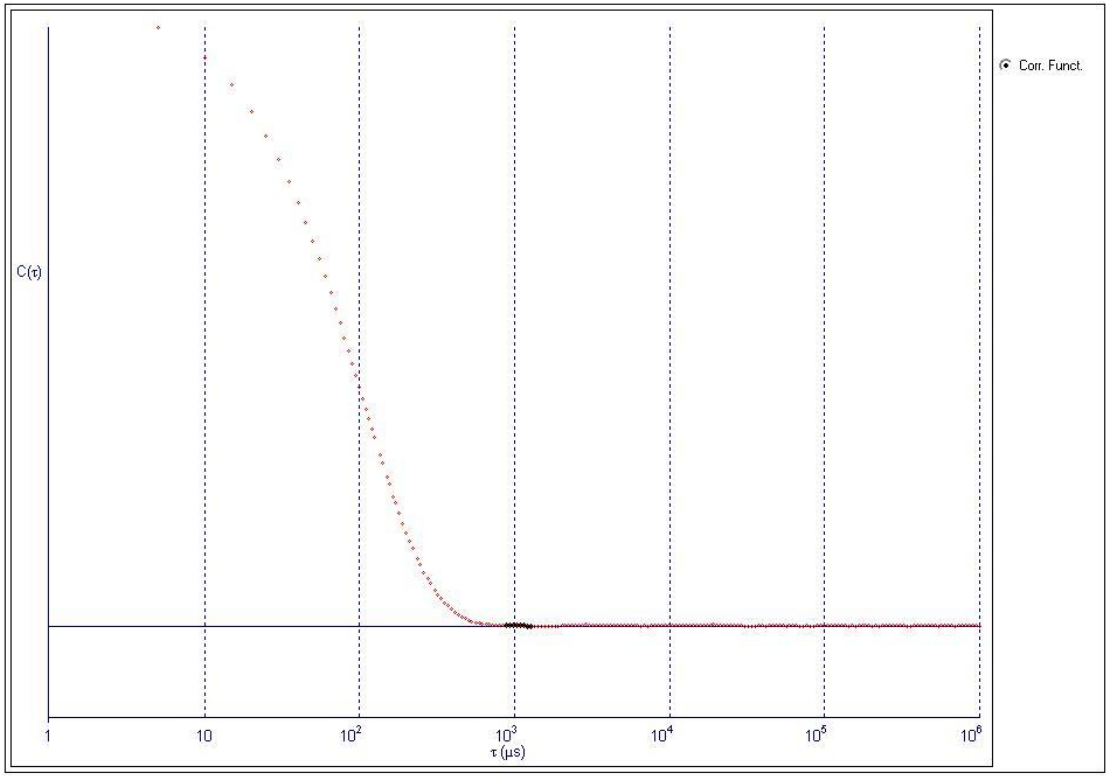
Correlation Function

Run	Eff. Diam. (nm)	Half Width (nm)	Polydispersity	Baseline Index
1	86.8	14.9	0.030	9.2/100.00%
2	82.2	29.9	0.132	6.6/ 88.94%
3	80.9	25.0	0.095	8.3/100.00%
4	82.3	20.9	0.064	8.6/ 84.89%
5	80.8	24.3	0.090	8.9/100.00%
6	80.7	23.9	0.087	9.4/ 95.58%
7	81.7	21.3	0.068	9.1/ 95.58%
8	81.8	18.4	0.051	9.0/100.00%
9	81.0	22.7	0.079	9.2/100.00%
10	80.6	20.9	0.068	9.6/100.00%
Mean	81.9	22.2	0.076	8.8/ 96.50%
Std. Error	0.6	1.3	0.009	0.3/ 1.72
Combined	81.9	22.2	0.073	9.3/ 96.50%

Figure A.8. DLS analysis of Sample 16.

110704_R7.5 (Combined)

Effective Diameter:	**75.1 nm**
Polydispersity:	**0.048**
Avg. Count Rate:	**313.5 kcps**
Baseline Index:	**9.5/ 97.68%**
Elapsed Time:	**00:10:00**

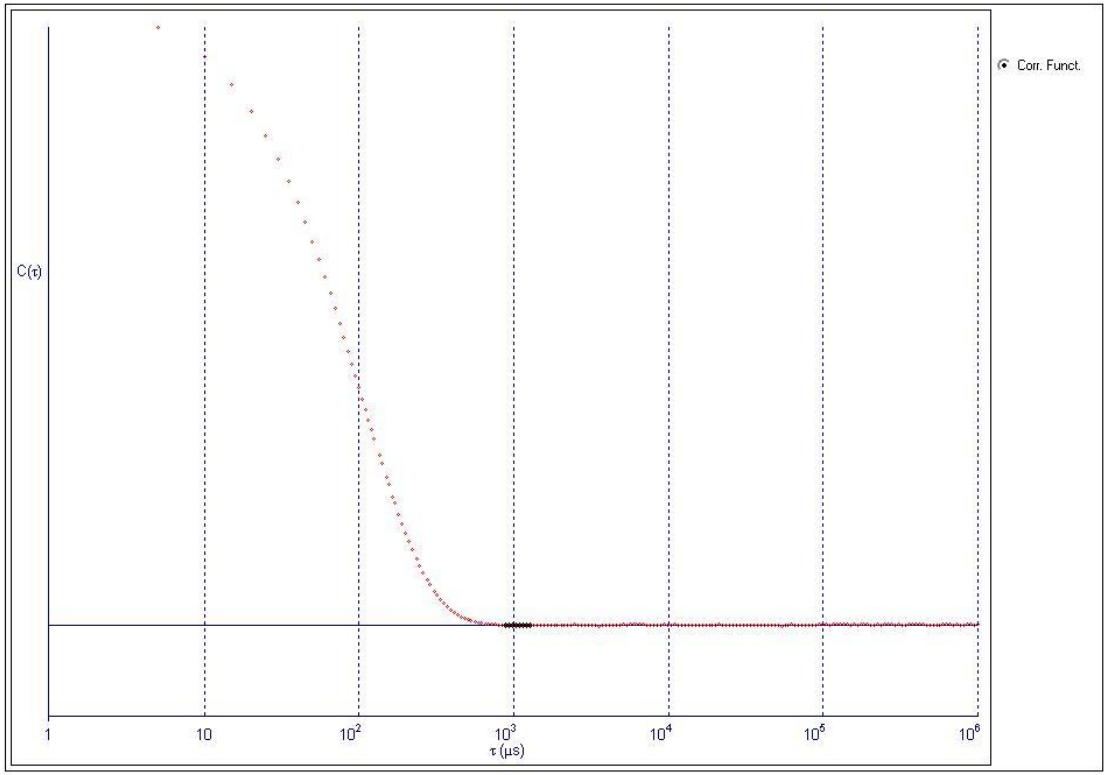


Run	Eff. Diam. (nm)	Half Width (nm)	Polydispersity	Baseline Index
1	73.8	20.5	0.077	9.1/ 95.54%
2	75.0	16.3	0.047	9.1/100.00%
3	76.1	18.2	0.057	9.7/ 95.54%
4	73.6	18.9	0.066	8.7/ 95.54%
5	76.0	15.9	0.044	9.5/ 90.22%
6	75.1	19.3	0.066	9.7/100.00%
7	74.7	10.7	0.020	7.9/100.00%
8	76.1	15.1	0.039	9.1/100.00%
9	74.9	17.7	0.056	9.4/100.00%
10	74.6	15.7	0.044	9.1/100.00%
Mean	75.0	16.8	0.052	9.1/ 97.68%
Std. Error	0.3	0.9	0.005	0.2/ 1.06
Combined	75.1	16.5	0.048	9.5/ 97.68%

Figure A.9. DLS analysis of Sample 18.

110823_R7.5 (Combined)

Effective Diameter: 80.4 nm
Polydispersity: 0.038
Avg. Count Rate: 354.5 kcps
Baseline Index: 9.4/ 98.27%
Elapsed Time: 00:10:00

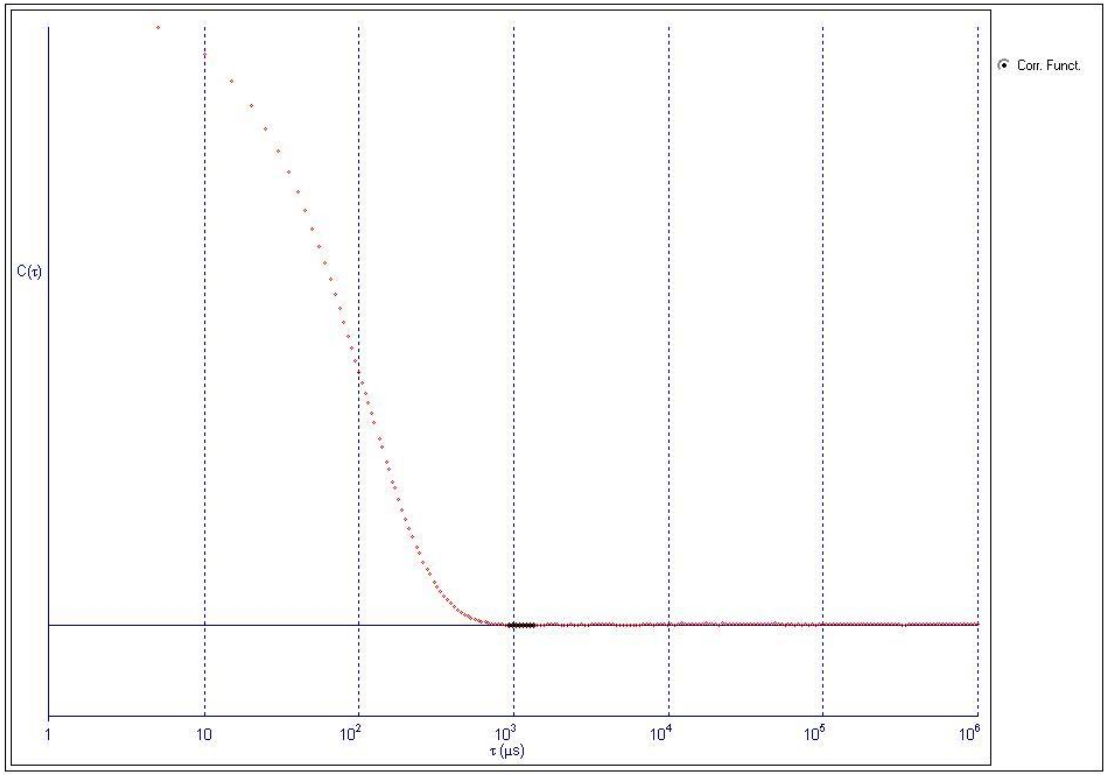


Run	Eff. Diam. (nm)	Half Width (nm)	Polydispersity	Baseline Index
1	79.7	25.1	0.099	8.1/ 95.56%
2	80.2	17.5	0.047	9.5/ 91.56%
3	79.9	10.0	0.016	9.1/ 95.56%
4	80.3	18.4	0.052	7.3/100.00%
5	79.6	12.4	0.024	9.1/100.00%
6	79.6	19.1	0.057	7.6/100.00%
7	81.7	5.8	0.005	9.8/100.00%
8	80.9	15.7	0.038	9.4/100.00%
9	80.8	12.4	0.024	8.9/100.00%
10	79.8	21.2	0.071	8.9/100.00%
Mean	80.2	15.7	0.043	8.7/ 98.27%
Std. Error	0.2	1.8	0.009	0.3/ 0.95
Combined	80.4	15.6	0.038	9.4/ 98.27%

Figure A.10. DLS analysis of Sample 19.

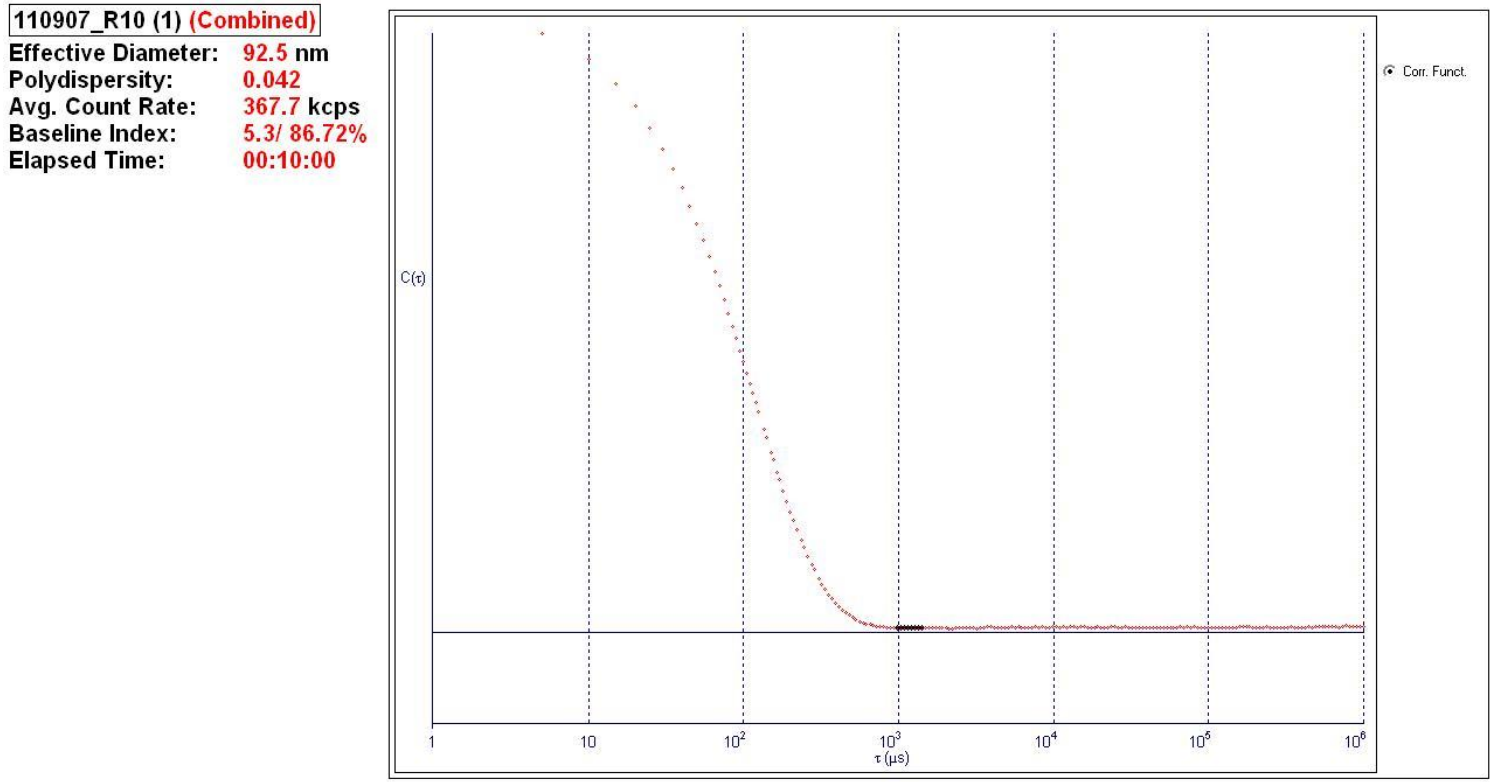
110823_R7.5(2) (Combined)

Effective Diameter: 85.9 nm
Polydispersity: 0.066
Avg. Count Rate: 427.3 kcps
Baseline Index: 9.4/ 97.26%
Elapsed Time: 00:10:00



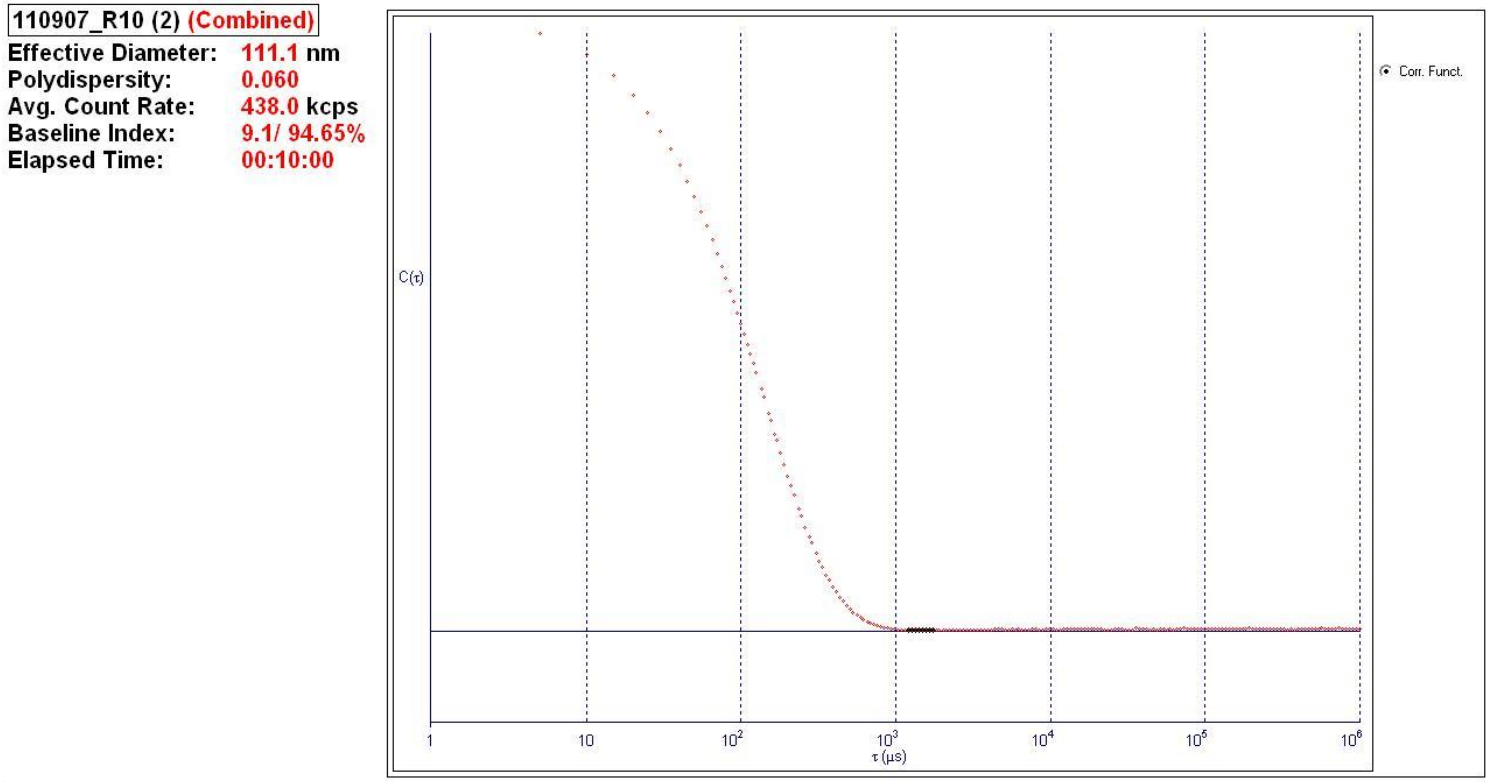
Run	Eff. Diam. (nm)	Half Width (nm)	Polydispersity	Baseline Index
1	88.5	18.8	0.045	8.8/100.00%
2	87.0	19.5	0.050	9.3/100.00%
3	85.8	28.0	0.106	8.1/100.00%
4	85.2	25.6	0.090	10.0/ 95.58%
5	85.6	22.9	0.071	8.9/ 95.58%
6	86.2	20.4	0.056	8.7/ 95.58%
7	84.0	24.1	0.082	9.8/100.00%
8	84.9	23.4	0.076	8.2/100.00%
9	85.6	16.6	0.038	8.7/100.00%
10	85.4	21.6	0.064	9.0/ 85.84%
Mean	85.8	22.1	0.068	9.0/ 97.26%
Std. Error	0.4	1.1	0.007	0.2/ 1.43
Combined	85.9	22.0	0.066	9.4/ 97.26%

Figure A.11. DLS analysis of Sample 20.



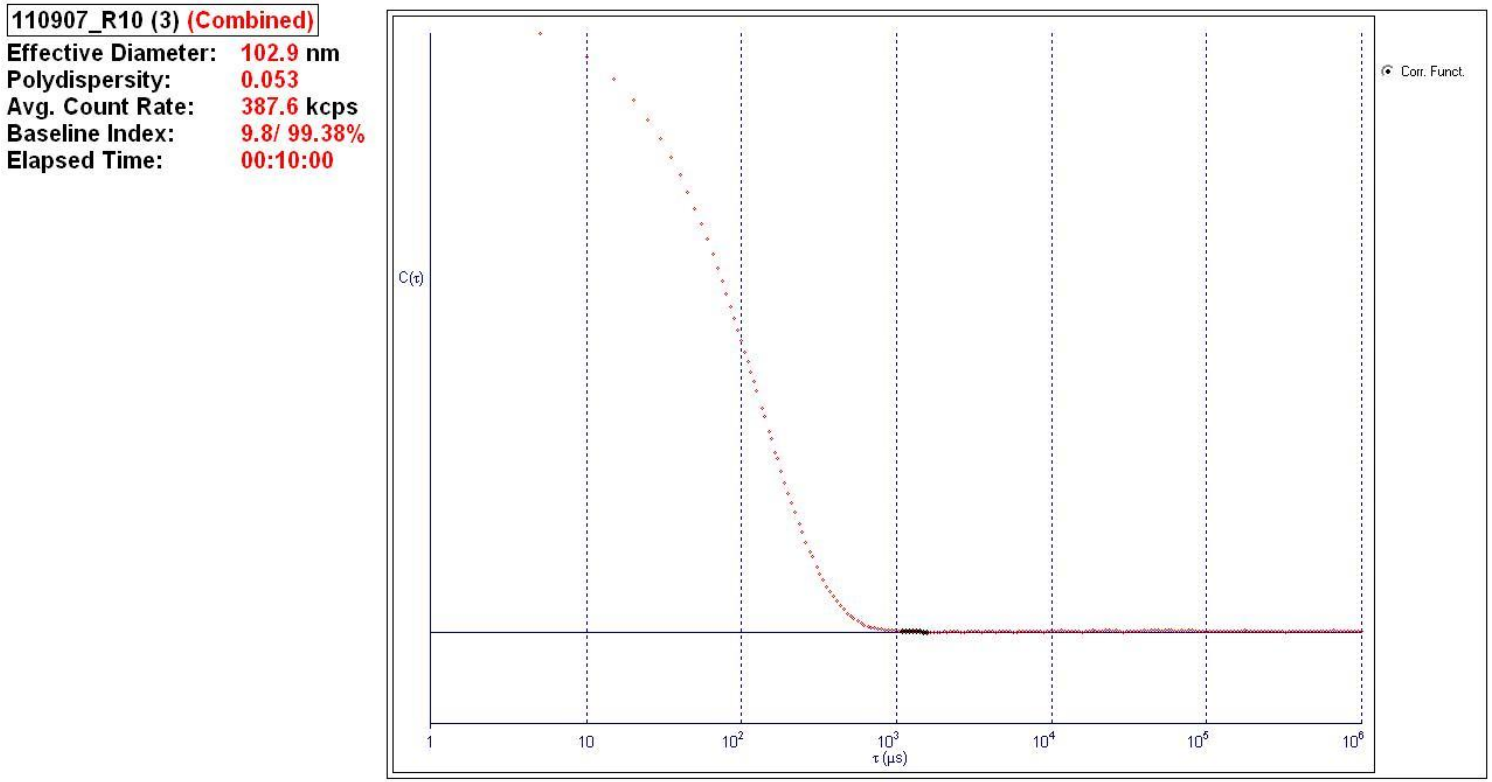
Run	Eff. Diam. (nm)	Half Width (nm)	Polydispersity	Baseline Index
1	92.8	15.5	0.028	9.7/ 95.58%
2	93.9	17.2	0.034	9.3/ 94.22%
3	93.1	24.1	0.067	10.0/100.00%
4	92.8	18.3	0.039	6.0/ 90.67%
5	92.7	15.8	0.029	9.8/ 69.64%
6	92.4	21.7	0.055	9.9/ 67.56%
7	92.1	18.4	0.040	9.1/ 77.78%
8	92.2	22.3	0.059	9.7/ 95.56%
9	91.0	25.4	0.078	7.5/ 93.36%
10	91.9	6.5	0.005	8.6/ 82.74%
Mean	92.5	18.5	0.043	9.0/ 86.71%
Std. Error	0.2	1.7	0.007	0.4/ 3.66
Combined	92.5	18.9	0.042	5.3/ 86.72%

Figure A.12. DLS analysis of Sample 22.



Run	Eff. Diam. (nm)	Half Width (nm)	Polydispersity	Baseline Index
1	112.4	25.3	0.051	7.6/100.00%
2	112.4	23.2	0.043	9.2/ 85.84%
3	110.4	26.9	0.060	9.9/ 91.15%
4	111.0	26.8	0.058	9.7/ 91.15%
5	110.4	32.1	0.084	9.1/ 95.58%
6	112.5	23.8	0.045	8.7/ 95.58%
7	109.9	35.5	0.105	7.3/100.00%
8	111.5	24.2	0.047	9.4/ 91.59%
9	109.7	26.3	0.058	9.7/100.00%
10	110.7	28.2	0.065	8.0/ 95.58%
Mean	111.1	27.2	0.061	8.9/ 94.65%
Std. Error	0.3	1.2	0.006	0.3/ 1.49
Combined	111.1	27.2	0.060	9.1/ 94.65%

Figure A.13. DLS analysis of Sample 23.

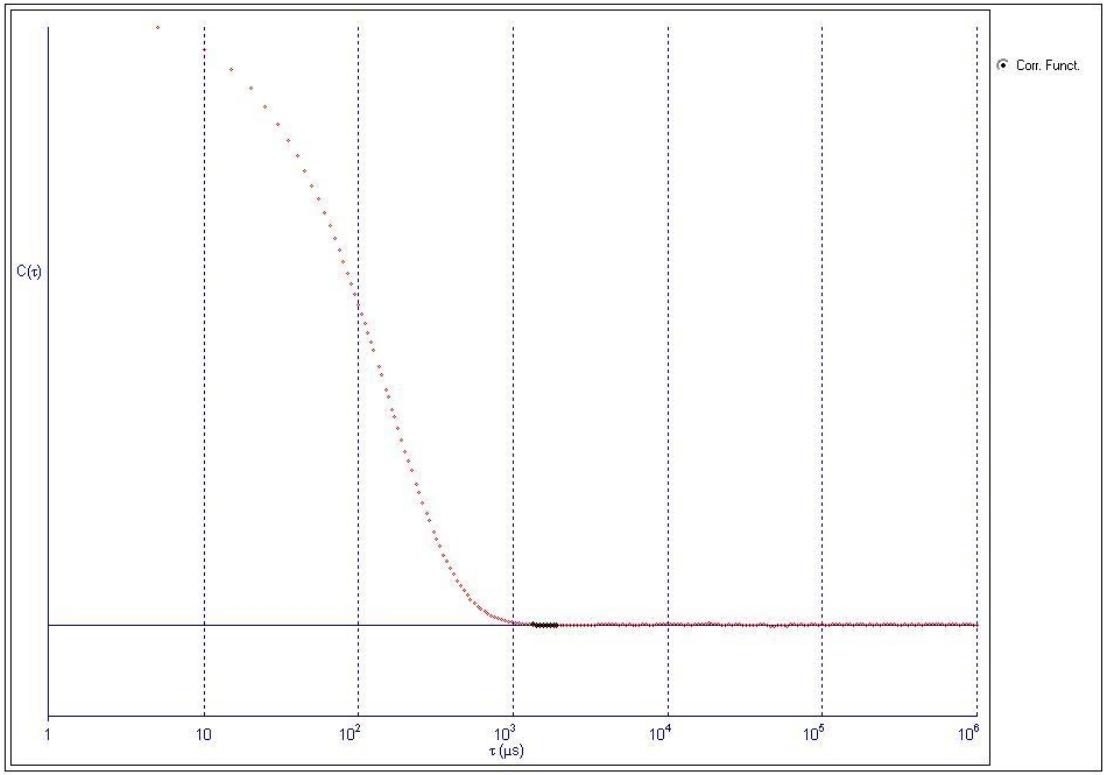


Run	Eff. Diam. (nm)	Half Width (nm)	Polydispersity	Baseline Index
1	102.8	25.5	0.062	9.8/ 93.81%
2	102.3	26.2	0.066	9.3/100.00%
3	104.3	17.5	0.028	8.8/100.00%
4	102.6	24.2	0.056	9.2/100.00%
5	100.7	30.9	0.094	8.1/100.00%
6	103.5	19.5	0.036	8.4/100.00%
7	102.9	25.9	0.063	9.3/100.00%
8	102.9	19.4	0.035	9.2/100.00%
9	101.8	31.3	0.094	6.1/100.00%
10	102.8	24.3	0.056	8.0/100.00%
Mean	102.7	24.5	0.059	8.6/ 99.38%
Std. Error	0.3	1.5	0.007	0.3/ 0.62
Combined	102.9	23.7	0.053	9.8/ 99.38%

Figure A.14. DLS analysis of Sample 24.

110516_R5d (Combined)

Effective Diameter: 120.3 nm
Polydispersity: 0.116
Avg. Count Rate: 343.5 kcps
Baseline Index: 9.5/ 99.60%
Elapsed Time: 00:10:00

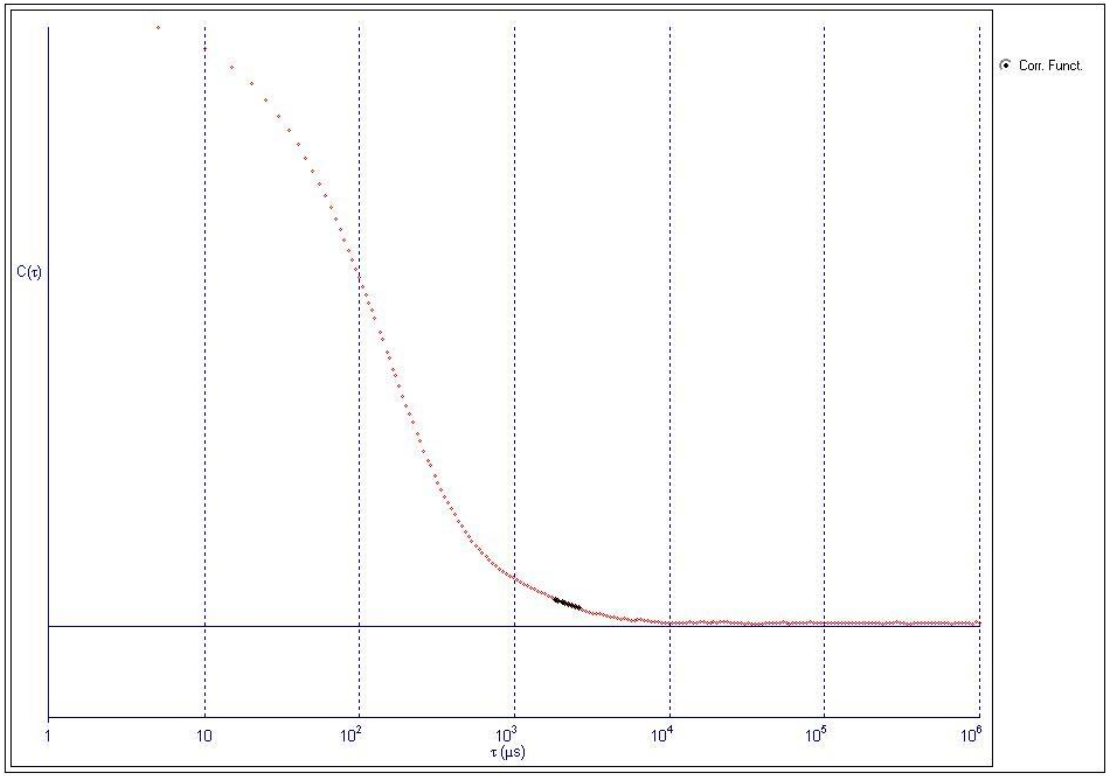


Run	Eff. Diam. (nm)	Half Width (nm)	Polydispersity	Baseline Index
1	120.5	40.1	0.111	9.6/100.00%
2	119.4	36.4	0.093	10.0/100.00%
3	121.2	42.3	0.122	8.0/ 96.00%
4	120.5	42.2	0.122	9.9/100.00%
5	121.0	41.1	0.115	8.5/100.00%
6	117.3	44.2	0.142	8.2/100.00%
7	119.5	42.2	0.124	9.4/100.00%
8	119.2	46.4	0.152	8.1/100.00%
9	121.4	35.9	0.087	9.3/100.00%
10	121.9	39.6	0.106	9.5/100.00%
Mean	120.2	41.0	0.117	9.1/ 99.60%
Std. Error	0.4	1.0	0.006	0.2/ 0.40
Combined	120.3	40.9	0.116	9.5/ 99.60%

Figure A.15. DLS analysis of Sample 25.

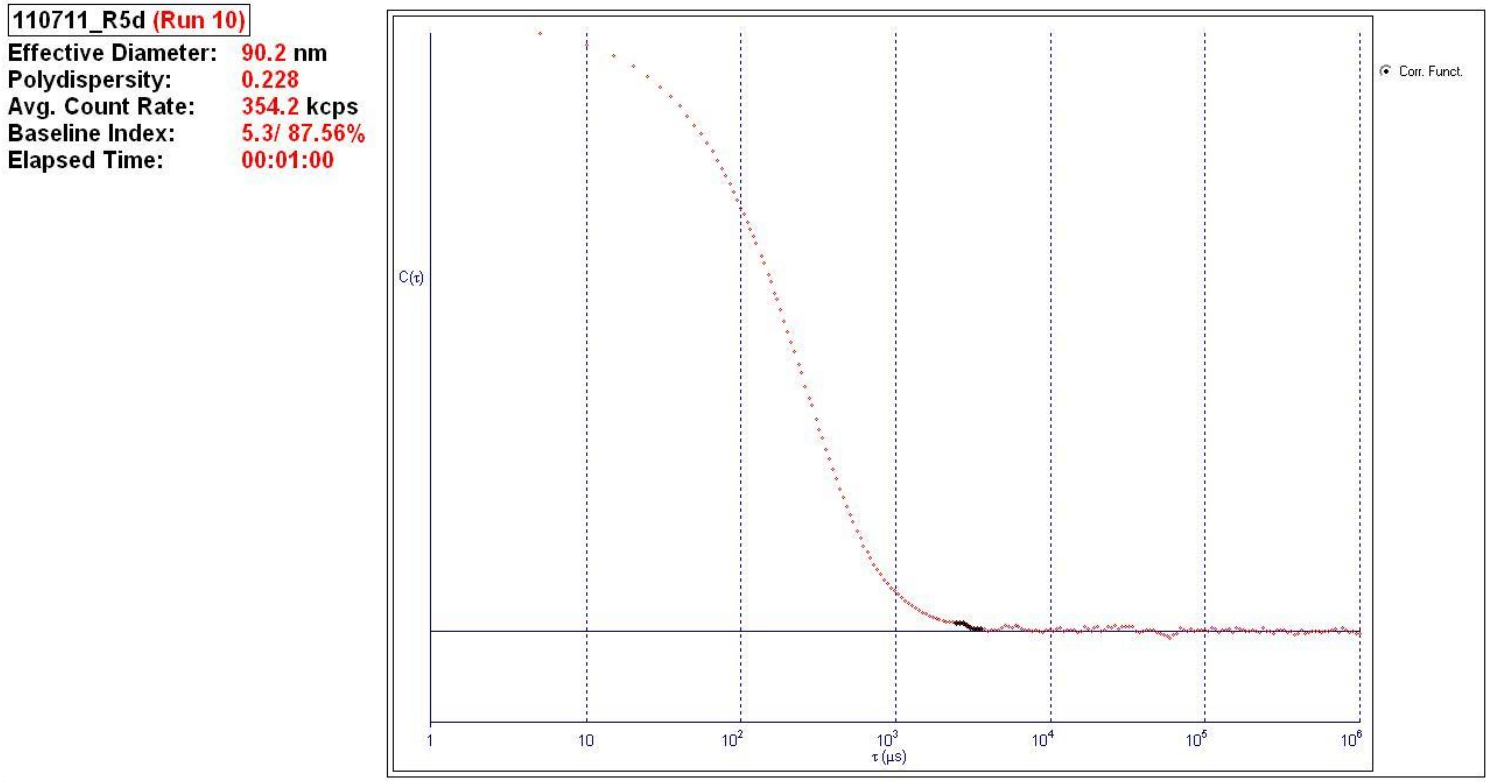
110621_R5d (Combined)

Effective Diameter: 136.8 nm
Polydispersity: 0.306
Avg. Count Rate: 186.3 kcps
Baseline Index: 0.0/ 90.69%
Elapsed Time: 00:10:00



Run	Eff. Diam. (nm)	Half Width (nm)	Polydispersity	Baseline Index
1	139.1	77.7	0.312	0.0/ 83.06%
2	139.5	77.5	0.309	0.0/ 82.77%
3	139.1	76.4	0.302	0.0/ 87.08%
4	136.4	75.3	0.305	0.0/ 95.90%
5	130.8	73.2	0.313	0.0/ 93.70%
6	137.3	75.9	0.306	0.0/ 91.37%
7	134.4	73.8	0.302	0.0/ 92.75%
8	137.8	75.6	0.301	0.0/ 89.35%
9	137.0	76.0	0.308	0.0/ 93.73%
10	134.4	74.8	0.310	0.0/ 95.67%
Mean	136.6	75.6	0.307	0.0/ 90.54%
Std. Error	0.9	0.5	0.001	0.0/ 1.53
Combined	136.8	75.7	0.306	0.0/ 90.69%

Figure A.16. DLS analysis of Sample 26.

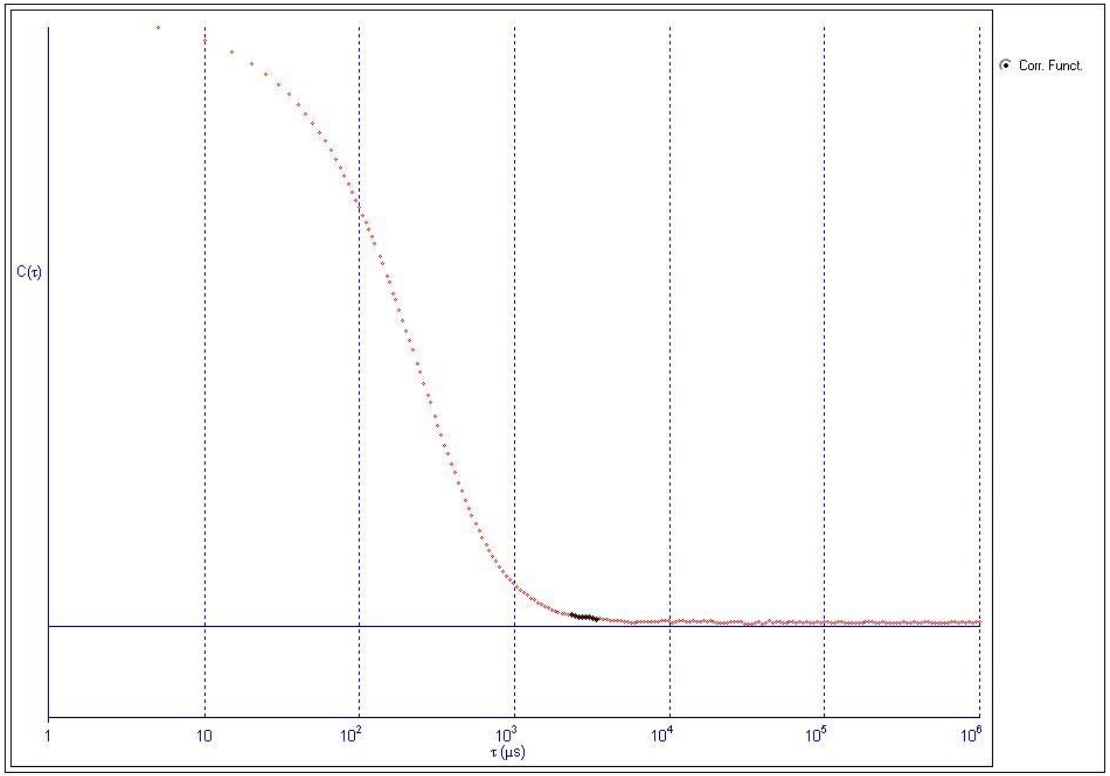


Run	Eff. Diam. (nm)	Half Width (nm)	Polydispersity	Baseline Index
1	86.7	39.7	0.210	4.4/ 71.11%
2	90.3	43.1	0.228	5.2/ 84.44%
3	89.8	41.1	0.210	4.0/ 56.44%
4	86.8	6.1	0.005	0.0/ 27.11%
5	91.3	38.5	0.178	3.6/ 94.22%
6	91.4	42.2	0.214	3.5/ 84.89%
7	91.3	43.4	0.225	9.0/ 73.33%
8	92.8	43.2	0.216	7.4/ 91.11%
9	89.5	43.0	0.231	7.0/ 87.56%
10	90.2	43.0	0.228	5.3/ 87.56%
Mean	90.0	38.3	0.195	4.9/ 75.78%
Std. Error	0.6	3.6	0.022	0.8/ 6.48
Combined	90.2	40.9	0.205	4.8/ 75.78%

Figure A.17. DLS analysis of Sample 28.

110621_R7.5d (Combined)

Effective Diameter: 205.0 nm
Polydispersity: 0.243
Avg. Count Rate: 398.9 kcps
Baseline Index: 0.4/ 79.13%
Elapsed Time: 00:10:00

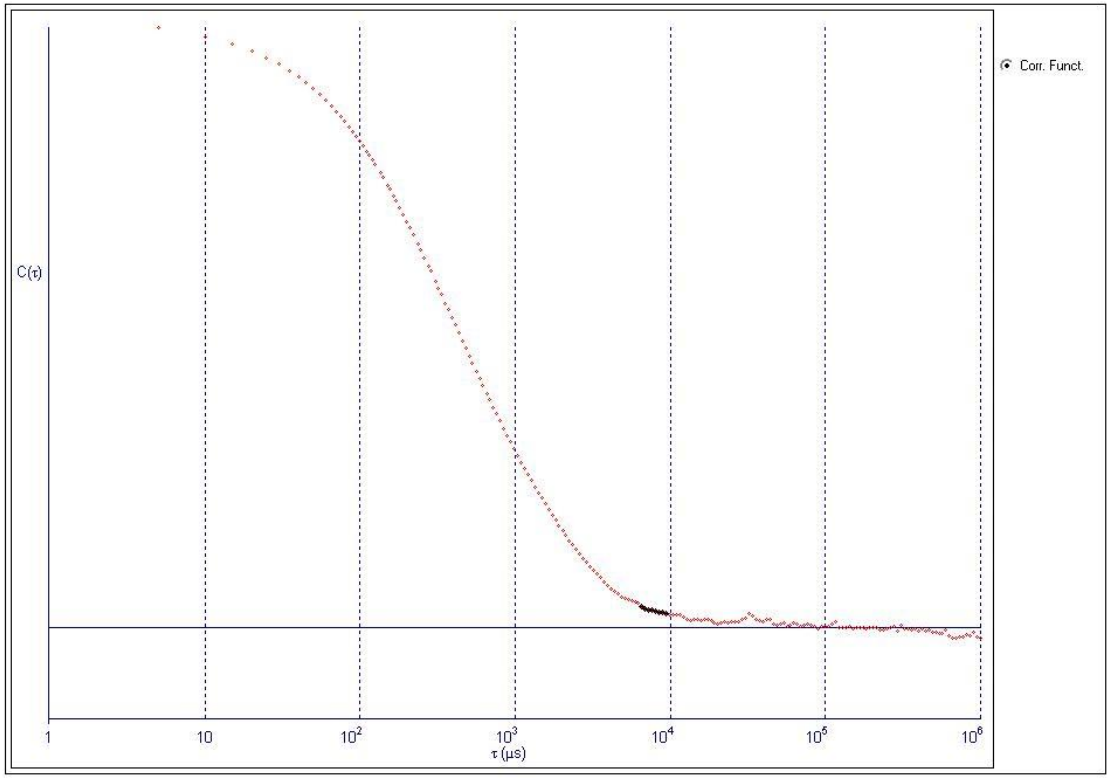


Run	Eff. Diam. (nm)	Half Width (nm)	Polydispersity	Baseline Index
1	205.6	100.5	0.239	4.7/ 34.07%
2	203.7	105.5	0.268	1.8/ 45.13%
3	203.8	94.1	0.213	2.5/ 81.42%
4	208.5	107.3	0.265	4.1/ 86.73%
5	204.3	101.2	0.245	4.7/ 95.58%
6	204.2	97.6	0.229	1.9/ 82.74%
7	204.3	100.6	0.243	3.7/ 96.02%
8	204.0	101.7	0.248	7.3/ 91.56%
9	204.2	103.3	0.256	5.0/ 91.11%
10	207.1	103.2	0.248	5.6/ 87.11%
Mean	205.0	101.5	0.245	4.1/ 79.15%
Std. Error	0.5	1.2	0.005	0.5/ 6.81
Combined	205.0	101.0	0.243	0.4/ 79.13%

Figure A.18. DLS analysis of Sample 29.

110711_R7.5d (Combined)

Effective Diameter:	**219.7 nm**
Polydispersity:	**0.387**
Avg. Count Rate:	**344.4 kcps**
Baseline Index:	**0.0/ 27.05%**
Elapsed Time:	**00:10:00**

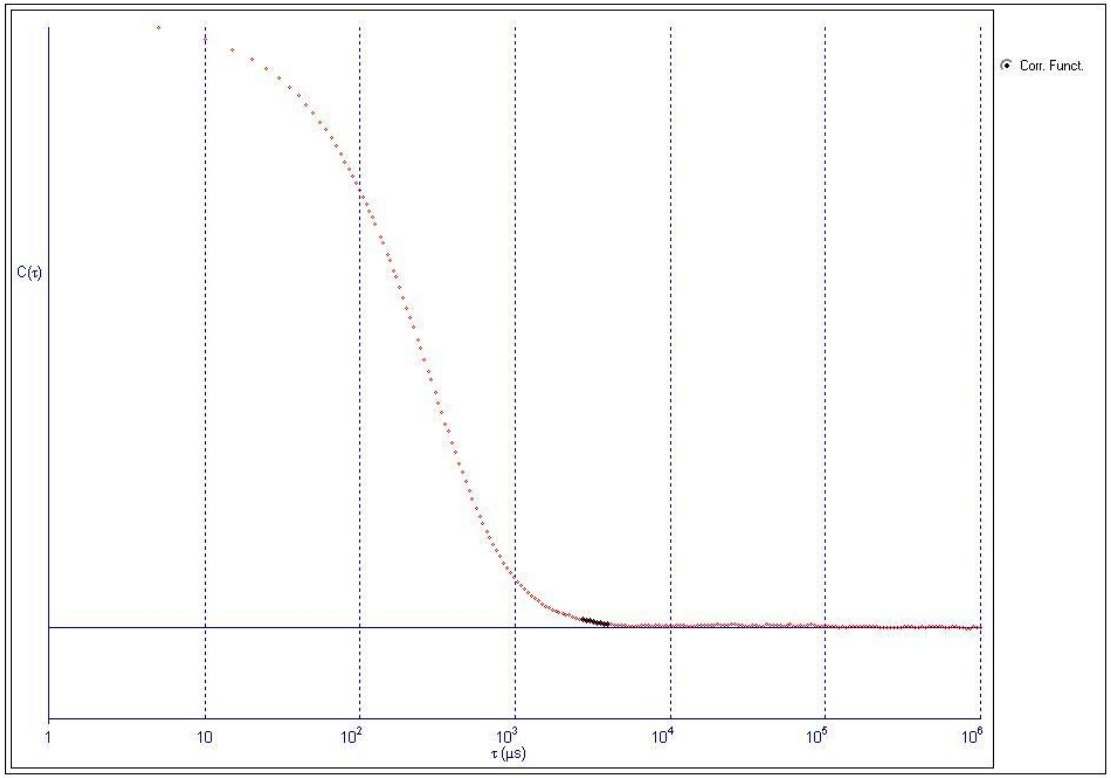


Run	Eff. Diam. (nm)	Half Width (nm)	Polydispersity	Baseline Index
1	219.8	137.2	0.390	0.0/ 37.78%
2	220.4	136.1	0.381	0.0/ 38.67%
3	206.1	129.2	0.393	0.0/ 39.56%
4	131.9	71.4	0.293	0.0/ 4.89%
5	228.9	143.9	0.395	4.7/ 17.33%
6	213.0	134.4	0.398	0.0/ 15.56%
7	206.3	127.9	0.384	2.2/ 42.48%
8	239.7	150.8	0.396	0.0/ 24.00%
9	229.4	145.3	0.401	0.0/ 39.56%
10	254.7	161.4	0.401	7.0/ 10.67%
Mean	215.0	133.7	0.383	1.4/ 27.05%
Std. Error	10.4	7.6	0.010	0.8/ 4.47
Combined	219.7	136.6	0.387	0.0/ 27.05%

Figure A.19. DLS analysis of Sample 30.

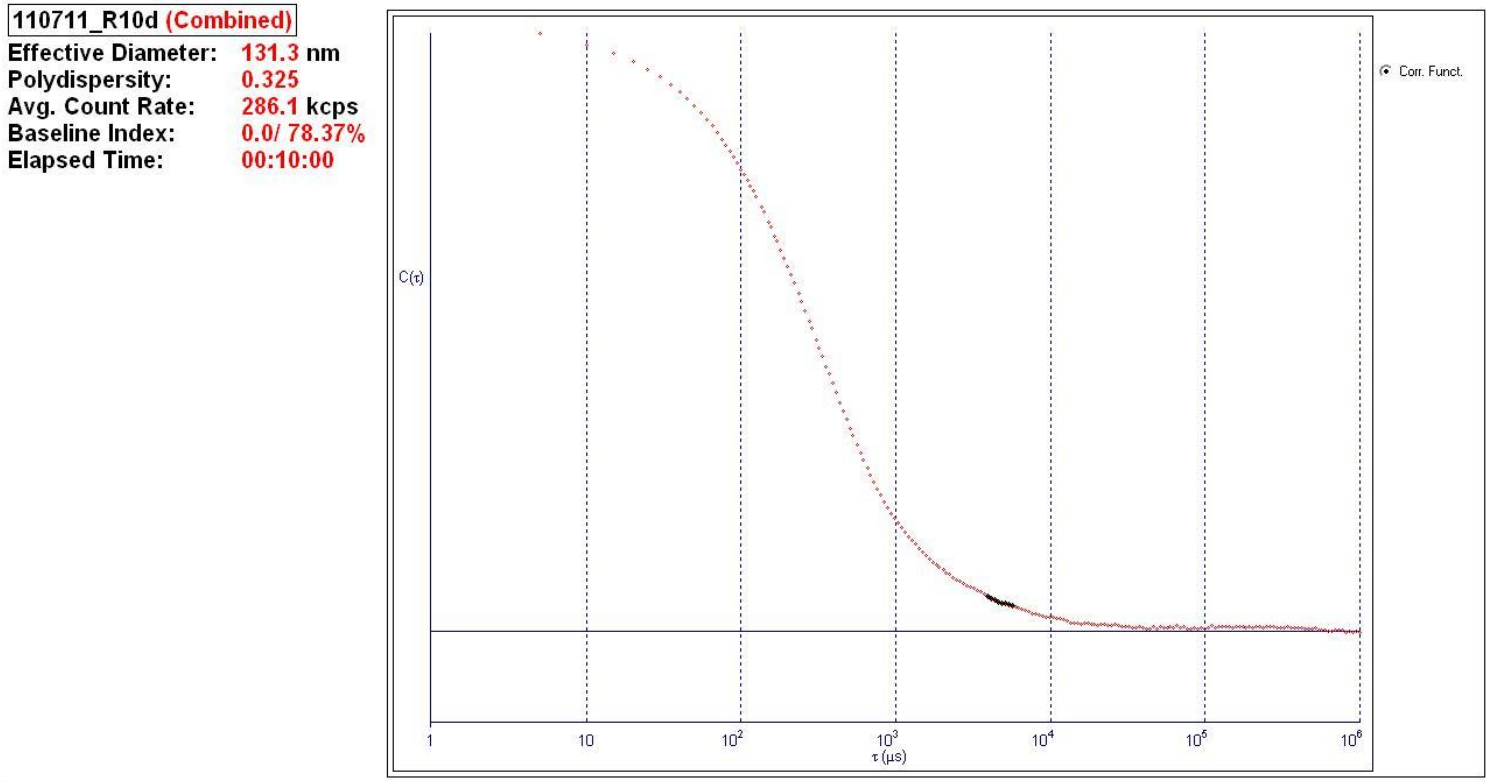
110621_R10d (Combined)

Effective Diameter:	**234.0 nm**
Polydispersity:	**0.244**
Avg. Count Rate:	**319.1 kcps**
Baseline Index:	**5.7/ 82.18%**
Elapsed Time:	**00:10:00**



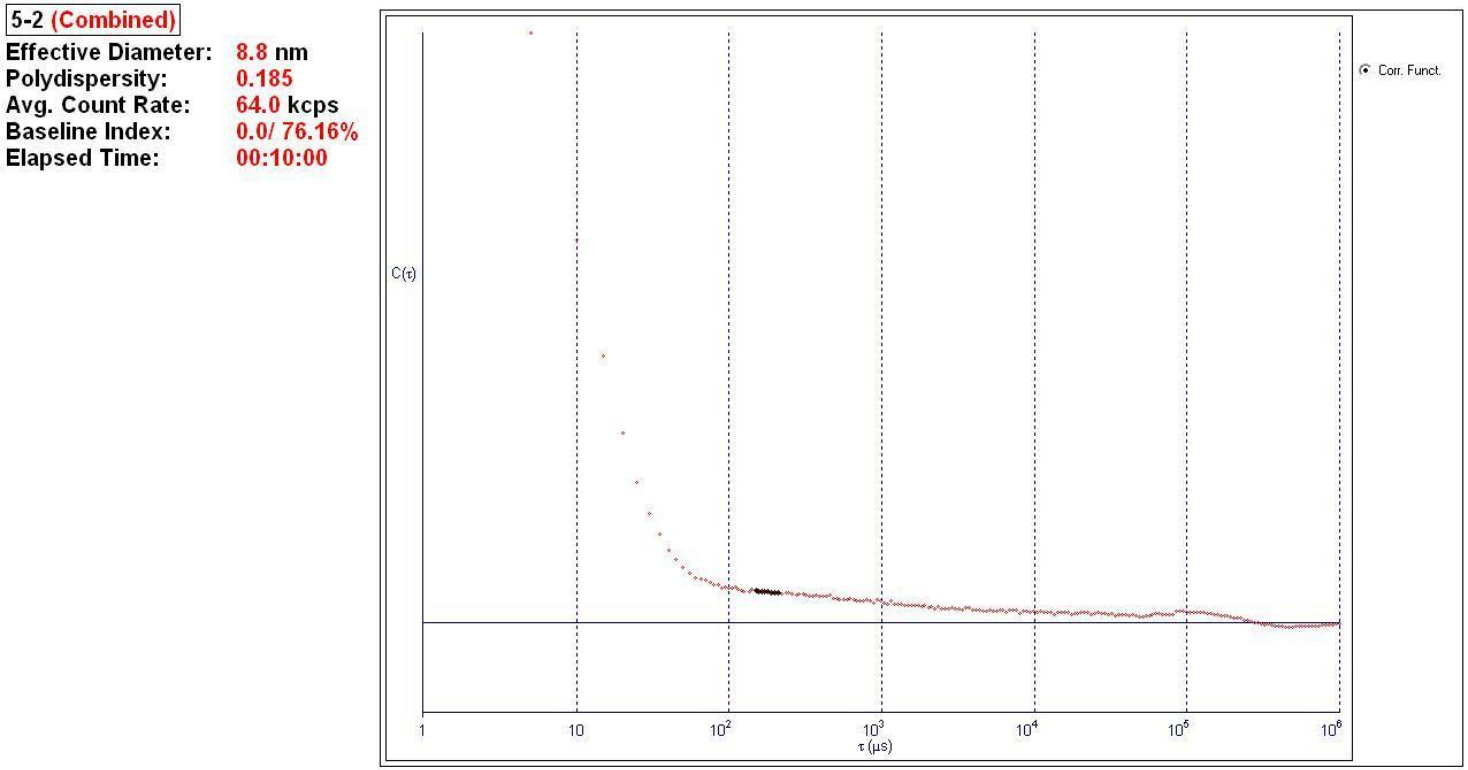
Run	Eff. Diam. (nm)	Half Width (nm)	Polydispersity	Baseline Index
1	239.0	115.4	0.233	6.8/ 78.22%
2	236.7	112.8	0.227	5.0/ 73.33%
3	238.4	120.7	0.256	7.7/ 63.56%
4	231.8	120.8	0.272	6.7/ 86.67%
5	232.9	113.6	0.238	6.7/ 80.44%
6	227.9	110.5	0.235	3.8/ 96.00%
7	234.2	118.8	0.257	8.4/ 87.56%
8	236.3	111.5	0.223	5.3/100.00%
9	235.2	119.1	0.256	5.5/ 68.89%
10	230.8	114.3	0.245	4.3/ 87.11%
Mean	234.3	115.7	0.244	6.0/ 82.18%
Std. Error	1.1	1.2	0.005	0.5/ 3.66
Combined	234.0	115.5	0.244	5.7/ 82.18%

Figure A.20. DLS analysis of Sample 31.



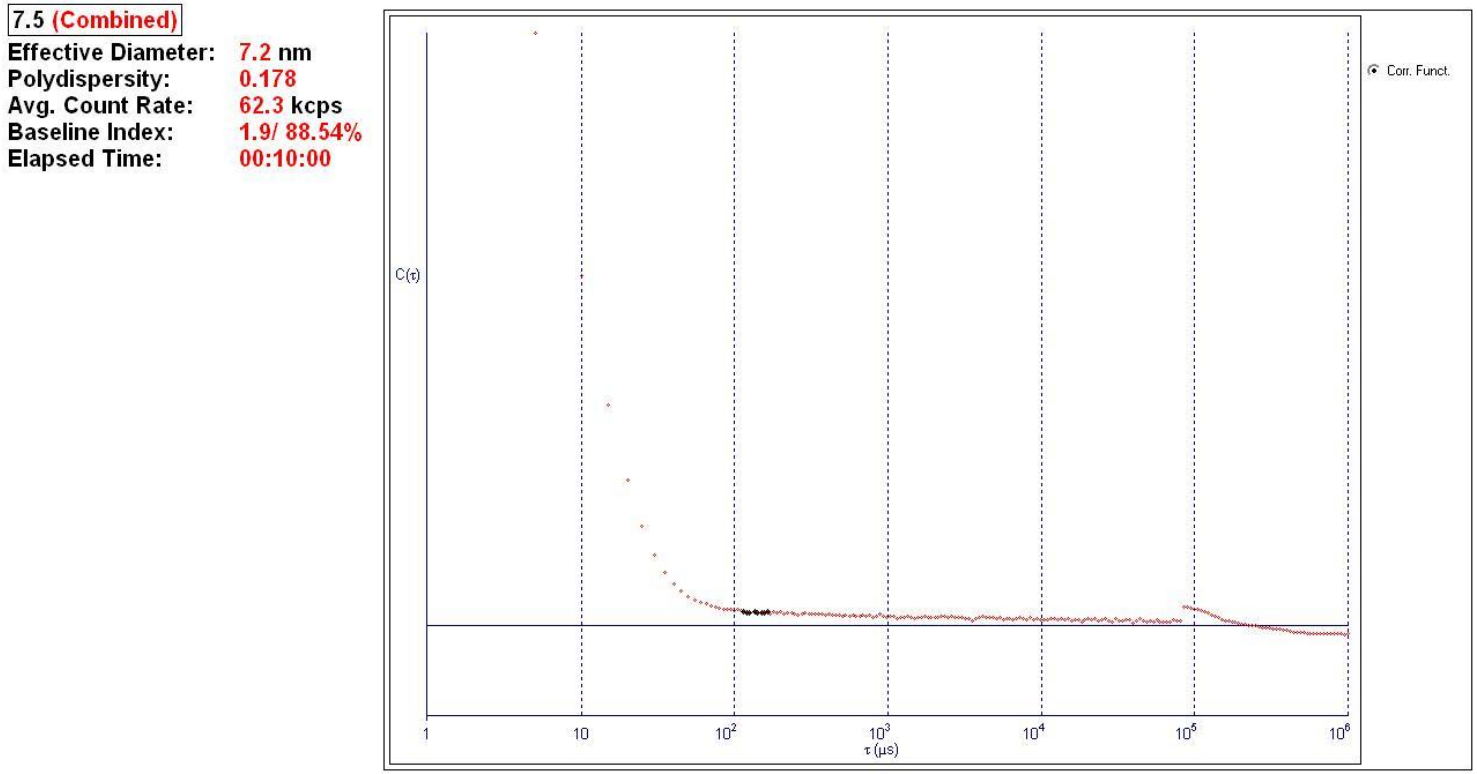
Run	Eff. Diam. (nm)	Half Width (nm)	Polydispersity	Baseline Index
1	123.4	69.5	0.317	7.9/ 53.78%
2	127.7	69.7	0.298	5.8/ 73.78%
3	135.0	76.9	0.324	5.2/ 91.56%
4	141.9	83.7	0.348	0.0/ 85.84%
5	148.9	87.7	0.347	0.0/ 80.44%
6	138.7	80.6	0.338	0.0/ 77.33%
7	138.8	81.6	0.346	0.0/ 67.56%
8	124.8	69.8	0.313	0.0/ 87.56%
9	127.5	72.1	0.320	0.0/ 91.56%
10	124.7	70.1	0.316	0.0/ 74.22%
Mean	133.1	76.2	0.327	1.9/ 78.36%
Std. Error	2.8	2.2	0.005	1.0/ 3.73
Combined	131.3	74.9	0.325	0.0/ 78.37%

Figure A.21. DLS analysis of Sample 32.



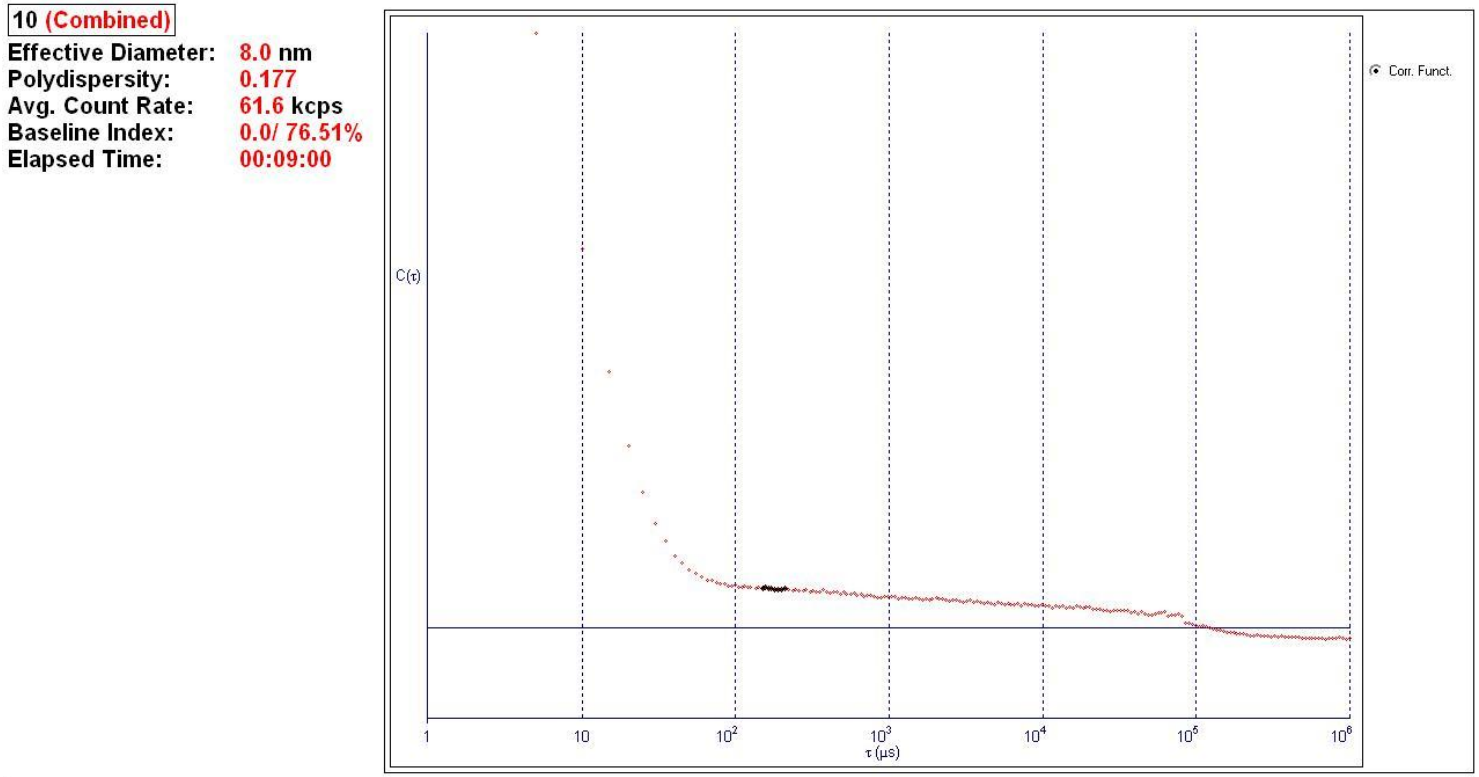
Run	Eff. Diam. (nm)	Half Width (nm)	Polydispersity	Baseline Index
1	8.3	3.8	0.207	0.0/ 68.75%
2	8.8	4.0	0.211	0.0/ 52.78%
3	8.8	3.9	0.197	0.0/ 81.60%
4	8.6	3.9	0.202	0.0/ 82.70%
5	8.7	3.8	0.189	0.0/ 74.31%
6	8.5	3.8	0.205	0.0/ 91.32%
7	8.6	3.9	0.202	0.0/ 90.97%
8	8.3	3.7	0.195	0.0/ 82.01%
9	8.2	3.7	0.207	0.0/ 67.71%
10	8.5	4.0	0.226	0.0/ 69.44%
Mean	8.5	3.9	0.204	0.0/ 76.16%
Std. Error	0.1	0.0	0.003	0.0/ 3.77
Combined	8.8	3.8	0.185	0.0/ 76.16%

Figure A.22. DLS analysis of w/o ME sample with $R = 5$.



Run	Eff. Diam. (nm)	Half Width (nm)	Polydispersity	Baseline Index
1	6.9	2.9	0.179	3.5/ 72.82%
2	7.1	3.2	0.195	2.1/ 86.46%
3	7.3	3.2	0.192	1.6/100.00%
4	7.3	3.2	0.192	0.0/ 94.77%
5	7.2	3.3	0.204	3.0/ 82.35%
6	7.3	3.0	0.173	2.5/ 86.51%
7	6.9	2.9	0.173	0.0/ 95.83%
8	6.8	2.9	0.187	4.8/ 77.78%
9	7.0	3.0	0.185	4.5/ 95.14%
10	6.7	3.1	0.210	4.6/ 93.73%
Mean	7.1	3.1	0.189	2.7/ 88.54%
Std. Error	0.1	0.0	0.004	0.6/ 2.80
Combined	7.2	3.0	0.178	1.9/ 88.54%

Figure A.23. DLS analysis of w/o ME sample with $R = 7.5$.



Run	Eff. Diam. (nm)	Half Width (nm)	Polydispersity	Baseline Index
1	7.9	3.4	0.189	0.0/ 91.32%
2	7.7	3.4	0.201	0.0/ 78.47%
3	1045642.6	73938.1	0.005	0.0/ 72.47%
4	7.4	3.2	0.186	0.0/ 51.39%
5	8.0	3.5	0.194	0.0/ 78.20%
6	7.9	3.4	0.184	0.0/ 78.82%
7	7.9	3.3	0.180	0.0/ 90.97%
8	7.5	3.3	0.196	0.0/ 61.11%
9	7.7	3.4	0.200	0.0/ 86.46%
10	7.8	3.4	0.195	0.0/ 71.88%
Mean	7.8	3.4	0.192	0.0/ 76.51%
Std. Error	0.1	0.0	0.002	0.0/ 4.46
Combined	8.0	3.3	0.177	0.0/ 76.51%

Figure A.24. DLS analysis of w/o ME sample with $R = 10$.

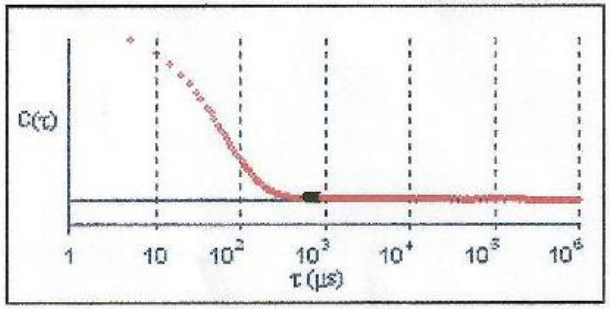
110413-R5 (Combined)

Effective Diameter: 62.6 nm

Polydispersity: 0.142

Baseline Index: 7.5/ 88.44%

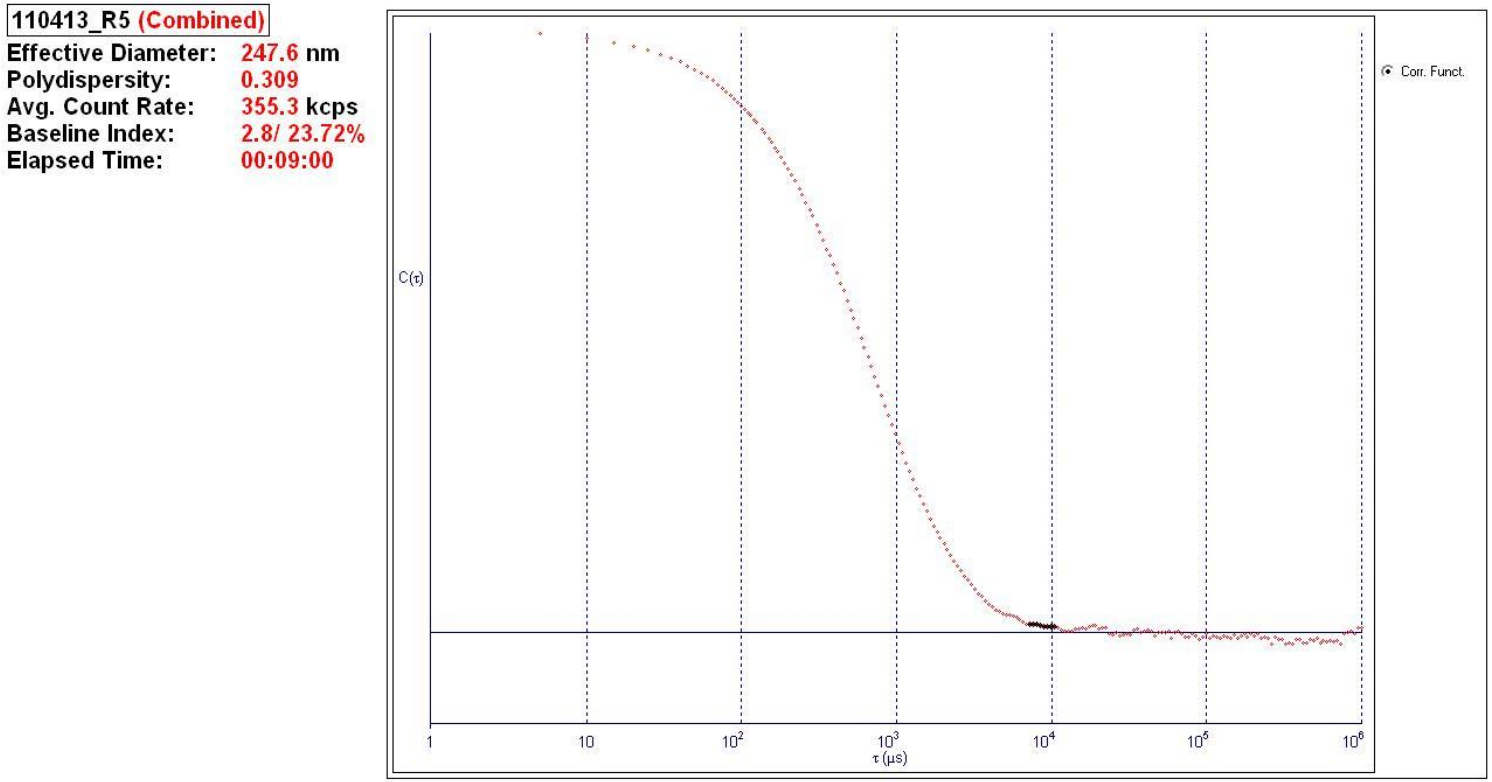
Elapsed Time: 00:10:00



Correlation Function

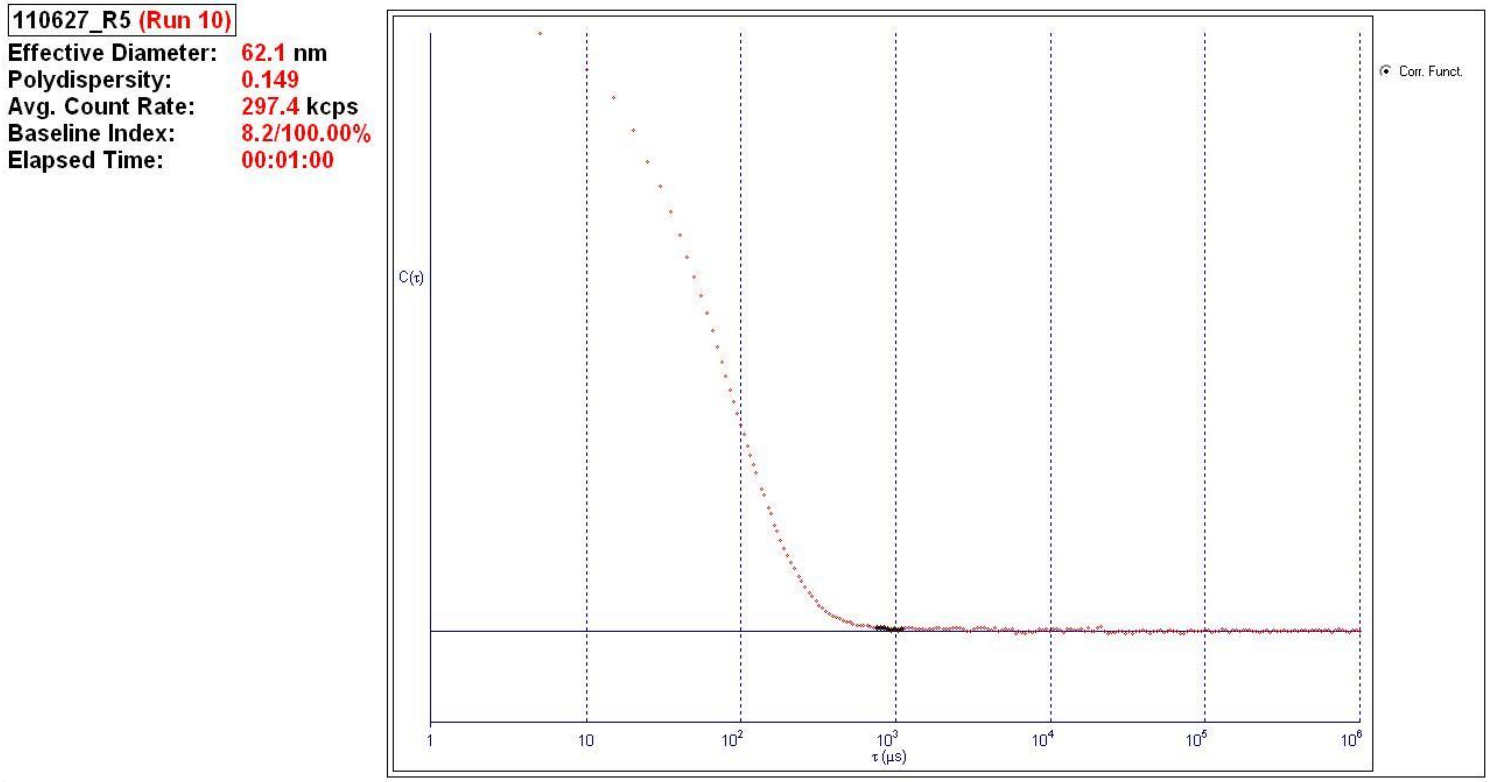
Run	Eff. Diam. (nm)	Half Width (nm)	Polydispersity	Baseline Index
1	68.0	26.4	0.151	7.2/ 82.59%
2	62.4	26.3	0.177	7.7/ 85.71%
3	61.6	25.7	0.174	9.0/ 87.05%
4	64.0	21.6	0.114	6.1/ 72.32%
5	61.7	23.1	0.140	8.5/ 95.54%
6	62.6	21.0	0.113	7.1/ 95.54%
7	61.1	24.9	0.166	8.4/ 91.07%
8	61.6	21.4	0.120	7.1/ 95.56%
9	61.4	22.2	0.130	7.4/ 95.54%
10	61.0	22.6	0.137	8.2/ 83.48%
Mean	62.5	23.5	0.142	7.7/ 88.44%
Std. Error	0.7	0.7	0.008	0.3/ 2.44
Combined	62.6	23.6	0.142	7.5/ 88.44%

Figure A.25. DLS analysis of Sample 1.



Run	Eff. Diam. (nm)	Half Width (nm)	Polydispersity	Baseline Index
1	247.5	137.7	0.310	7.0/ 37.78%
2	208.6	76.0	0.133	0.0/ 7.08%
3	263.1	156.7	0.355	6.5/ 28.32%
4	0.0	0.0	0.000	0.0/ 0.44%
5	247.1	131.4	0.283	7.8/ 27.88%
6	216.6	125.4	0.335	0.0/ 13.78%
7	303.8	170.2	0.314	9.5/ 21.33%
8	214.5	113.6	0.280	5.9/ 8.89%
9	238.1	135.7	0.325	3.1/ 35.11%
10	241.3	133.3	0.305	4.9/ 33.33%
Mean	242.3	131.1	0.293	5.0/ 23.72%
Std. Error	9.8	8.8	0.022	1.1/ 3.84
Combined	247.6	137.6	0.309	2.8/ 23.72%

Figure A.26. DLS analysis of Sample 1 suspended in water.

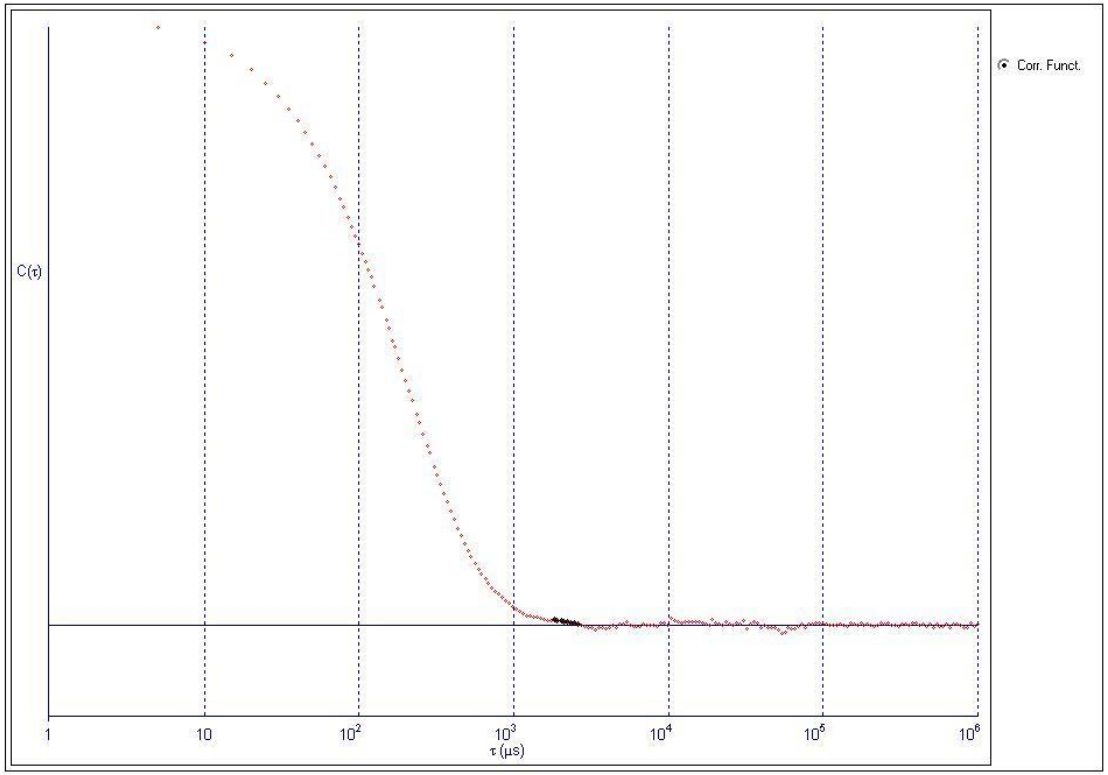


Run	Eff. Diam. (nm)	Half Width (nm)	Polydispersity	Baseline Index
1	70.3	33.5	0.228	0.0/ 38.67%
2	66.2	26.7	0.163	5.6/ 67.56%
3	63.5	26.0	0.168	4.0/ 74.22%
4	63.2	29.6	0.219	6.8/ 54.02%
5	65.1	25.9	0.158	5.0/ 95.56%
6	63.2	25.4	0.161	6.9/100.00%
7	64.7	26.6	0.168	5.1/100.00%
8	62.2	26.4	0.180	5.6/100.00%
9	62.0	22.4	0.130	5.6/100.00%
10	62.1	24.0	0.149	8.2/100.00%
Mean	63.6	25.9	0.166	5.9/ 87.93%
Std. Error	0.5	0.7	0.008	0.4/ 5.94
Combined	63.5	25.7	0.163	1.9/ 87.92%

Figure A.27. DLS analysis of Sample 2.

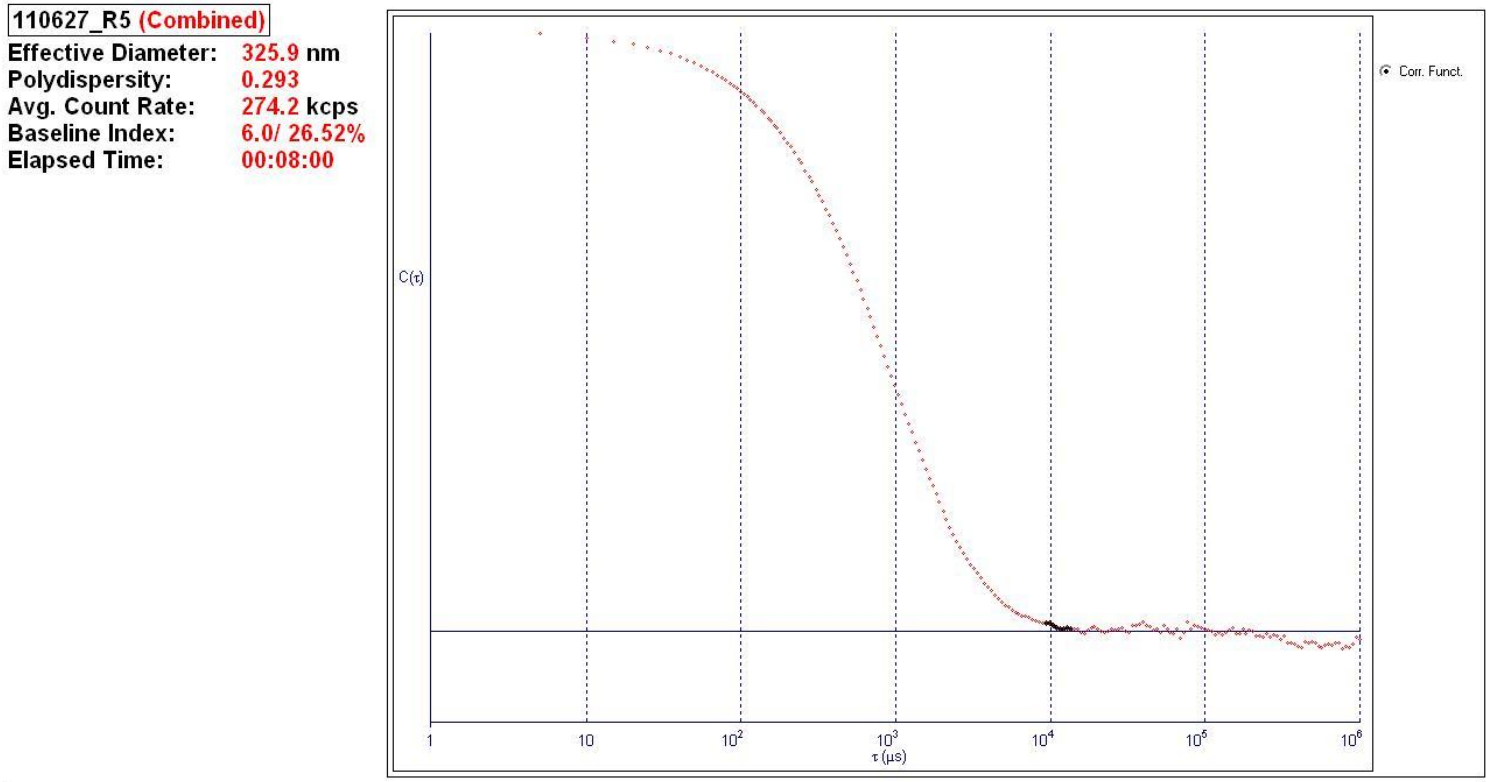
110627_R5 (Run 10)

Effective Diameter: 55.8 nm
Polydispersity: 0.200
Avg. Count Rate: 358.4 kcps
Baseline Index: 6.5/ 78.67%
Elapsed Time: 00:01:00



Run	Eff. Diam. (nm)	Half Width (nm)	Polydispersity	Baseline Index
1	56.0	25.1	0.202	7.4/ 35.40%
2	55.6	25.2	0.206	6.3/ 70.35%
3	57.6	25.2	0.191	5.8/ 82.30%
4	56.0	25.1	0.201	8.1/ 54.42%
5	56.2	24.7	0.193	7.7/100.00%
6	55.6	26.5	0.227	5.5/100.00%
7	56.5	25.5	0.204	8.1/ 76.44%
8	56.4	24.0	0.182	9.5/ 95.56%
9	54.9	25.9	0.223	8.8/ 87.11%
10	55.8	24.9	0.200	6.5/ 78.67%
Mean	56.1	25.2	0.203	7.4/ 78.03%
Std. Error	0.2	0.2	0.004	0.4/ 6.51
Combined	56.1	25.1	0.200	3.2/ 77.99%

Figure A.28. DLS analysis of Sample 2 suspended in ethanol.

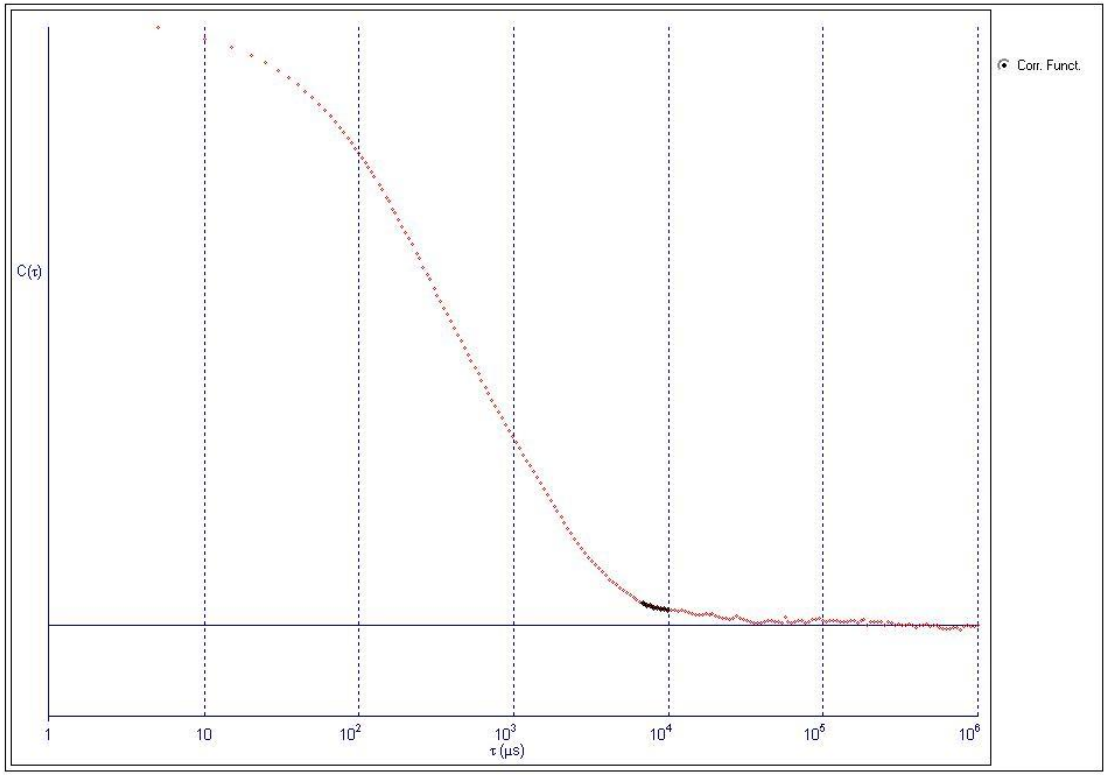


Run	Eff. Diam. (nm)	Half Width (nm)	Polydispersity	Baseline Index
1	344.1	187.1	0.296	0.0/ 20.26%
2	336.1	196.8	0.343	4.5/ 33.19%
3	356.2	212.2	0.355	2.3/ 26.11%
4	415.7	243.0	0.342	0.8/ 10.62%
5	278.3	141.2	0.258	0.0/ 10.67%
6	318.7	178.1	0.312	8.3/ 33.63%
7	260.6	18.4	0.005	0.0/ 16.44%
8	331.2	169.4	0.262	0.0/ 33.78%
9	0.0	0.0	0.000	0.0/ 0.00%
10	303.7	168.9	0.309	7.1/ 22.22%
Mean	281.3	141.4	0.235	2.8/ 23.20%
Std. Error	41.5	29.3	0.052	1.2/ 4.06
Combined	325.9	176.5	0.293	6.0/ 26.52%

Figure A.29. DLS analysis of Sample 2 suspended in water.

110704_R5d (Combined)

Effective Diameter:	**235.7 nm**
Polydispersity:	**0.410**
Avg. Count Rate:	**267.3 kcps**
Baseline Index:	**0.0/ 41.77%**
Elapsed Time:	**00:10:00**

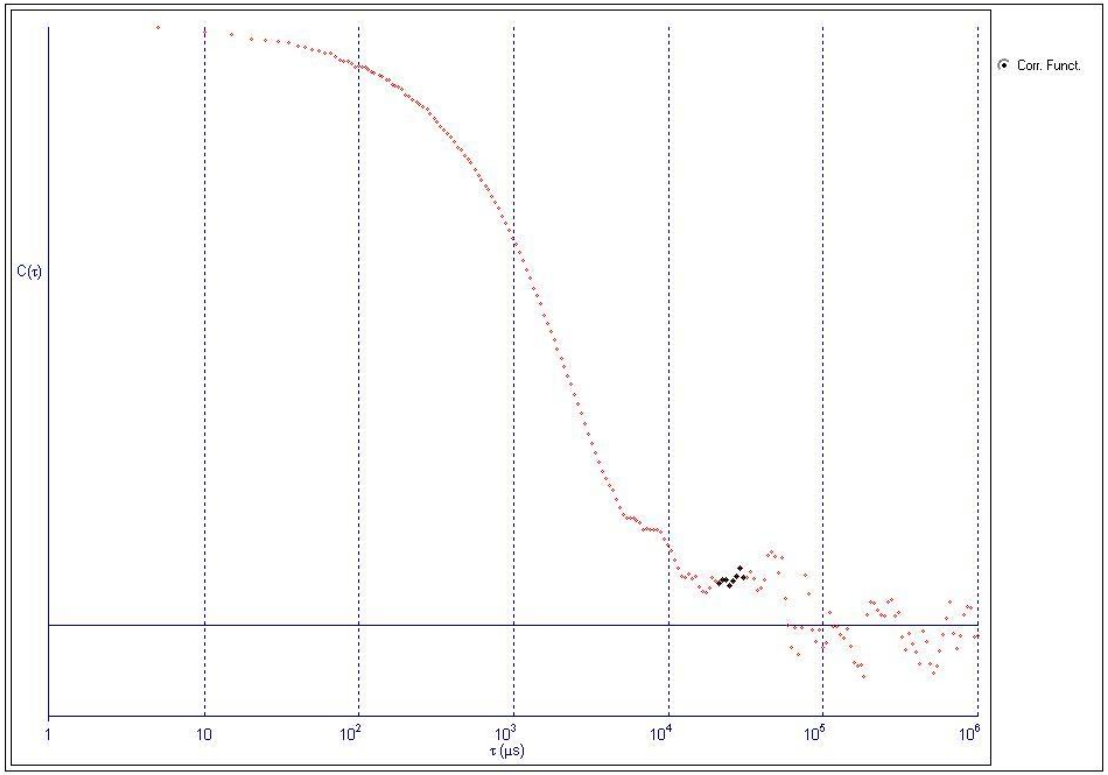


Run	Eff. Diam. (nm)	Half Width (nm)	Polydispersity	Baseline Index
1	248.5	155.4	0.391	4.8/ 39.38%
2	210.1	138.1	0.432	0.0/ 50.66%
3	228.0	141.9	0.387	0.0/ 44.05%
4	232.5	146.5	0.397	0.0/ 60.62%
5	226.3	145.0	0.411	0.0/ 42.92%
6	239.1	145.7	0.371	2.4/ 34.07%
7	219.4	146.4	0.446	0.0/ 11.06%
8	269.1	178.2	0.438	0.2/ 35.84%
9	251.9	165.8	0.434	0.0/ 46.67%
10	216.1	137.2	0.403	0.0/ 52.44%
Mean	234.1	150.0	0.411	0.7/ 41.77%
Std. Error	5.8	4.1	0.008	0.5/ 4.25
Combined	235.7	150.9	0.410	0.0/ 41.77%

Figure A.30. DLS analysis of Sample 27.

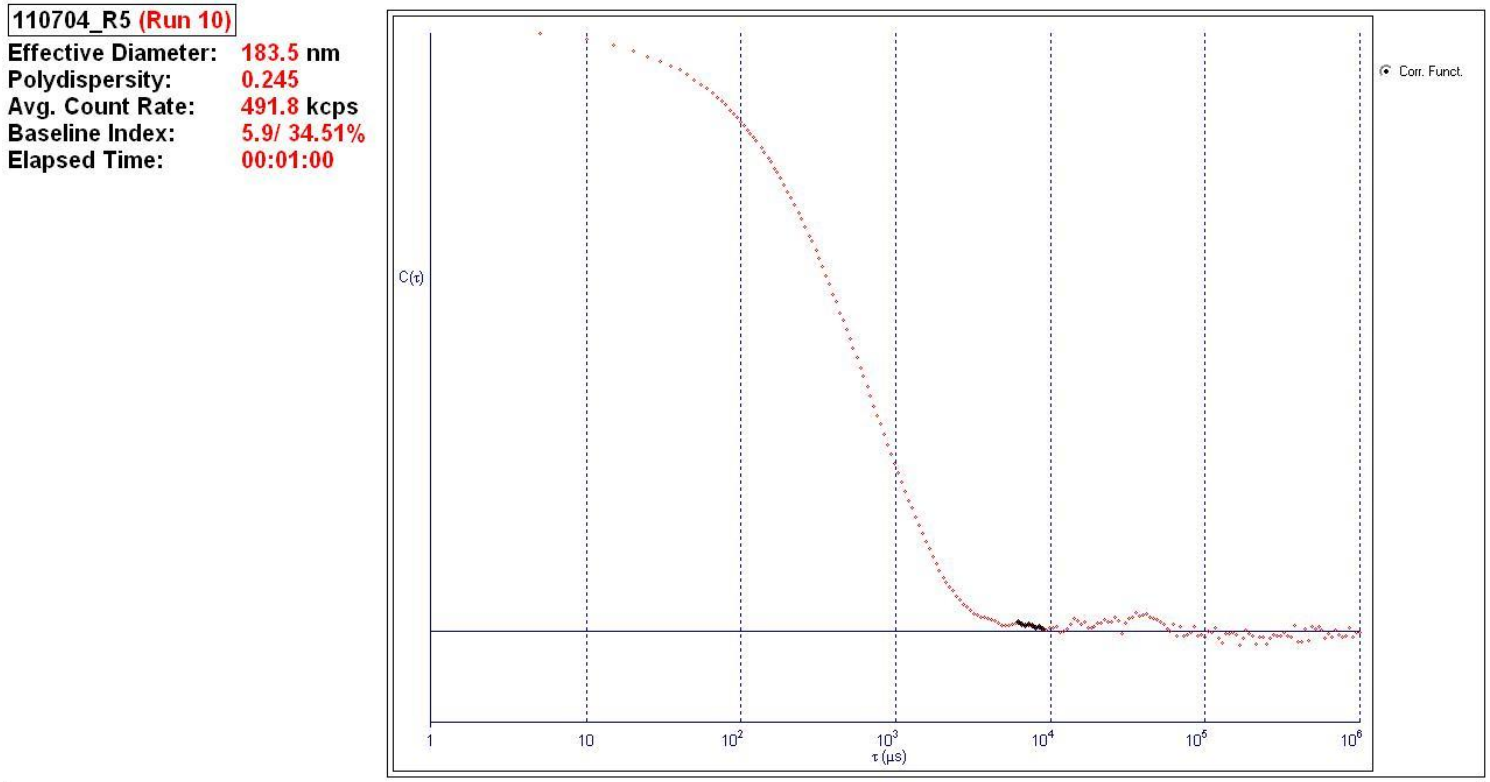
110704_R5d (Run 10)

Effective Diameter: 543.8 nm
Polydispersity: 0.356
Avg. Count Rate: 476.8 kcps
Baseline Index: 0.0/ 12.39%
Elapsed Time: 00:01:00



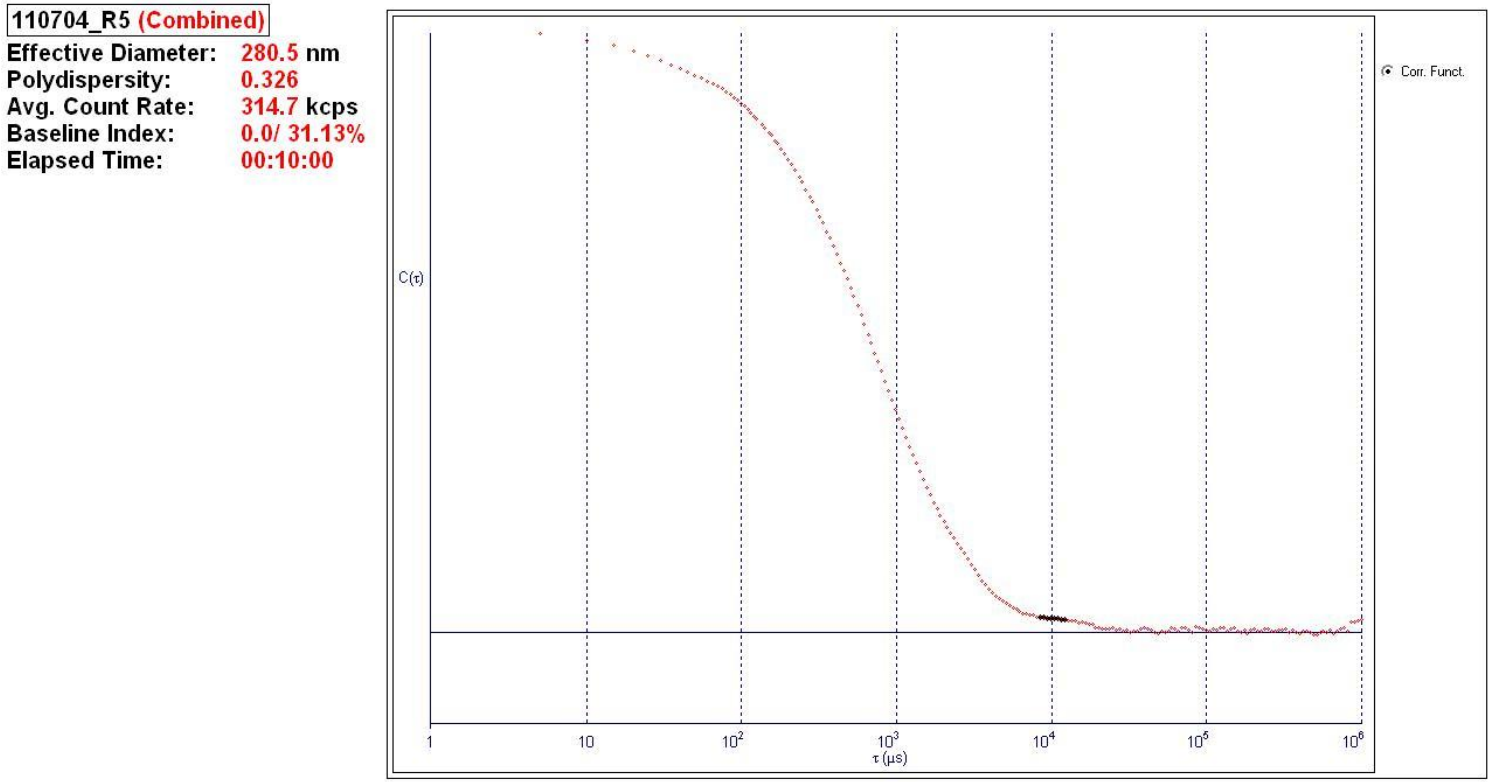
Run	Eff. Diam. (nm)	Half Width (nm)	Polydispersity	Baseline Index
1	719.6	400.7	0.310	9.1/ 48.02%
2	814.2	554.8	0.464	0.0/ 11.50%
3	0.0	0.0	0.000	0.0/ 0.00%
4	801.6	439.9	0.301	0.0/ 41.15%
5	746.3	469.7	0.396	7.8/ 19.91%
6	604.2	42.7	0.005	0.0/ 2.21%
7	1451.1	1038.8	0.512	0.0/ 2.21%
8	0.0	0.0	0.000	0.0/ 0.00%
9	739.1	441.7	0.357	0.0/ 10.62%
10	543.8	324.6	0.356	0.0/ 12.39%
Mean	713.3	412.6	0.300	1.9/ 16.45%
Std. Error	124.4	100.8	0.061	1.3/ 5.74
Combined	731.8	414.9	0.321	0.0/ 18.52%

Figure A.31. DLS analysis of Sample 27 suspended in ethanol.



Run	Eff. Diam. (nm)	Half Width (nm)	Polydispersity	Baseline Index
1	195.4	110.1	0.318	1.0/ 50.00%
2	196.2	102.8	0.274	7.1/ 51.77%
3	196.2	101.7	0.269	0.0/ 21.24%
4	195.1	102.4	0.275	8.6/ 66.37%
5	181.9	101.1	0.309	5.9/ 12.83%
6	196.0	102.4	0.273	8.0/ 51.98%
7	193.2	104.2	0.291	8.2/ 52.21%
8	203.6	113.2	0.309	5.9/ 50.44%
9	185.2	96.5	0.271	10.0/ 33.92%
10	183.5	90.8	0.245	5.9/ 34.51%
Mean	192.6	102.5	0.283	6.1/ 42.53%
Std. Error	2.2	2.0	0.007	1.0/ 5.20
Combined	194.2	103.9	0.286	5.1/ 42.53%

Figure A.32. DLS analysis of Sample 33 suspended in ethanol.

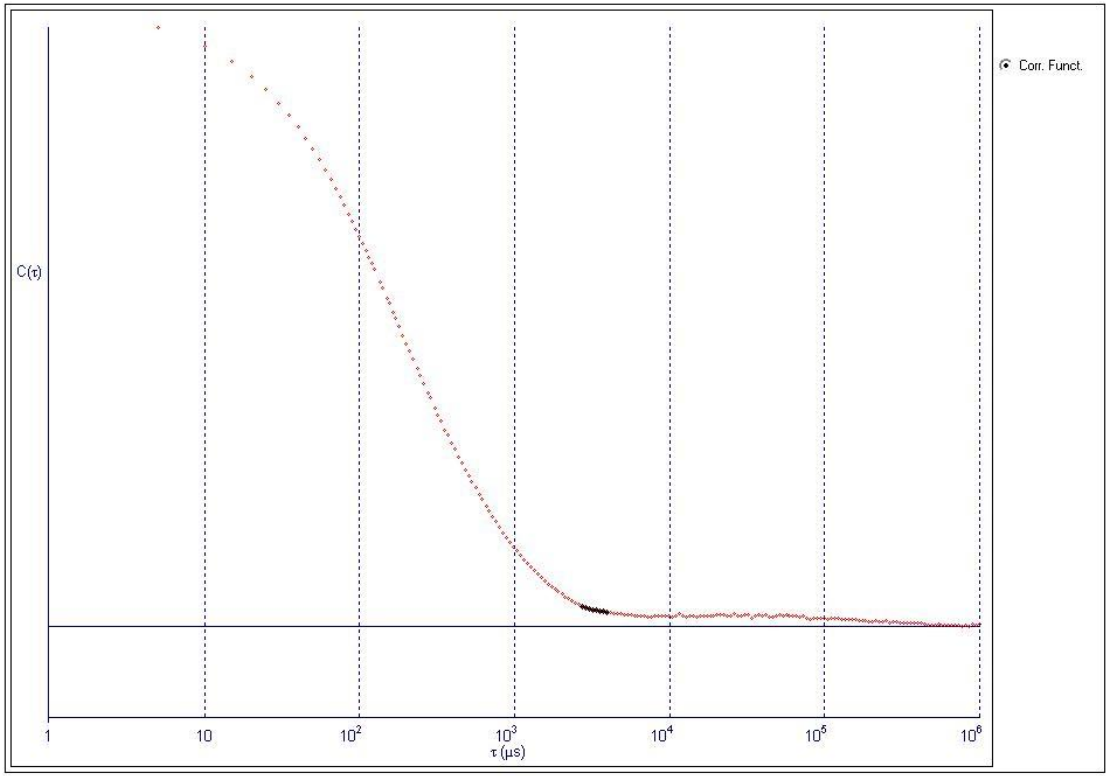


Run	Eff. Diam. (nm)	Half Width (nm)	Polydispersity	Baseline Index
1	301.3	169.5	0.317	0.0/ 44.00%
2	287.0	170.0	0.351	3.2/ 34.67%
3	237.5	130.0	0.299	0.0/ 14.67%
4	266.5	151.4	0.323	2.4/ 31.86%
5	273.3	157.2	0.331	0.0/ 40.89%
6	273.0	152.6	0.312	0.0/ 35.11%
7	285.5	136.6	0.229	0.0/ 13.33%
8	263.7	144.0	0.298	7.6/ 9.78%
9	297.4	170.1	0.327	3.3/ 60.89%
10	290.1	162.9	0.315	0.0/ 26.11%
Mean	277.5	154.4	0.310	1.6/ 31.13%
Std. Error	6.0	4.5	0.010	0.8/ 4.99
Combined	280.5	160.1	0.326	0.0/ 31.13%

Figure A.33. DLS analysis of Sample 33 suspended in water.

110727_R5m1 (Combined)

Effective Diameter: 219.9 nm
Polydispersity: 0.376
Avg. Count Rate: 267.1 kcps
Baseline Index: 0.0/ 55.18%
Elapsed Time: 00:10:00

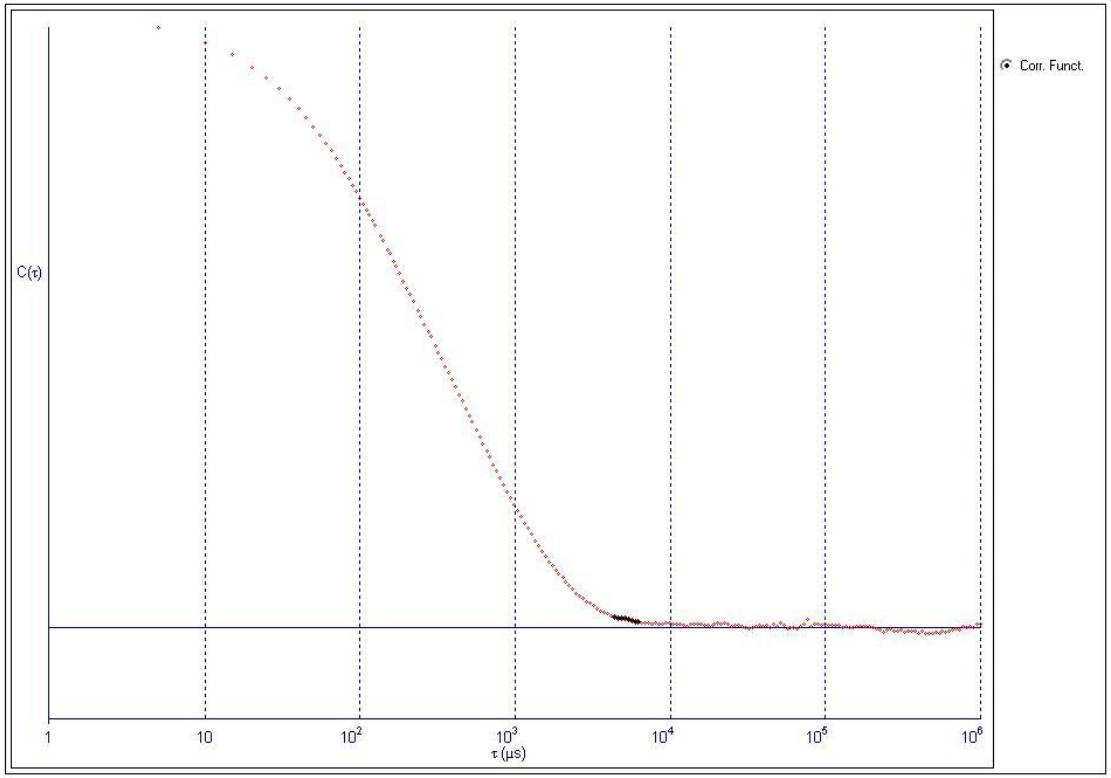


Run	Eff. Diam. (nm)	Half Width (nm)	Polydispersity	Baseline Index
1	238.7	149.4	0.392	0.0/ 64.89%
2	221.6	136.7	0.381	0.0/ 42.67%
3	239.2	148.3	0.384	0.0/ 34.67%
4	226.2	134.9	0.355	3.1/ 54.67%
5	218.7	136.3	0.388	3.6/ 65.78%
6	212.2	127.0	0.358	0.0/ 67.11%
7	222.1	136.1	0.376	0.0/ 60.44%
8	192.9	114.3	0.351	0.0/ 57.08%
9	214.6	131.4	0.375	4.7/ 61.33%
10	218.8	134.4	0.377	9.4/ 43.11%
Mean	220.5	134.9	0.374	2.1/ 55.17%
Std. Error	4.2	3.1	0.004	1.0/ 3.56
Combined	219.9	134.8	0.376	0.0/ 55.18%

Figure A.34. DLS analysis of Sample 34.

110727_R5m2 (Combined)

Effective Diameter: 353.5 nm
Polydispersity: 0.395
Avg. Count Rate: 276.6 kcps
Baseline Index: 0.4/ 33.66%
Elapsed Time: 00:10:00

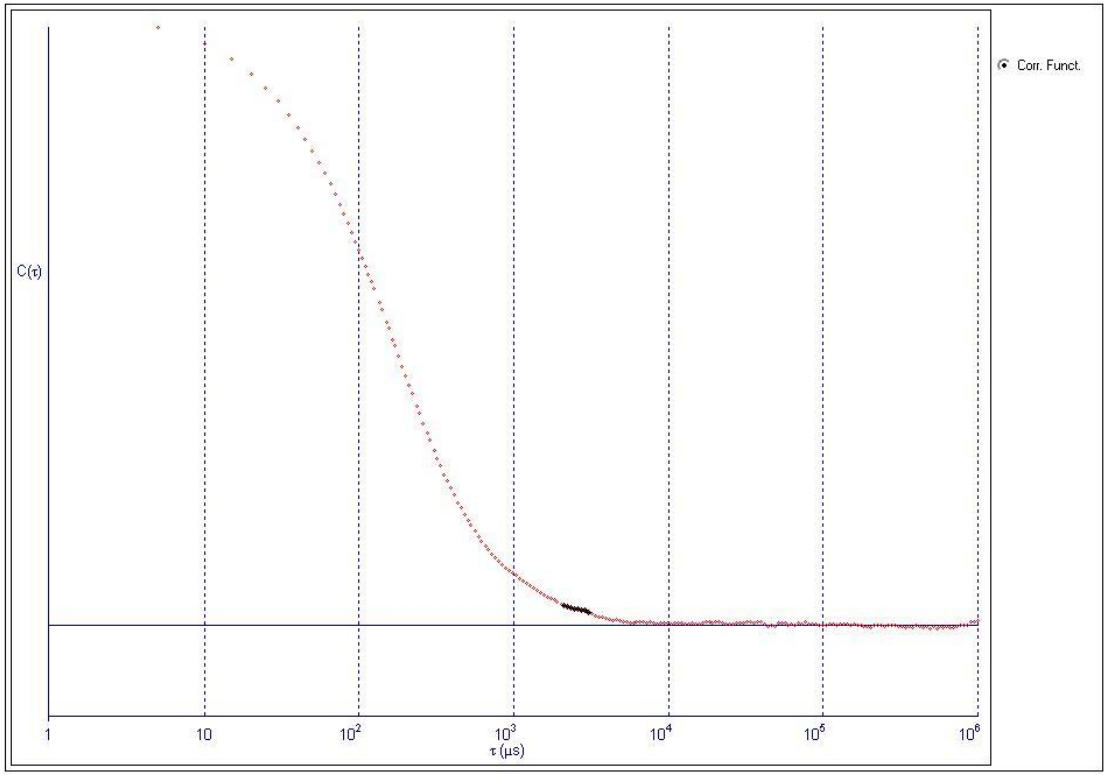


Run	Eff. Diam. (nm)	Half Width (nm)	Polydispersity	Baseline Index
1	359.6	236.2	0.431	0.0/ 51.56%
2	327.5	208.9	0.407	0.0/ 32.44%
3	372.8	233.0	0.390	5.5/ 31.56%
4	330.3	205.4	0.387	0.0/ 46.22%
5	406.2	256.8	0.400	8.0/ 19.11%
6	388.6	238.1	0.375	2.3/ 14.22%
7	388.7	255.5	0.432	6.9/ 16.00%
8	354.7	220.9	0.388	5.2/ 39.11%
9	368.5	224.4	0.371	6.2/ 24.11%
10	336.7	205.4	0.372	0.0/ 62.22%
Mean	363.4	228.5	0.395	3.4/ 33.66%
Std. Error	8.4	6.0	0.007	1.0/ 5.08
Combined	353.5	222.2	0.395	0.4/ 33.66%

Figure A.35. DLS analysis of Sample 35.

110817_R5_M1 (Combined)

Effective Diameter: 162.5 nm
Polydispersity: 0.322
Avg. Count Rate: 406.4 kcps
Baseline Index: 0.0/ 36.02%
Elapsed Time: 00:10:00

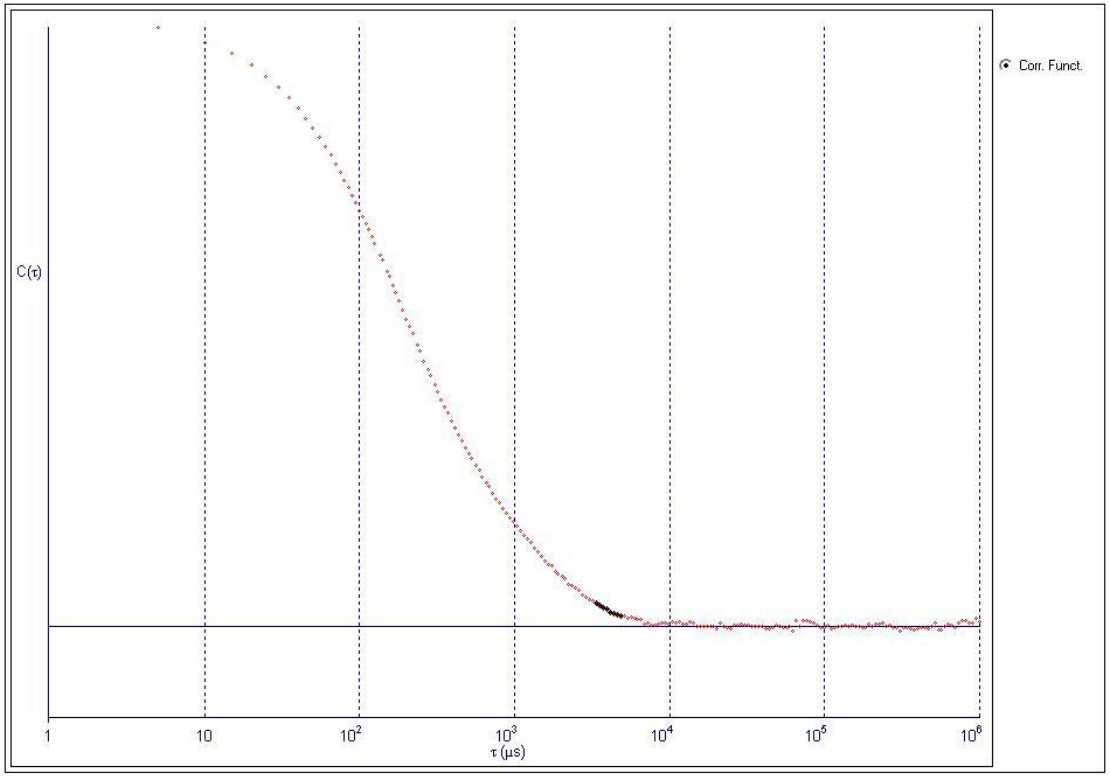


Run	Eff. Diam. (nm)	Half Width (nm)	Polydispersity	Baseline Index
1	162.9	91.9	0.318	0.0/ 25.22%
2	178.0	105.6	0.352	0.0/ 39.82%
3	185.4	111.0	0.358	0.0/ 13.27%
4	170.1	99.7	0.344	0.0/ 26.55%
5	180.5	103.5	0.329	0.0/ 26.55%
6	164.4	94.5	0.330	1.7/ 38.50%
7	156.0	85.8	0.303	0.0/ 32.74%
8	160.5	90.4	0.317	0.0/ 37.61%
9	154.6	86.1	0.310	0.0/ 46.02%
10	150.5	83.2	0.306	0.0/ 73.89%
Mean	166.3	95.2	0.327	0.2/ 36.02%
Std. Error	3.7	3.0	0.006	0.2/ 5.14
Combined	162.5	92.3	0.322	0.0/ 36.02%

Figure A.36. DLS analysis of Sample 36.

110817_R5_M2 (Combined)

Effective Diameter: 267.3 nm
Polydispersity: 0.380
Avg. Count Rate: 294.9 kcps
Baseline Index: 0.0/ 22.43%
Elapsed Time: 00:10:00

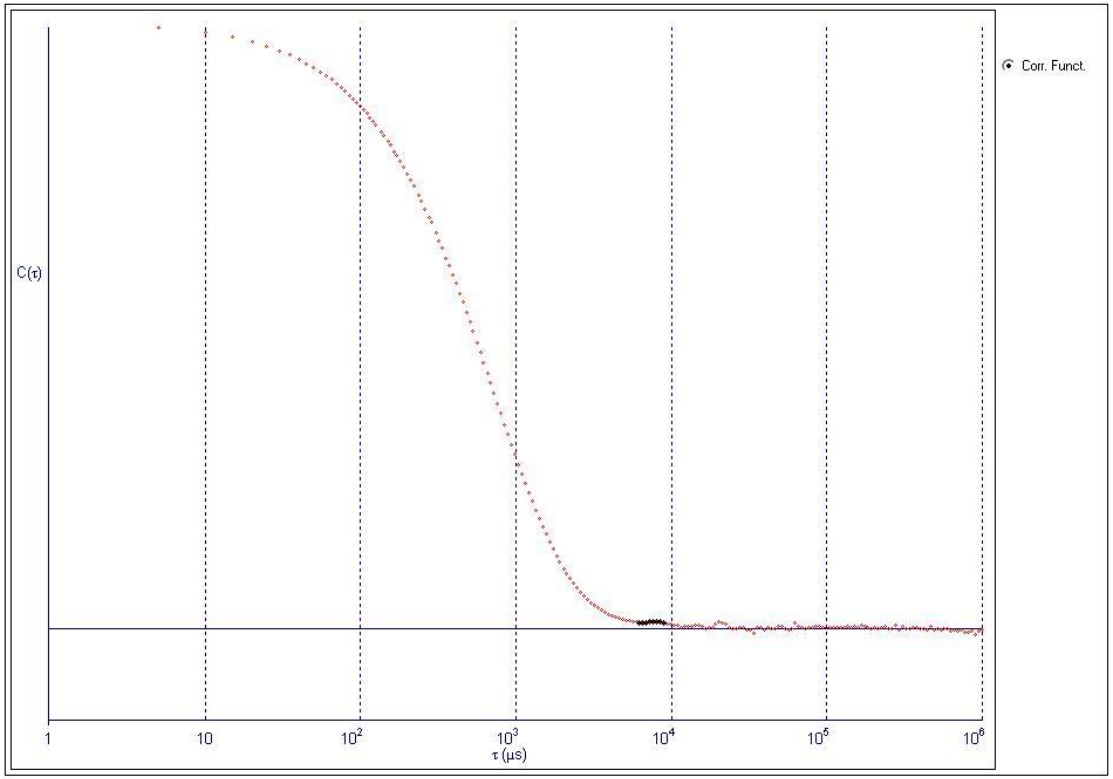


Run	Eff. Diam. (nm)	Half Width (nm)	Polydispersity	Baseline Index
1	268.1	178.6	0.444	0.0/ 12.44%
2	282.4	170.7	0.366	0.0/ 38.50%
3	264.5	164.1	0.385	0.0/ 8.44%
4	218.7	125.7	0.330	4.0/ 24.89%
5	247.3	153.7	0.386	0.0/ 32.00%
6	274.0	170.3	0.386	0.0/ 50.67%
7	281.9	176.2	0.391	0.0/ 23.11%
8	320.7	214.8	0.449	0.0/ 0.44%
9	287.6	179.7	0.391	0.0/ 17.78%
10	243.8	149.6	0.376	0.9/ 16.00%
Mean	268.9	168.3	0.390	0.5/ 22.43%
Std. Error	8.8	7.4	0.011	0.4/ 4.71
Combined	267.3	164.7	0.380	0.0/ 22.43%

Figure A.37. DLS analysis of Sample 37.

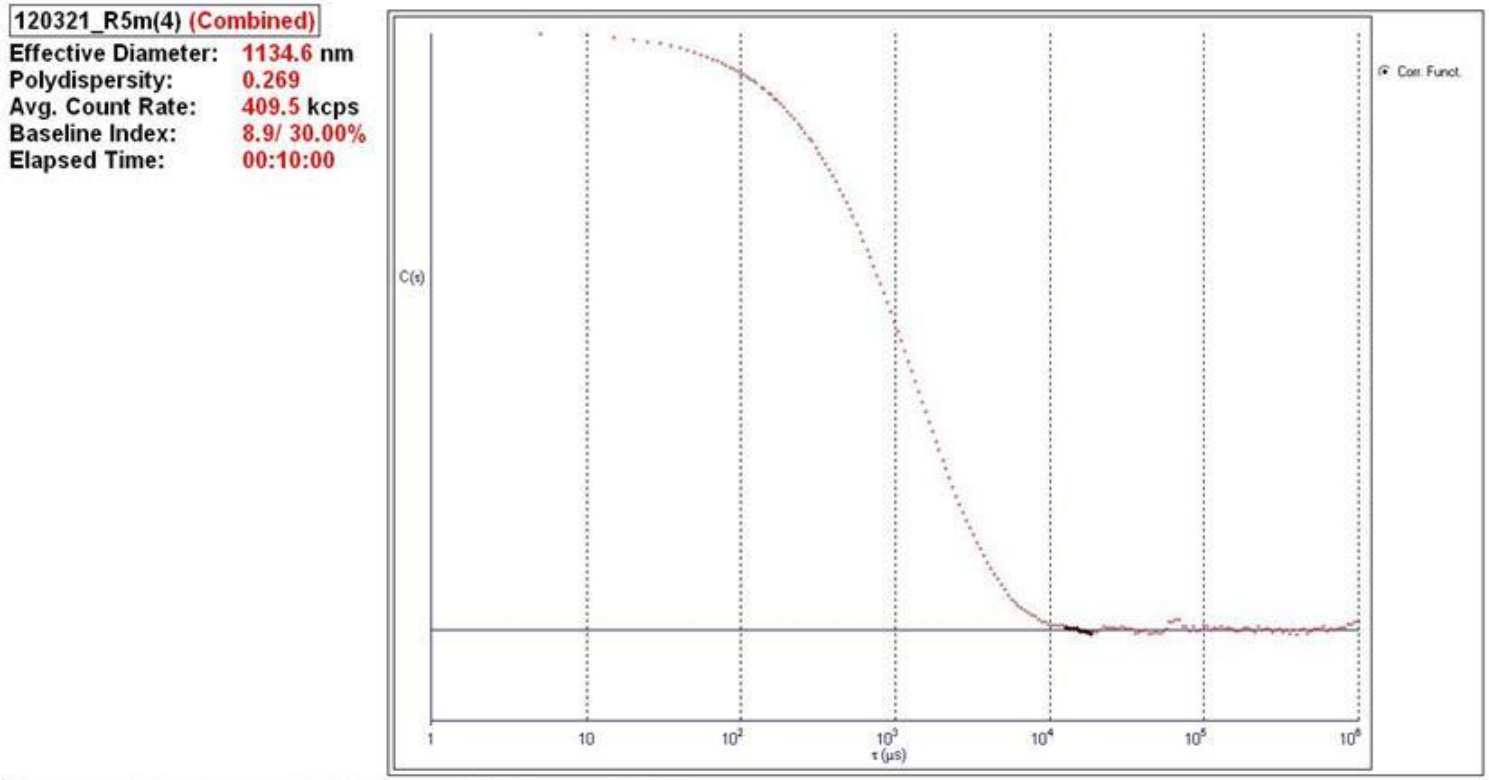
111020_R5m (Combined)

Effective Diameter:	**562.6 nm**
Polydispersity:	**0.214**
Avg. Count Rate:	**392.0 kcps**
Baseline Index:	**2.9/ 37.78%**
Elapsed Time:	**00:10:00**



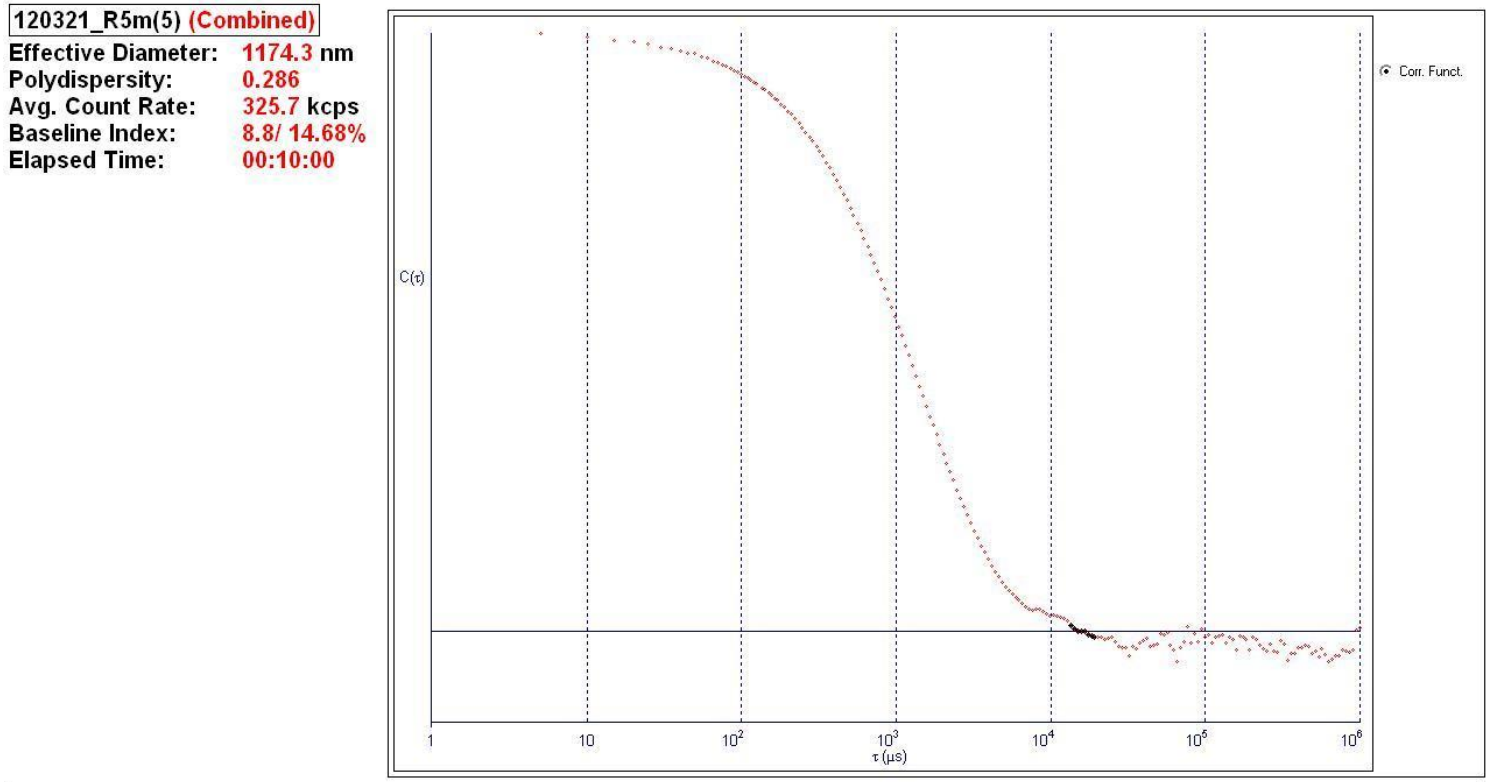
Run	Eff. Diam. (nm)	Half Width (nm)	Polydispersity	Baseline Index
1	607.2	327.8	0.291	0.0/ 23.45%
2	591.1	257.2	0.189	9.0/ 38.50%
3	550.3	201.3	0.134	2.5/ 22.57%
4	571.3	237.1	0.172	0.0/ 38.50%
5	528.4	268.9	0.259	0.0/ 14.67%
6	523.2	176.6	0.114	0.0/ 44.69%
7	584.4	296.9	0.258	5.8/ 45.33%
8	564.5	287.5	0.259	8.0/ 54.42%
9	543.8	273.8	0.254	9.8/ 36.73%
10	553.6	267.8	0.234	10.0/ 58.85%
Mean	561.8	259.5	0.216	4.5/ 37.77%
Std. Error	8.6	14.1	0.019	1.4/ 4.47
Combined	562.6	260.2	0.214	2.9/ 37.78%

Figure A.38. DLS analysis of Sample 38.



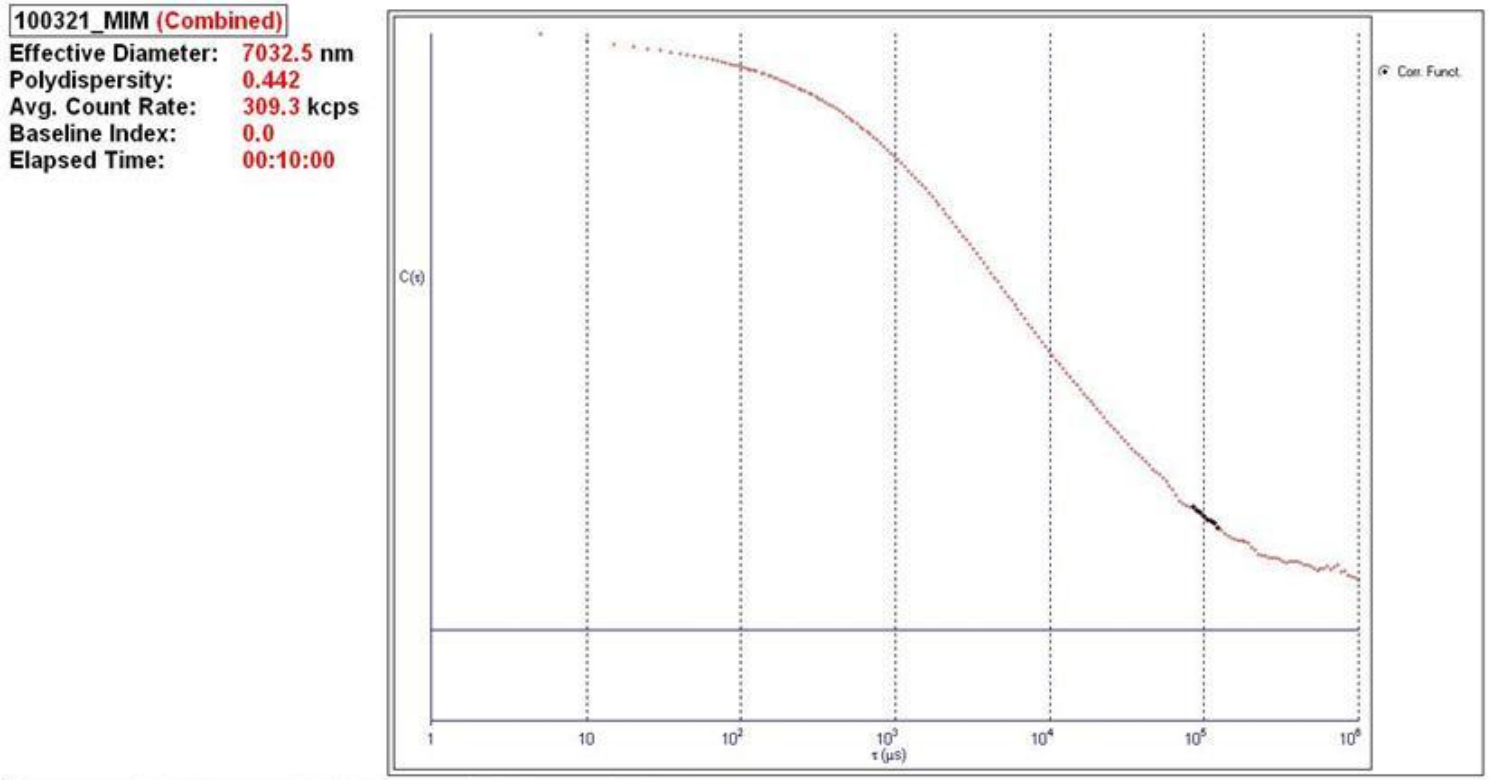
Run	Eff. Diam. (nm)	Half Width (nm)	Polydispersity	Baseline Index
1	1204.6	657.1	0.298	0.4/ 50.88%
2	1078.6	571.2	0.280	8.6/ 33.63%
3	1060.5	216.4	0.042	0.0/ 30.53%
4	1137.0	552.4	0.236	4.4/ 52.21%
5	1101.6	562.9	0.261	8.0/ 63.72%
6	1051.7	454.1	0.186	0.0/ 10.18%
7	1232.3	838.3	0.463	0.0/ 13.33%
8	1092.1	712.6	0.426	0.0/ 11.06%
9	1109.7	570.4	0.264	2.2/ 21.33%
10	1372.0	867.3	0.400	0.0/ 12.89%
Mean	1144.0	600.3	0.286	2.4/ 29.98%
Std. Error	31.4	59.4	0.039	1.1/ 6.22
Combined	1134.6	588.6	0.269	8.9/ 30.00%

Figure A.39. DLS analysis of Sample 39.



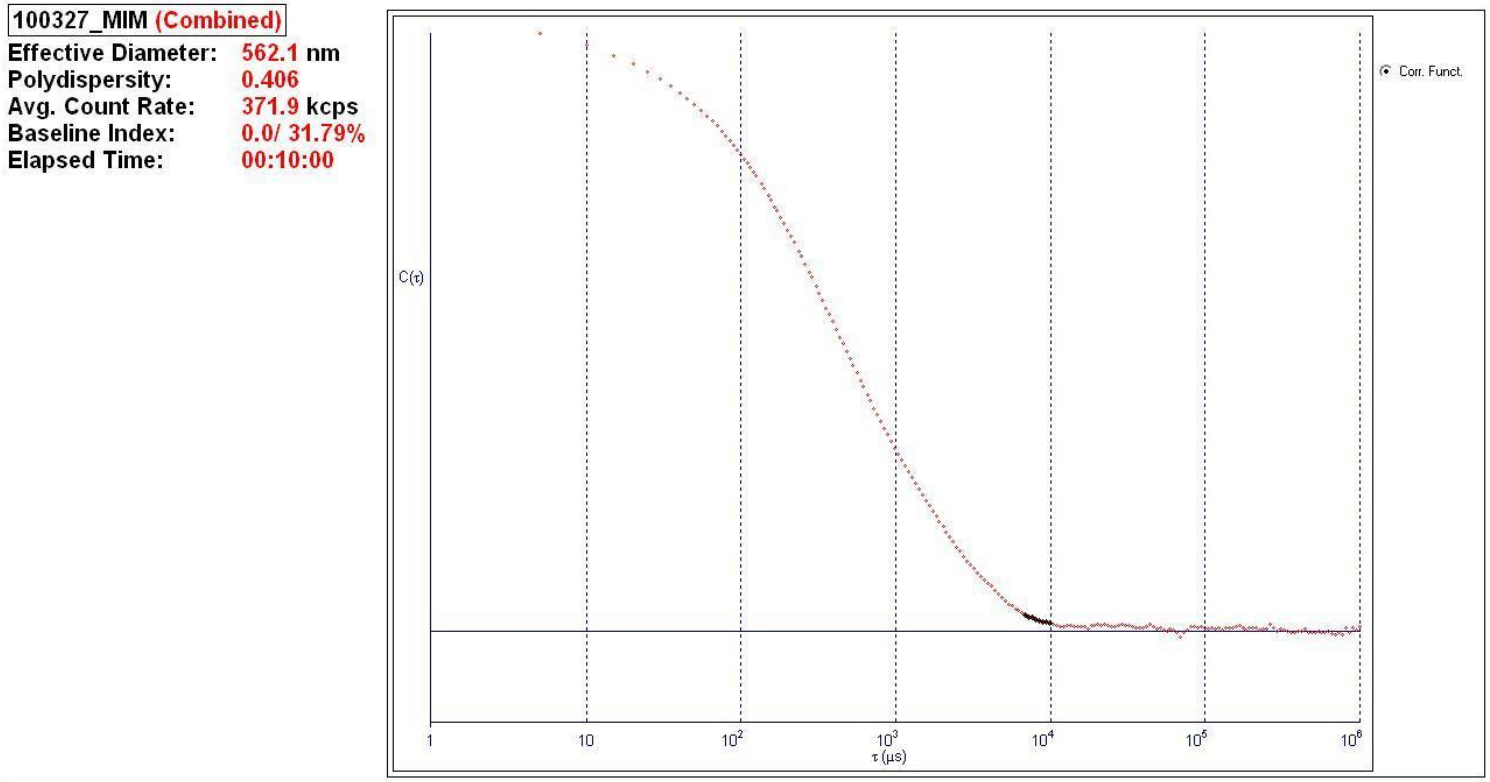
Run	Eff. Diam. (nm)	Half Width (nm)	Polydispersity	Baseline Index
1	1037.2	543.8	0.275	0.0/ 25.66%
2	1112.3	530.6	0.228	0.0/ 15.04%
3	0.0	0.0	0.000	0.0/ 0.00%
4	1122.4	633.8	0.319	5.6/ 14.67%
5	1468.1	857.6	0.341	0.0/ 15.11%
6	1271.9	696.7	0.300	0.0/ 19.91%
7	1133.1	607.5	0.287	1.1/ 17.70%
8	1989.2	1527.7	0.590	9.5/ 7.11%
9	1297.9	860.3	0.439	0.0/ 8.44%
10	1517.7	783.1	0.266	0.0/ 8.41%
Mean	1195.0	704.1	0.305	1.6/ 13.21%
Std. Error	159.7	120.1	0.047	1.0/ 2.33
Combined	1174.3	627.5	0.286	8.8/ 14.68%

Figure A.40. DLS analysis of Sample 40.



Run	Eff. Diam. (nm)	Half Width (nm)	Polydispersity	Baseline Index
1	8064.6	5235.6	0.421	0.0
2	5778.6	3737.7	0.418	0.0
3	9238.3	6354.7	0.473	0.0
4	6053.5	4366.0	0.520	0.0
5	6075.6	4089.0	0.453	0.0
6	6648.4	4466.4	0.451	0.0
7	4659.8	2793.1	0.359	0.0
8	8136.0	5168.9	0.404	0.0
9	6329.8	4007.2	0.401	0.0
10	10262.1	7441.5	0.526	0.0
Mean	7124.7	4766.0	0.443	0.0
Std. Error	549.9	425.6	0.017	0.0
Combined	7032.5	4677.5	0.442	0.0

Figure A.41. DLS analysis of Sample 41.

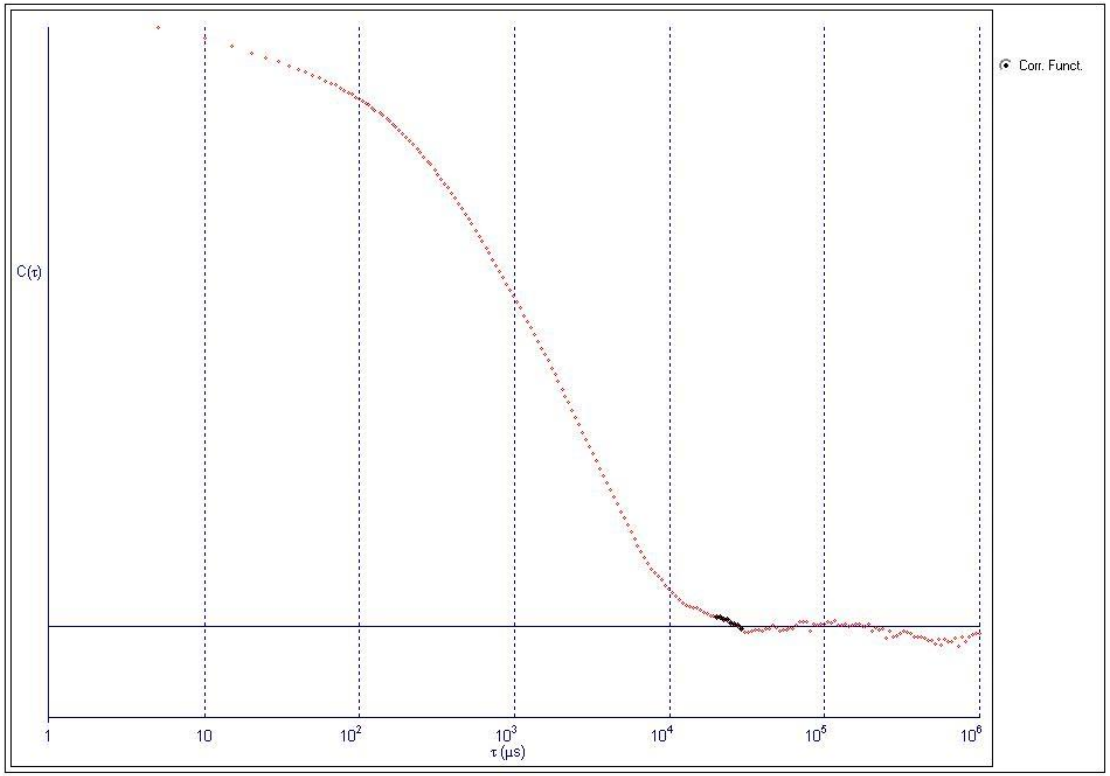


Run	Eff. Diam. (nm)	Half Width (nm)	Polydispersity	Baseline Index
1	586.5	363.7	0.384	0.0/ 49.78%
2	528.2	328.8	0.388	0.0/ 28.44%
3	589.2	380.2	0.416	7.5/ 29.78%
4	540.0	346.5	0.412	0.0/ 34.67%
5	569.4	351.0	0.380	0.2/ 41.78%
6	619.9	416.0	0.450	4.7/ 20.89%
7	493.3	322.9	0.428	0.0/ 21.68%
8	525.6	328.9	0.392	0.0/ 28.76%
9	566.2	363.5	0.412	0.0/ 34.22%
10	604.7	397.1	0.431	8.5/ 28.00%
Mean	562.3	359.9	0.409	2.1/ 31.80%
Std. Error	12.6	9.7	0.007	1.1/ 2.78
Combined	562.1	358.3	0.406	0.0/ 31.79%

Figure A.42. DLS analysis of Sample 42.

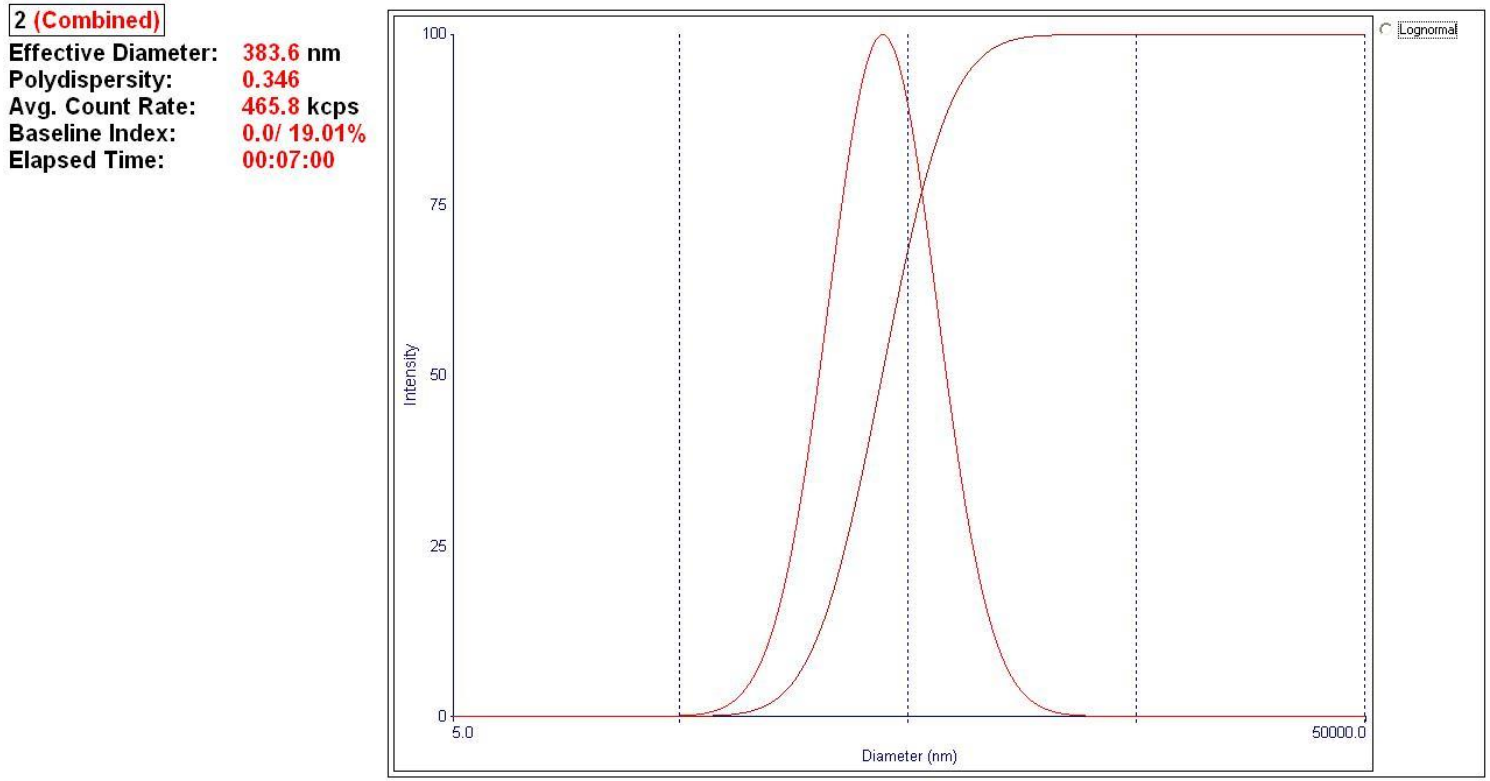
1 (Combined)

Effective Diameter:	**1671.9 nm**
Polydispersity:	**0.386**
Avg. Count Rate:	**236.8 kcps**
Baseline Index:	**5.6/ 26.35%**
Elapsed Time:	**00:10:00**



Run	Eff. Diam. (nm)	Half Width (nm)	Polydispersity	Baseline Index
1	1503.4	951.9	0.401	6.0/ 28.45%
2	1837.5	1082.5	0.347	0.0/ 32.77%
3	1879.5	1157.9	0.380	8.3/ 49.79%
4	1529.0	858.2	0.315	0.0/ 22.88%
5	1765.3	1169.4	0.439	0.0/ 19.66%
6	1670.6	989.3	0.351	7.9/ 33.33%
7	1485.5	987.4	0.442	0.0/ 15.38%
8	1323.1	816.1	0.380	0.0/ 10.73%
9	1606.7	995.7	0.384	0.0/ 22.65%
10	1511.1	1078.1	0.509	0.0/ 27.85%
Mean	1611.2	1008.6	0.395	2.2/ 26.35%
Std. Error	55.5	36.9	0.018	1.1/ 3.46
Combined	1671.9	1038.8	0.386	5.6/ 26.35%

Figure A.43. DLS analysis of Sample 43.



Run	Eff. Diam. (nm)	Half Width (nm)	Polydispersity	Baseline Index
1	512.7	353.5	0.475	0.8/ 8.85%
2	381.1	219.9	0.333	9.4/ 3.98%
3	388.3	236.6	0.371	0.0/ 35.68%
4	387.8	230.4	0.353	0.0/ 10.62%
5	0.0	0.0	0.000	0.0/ 0.00%
6	397.5	223.7	0.317	0.0/ 27.88%
7	369.7	209.8	0.322	0.0/ 32.74%
8	305.8	197.8	0.419	0.0/ 6.64%
9	0.0	0.0	0.000	0.0/ 2.21%
10	424.6	244.5	0.332	0.0/ 15.49%
Mean	379.3	223.3	0.349	1.3/ 19.00%
Std. Error	13.8	6.0	0.014	1.3/ 4.90
Combined	383.6	225.7	0.346	0.0/ 19.01%

Figure A.44. DLS analysis of Sample 44.

APPENDIX B: SEM IMAGES AND MEASUREMENTS

The following pages (110-127) include SEM images of samples mentioned at Chapter 5.

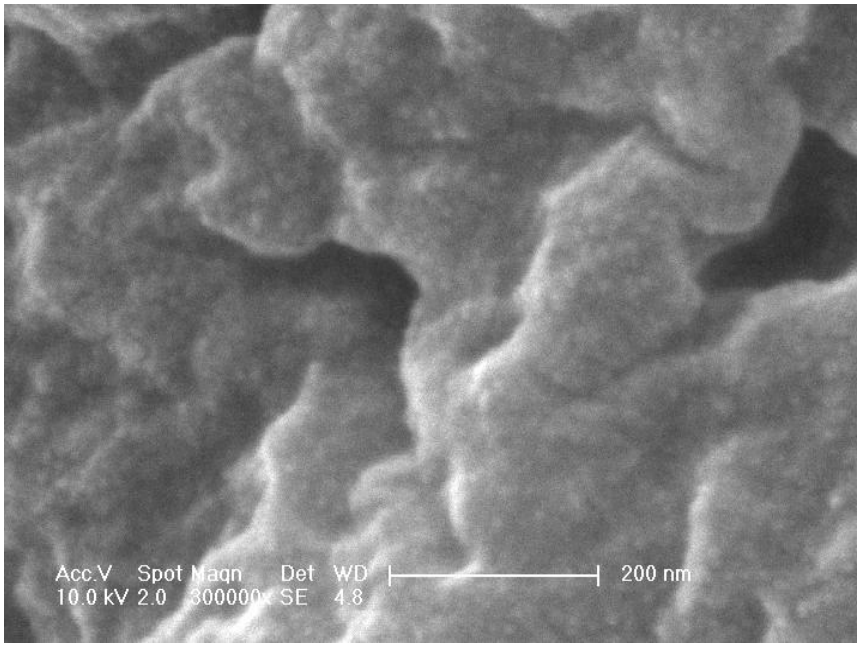


Figure B.1. SEM image of Sample 41.

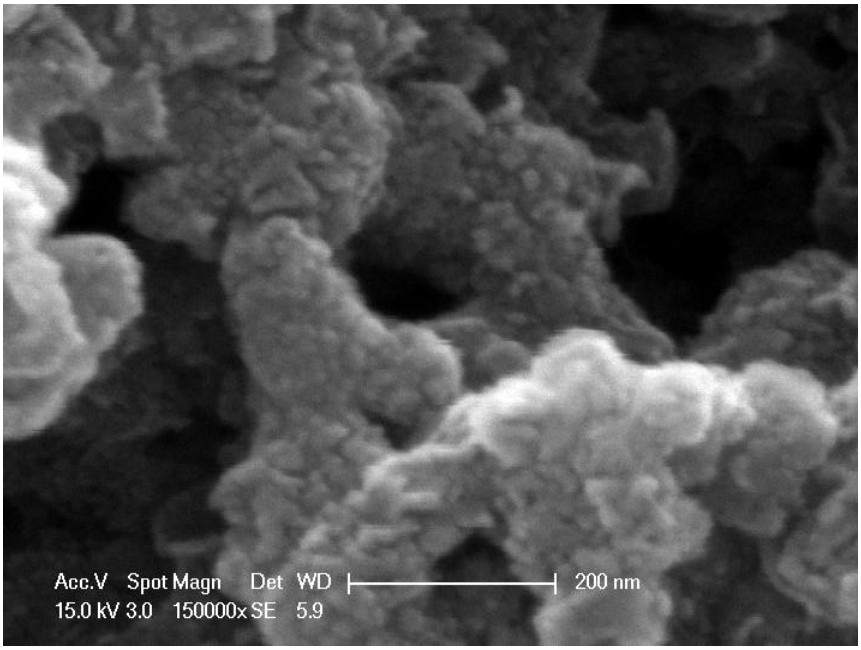


Figure B.2. SEM image of Sample 42.

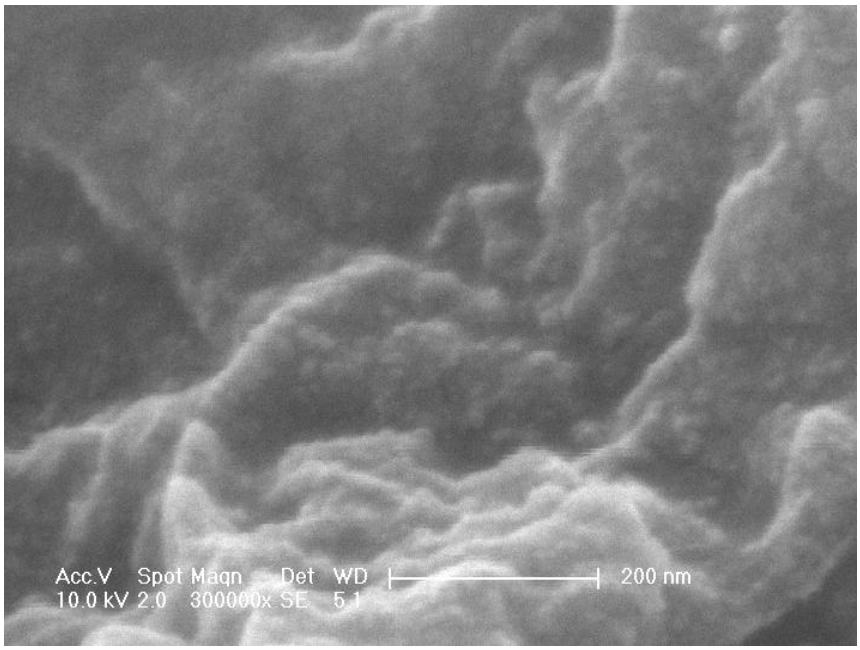


Figure B.3. SEM image of Sample 43.

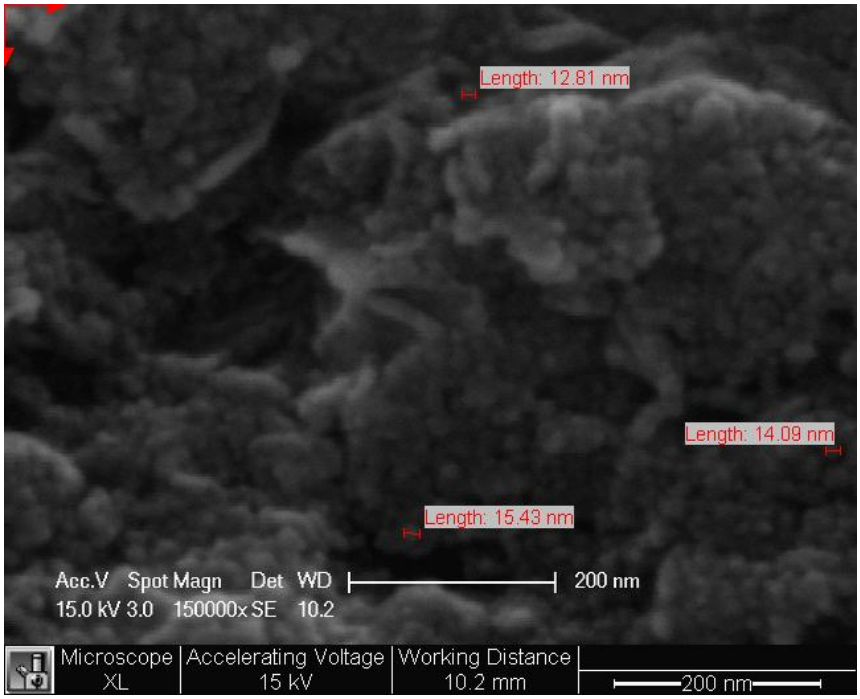


Figure B.4. SEM image of Sample 44 with measurements.

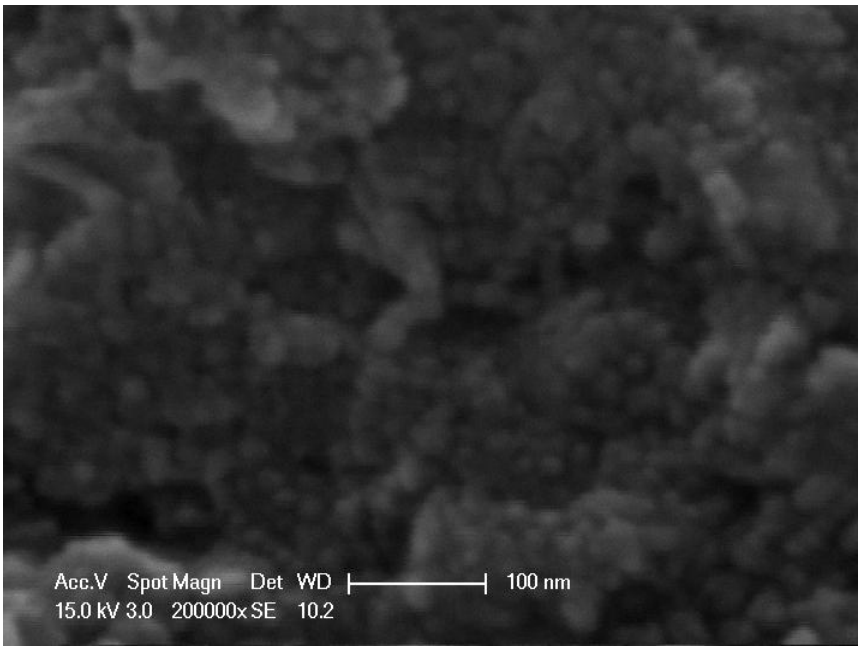


Figure B.5 SEM image of Sample 44 from another part.

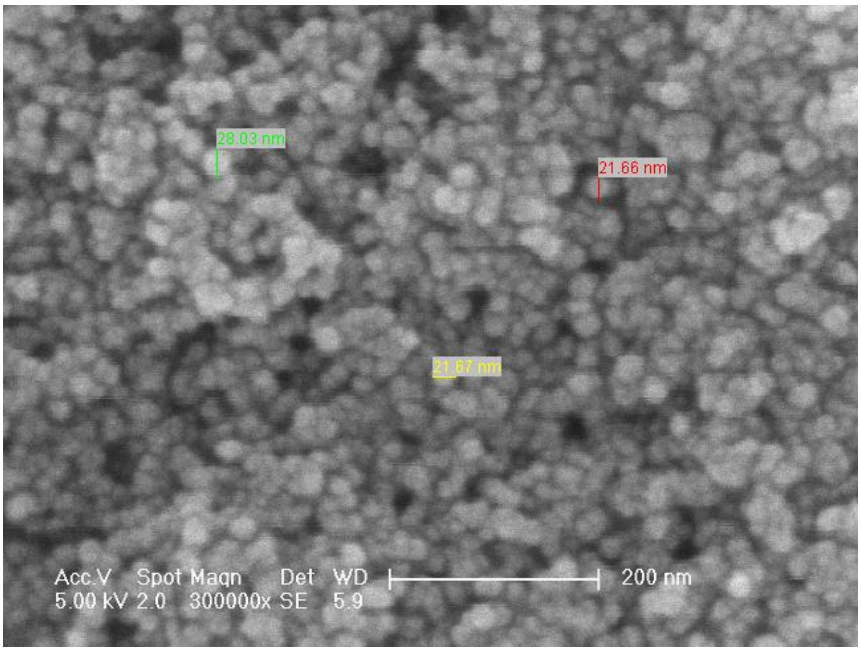


Figure B.6 SEM image of Sample 38.

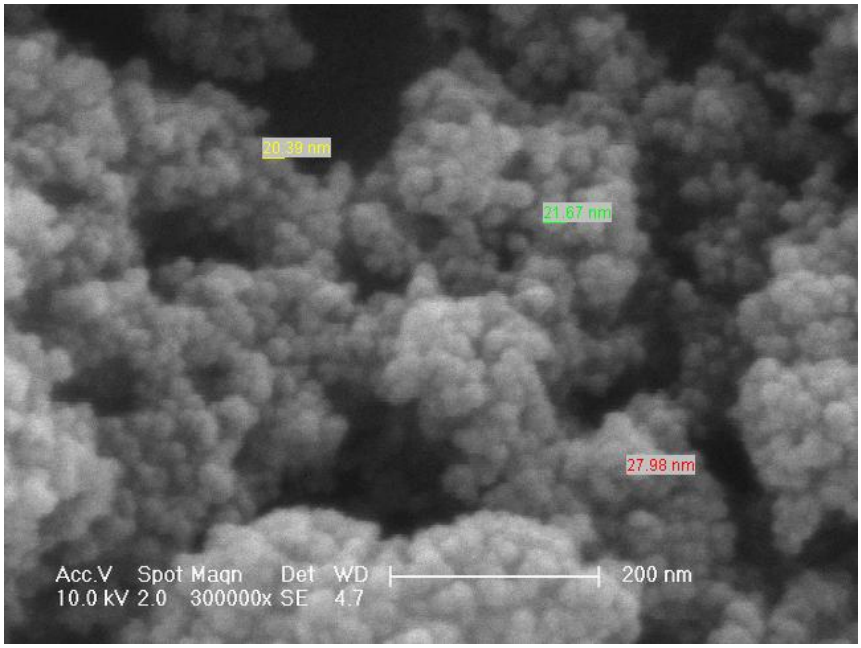


Figure B.7. SEM image of Sample 40.

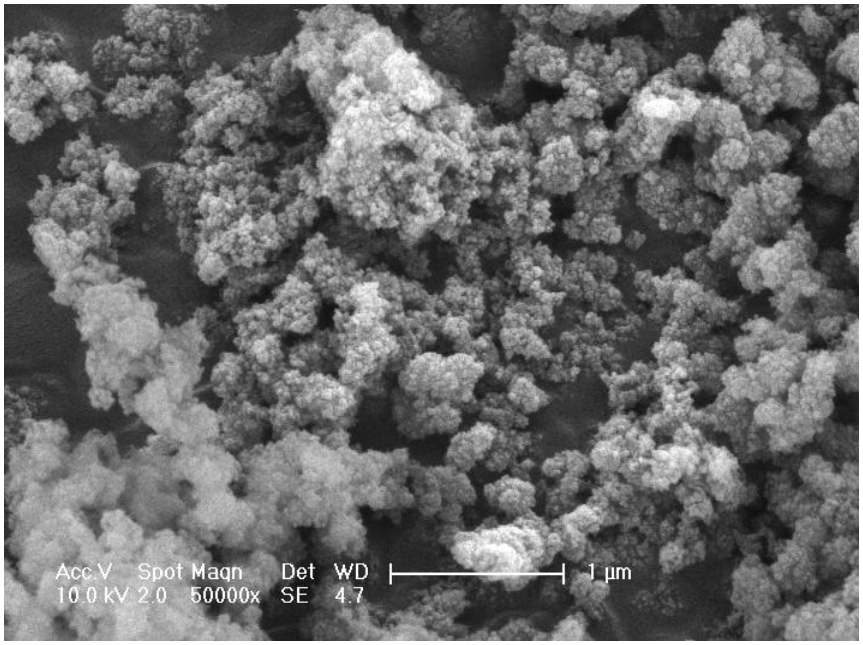


Figure B.8. SEM image of Sample 40 from another part.

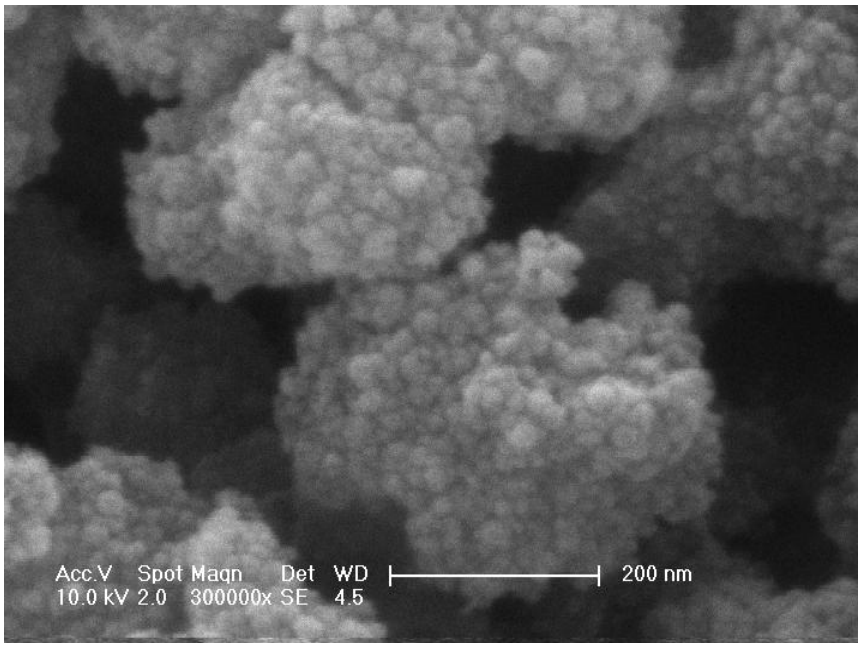


Figure B.9. SEM image of Sample 39.

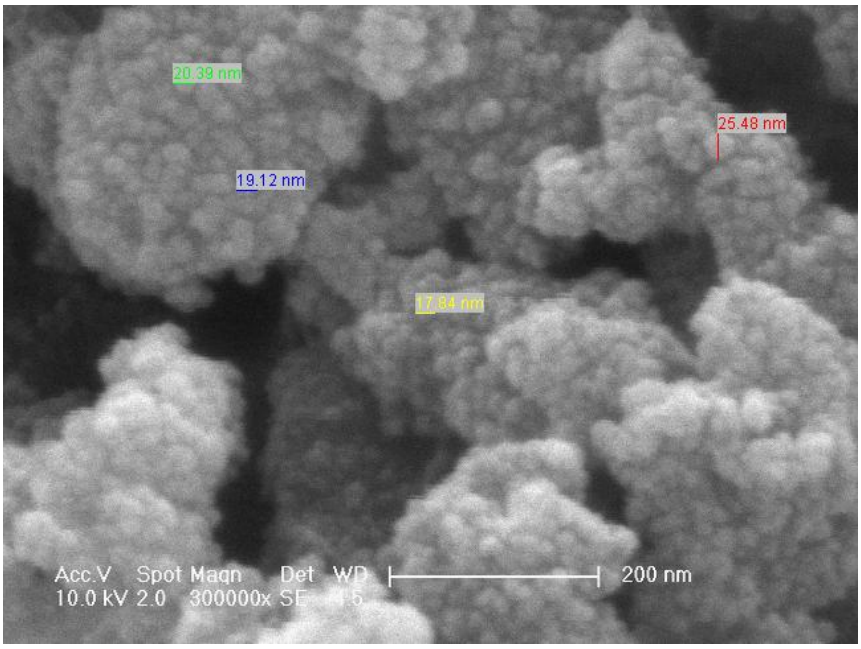


Figure B.10. SEM image of Sample 39 from another part, with measurements.

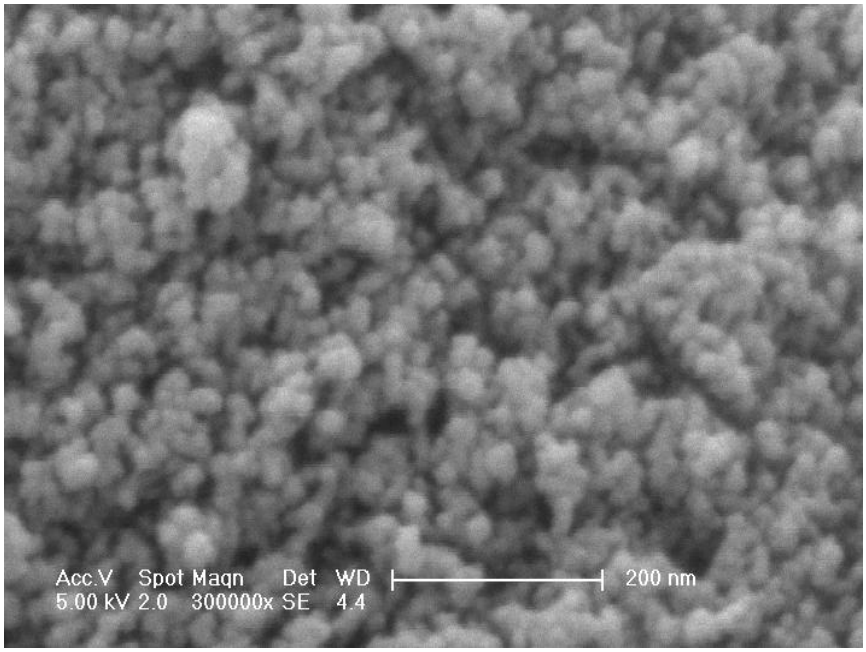


Figure B.11. SEM image of Sample 47.

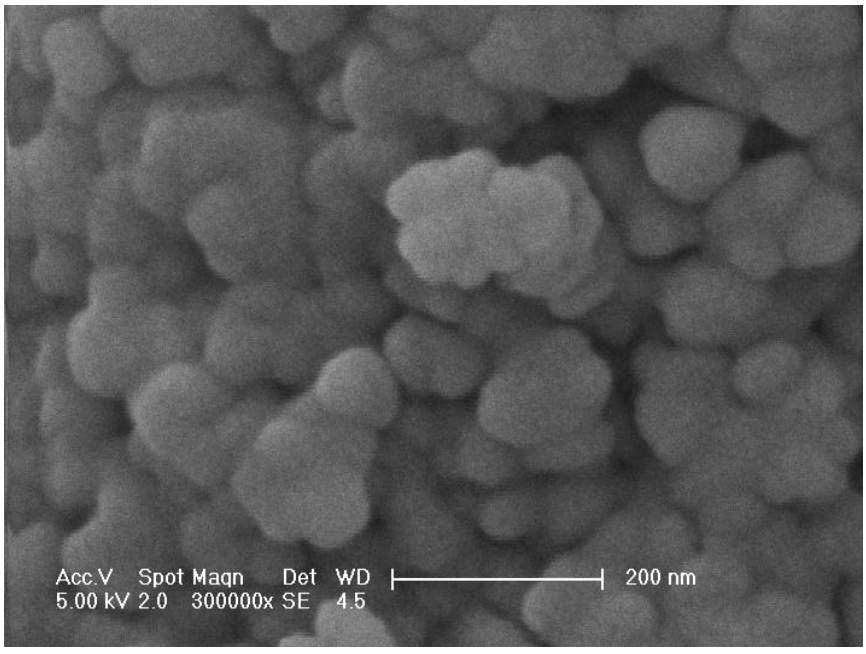


Figure B.12. SEM image of Sample 47 from another part.

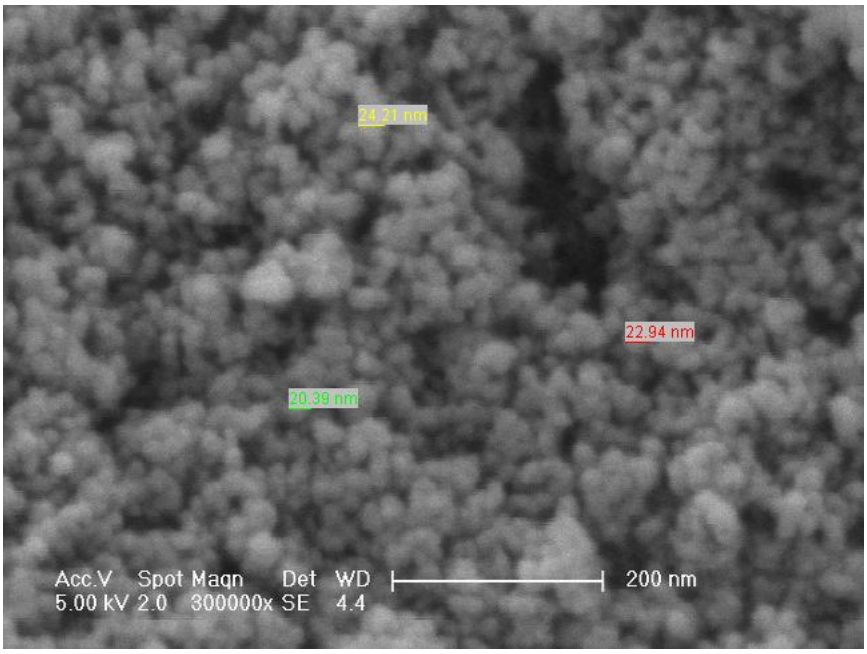


Figure B.13. SEM image of Sample 47 from another part, with measurements.

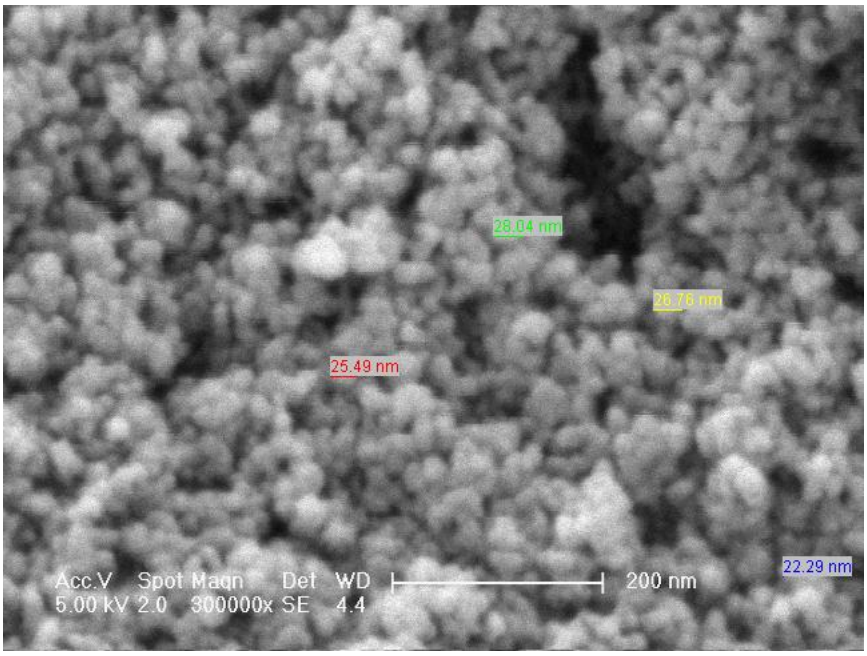


Figure B.14. SEM image of Sample 47 from another part, with measurements.

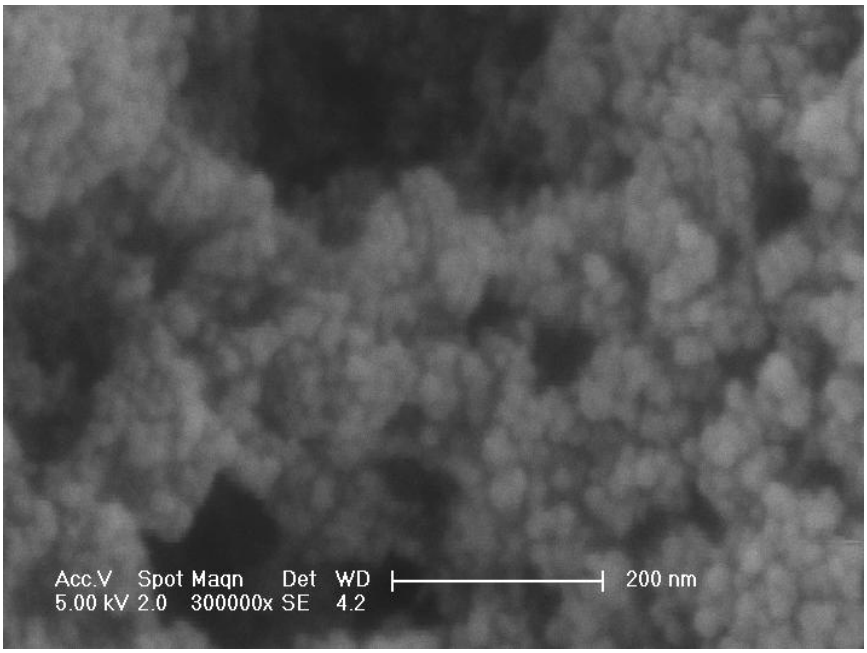


Figure B.15. SEM image of Sample 48.

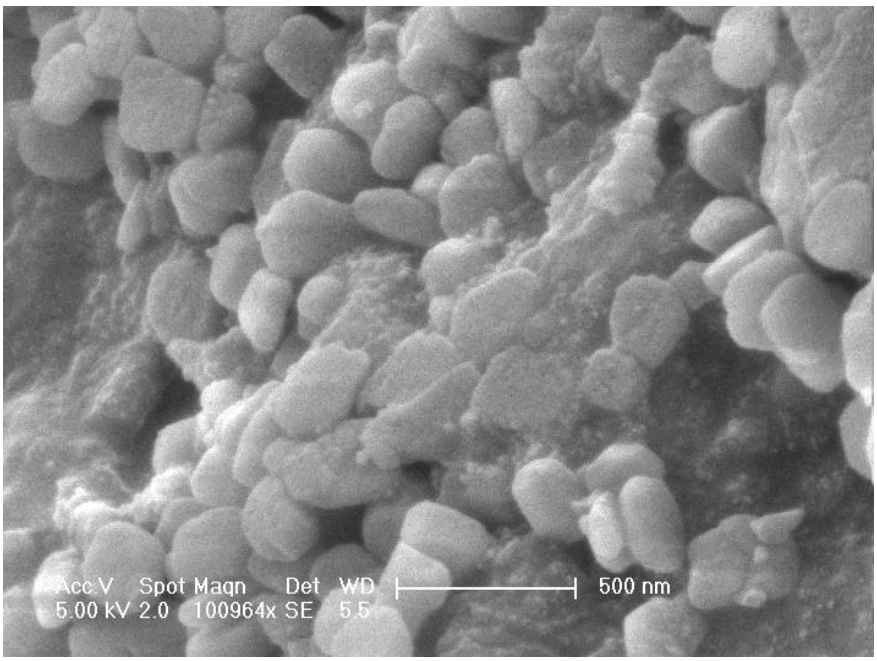


Figure B.16. SEM image of Sample 53.

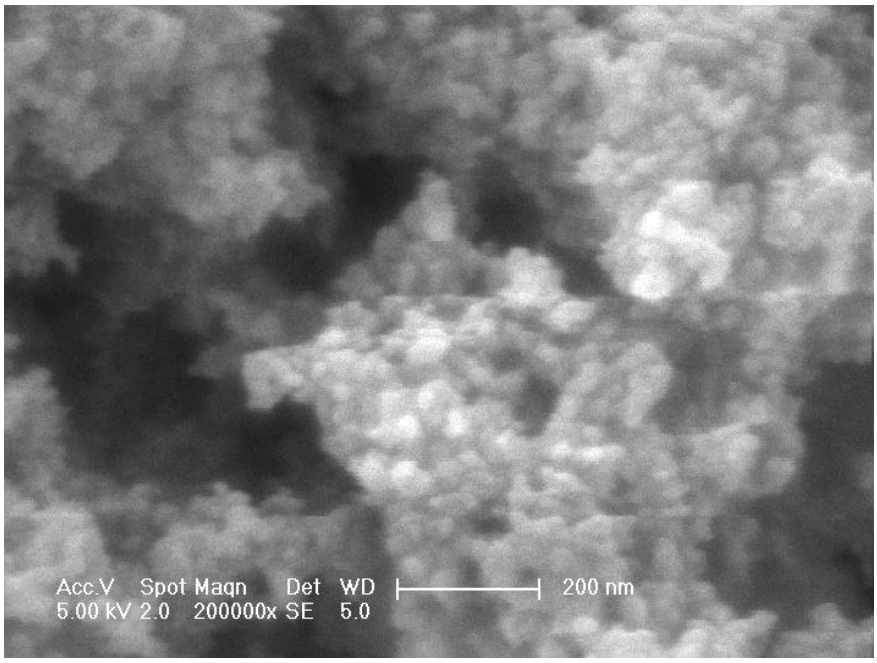


Figure B.17. SEM image of Sample 53 from another part.

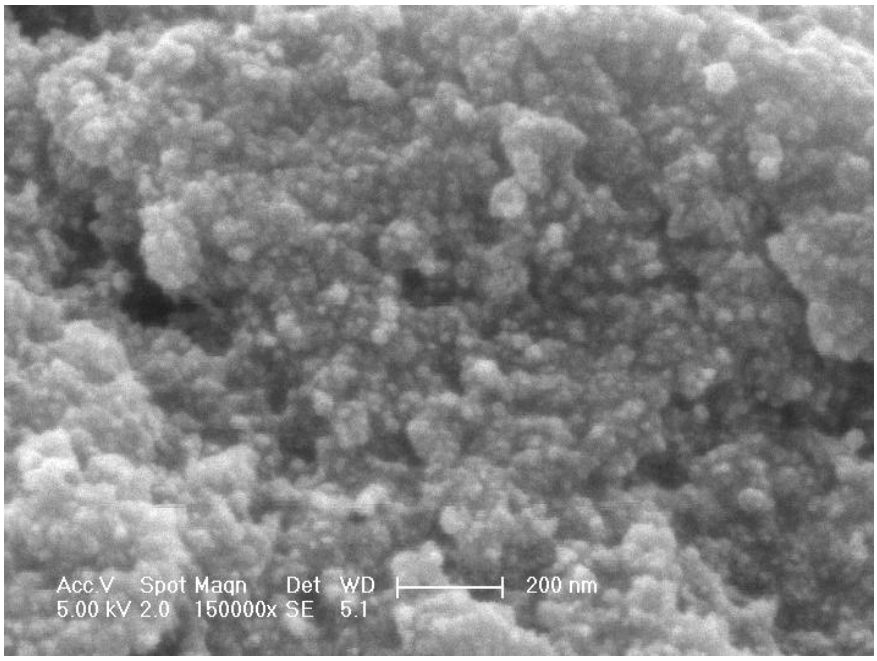


Figure B.18. SEM image of Sample 54.

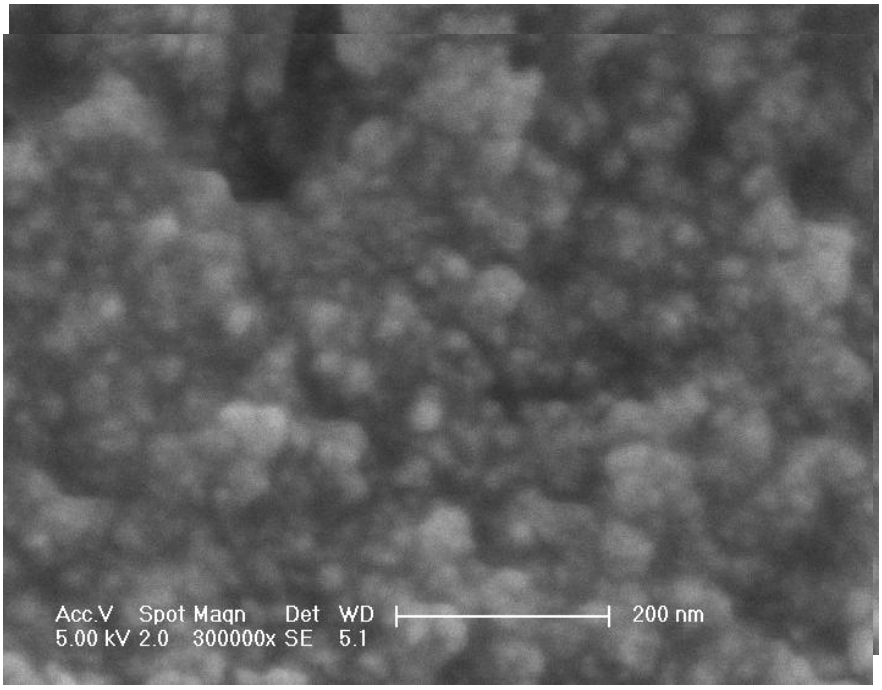


Figure B.19. SEM image of Sample 54 from another part.

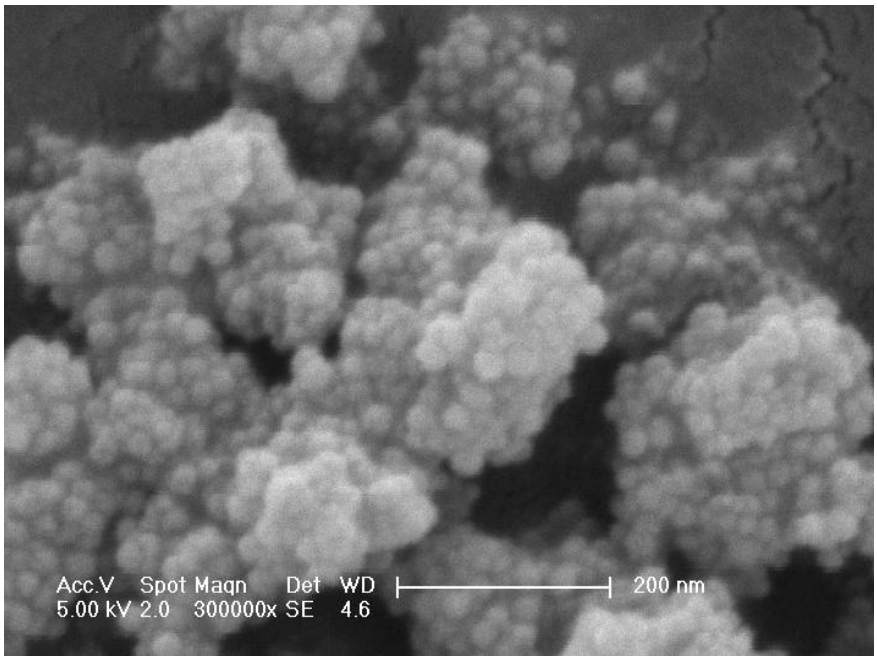


Figure B.20. SEM image of Sample 56.

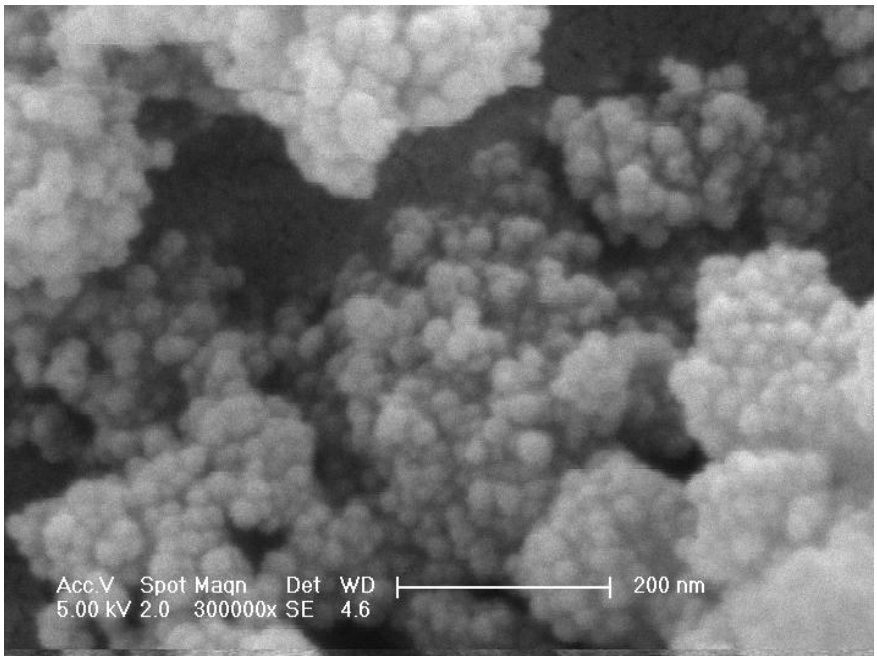


Figure B.21. SEM image of Sample 56 from another part.

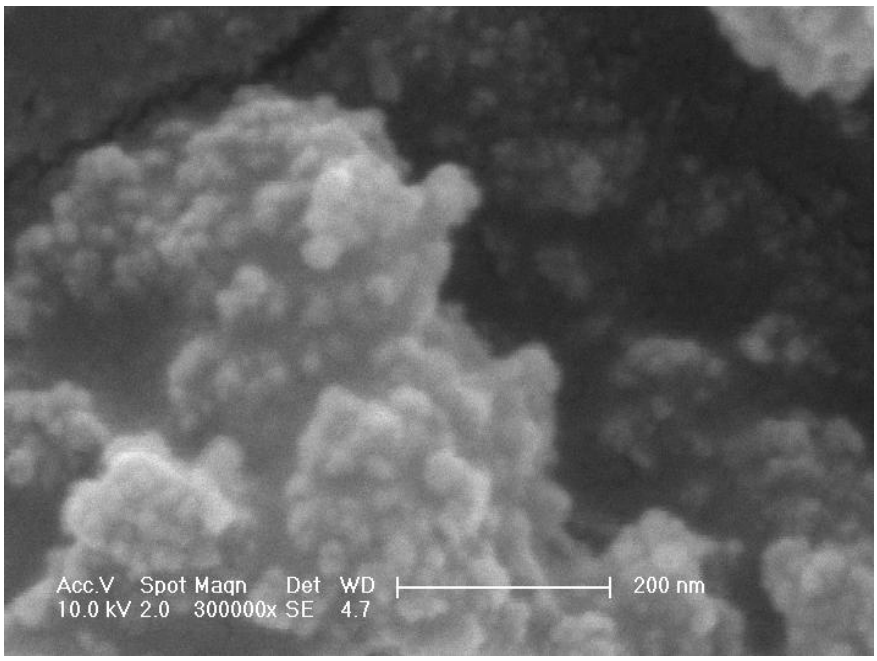


Figure B.22. SEM image of Sample 57.

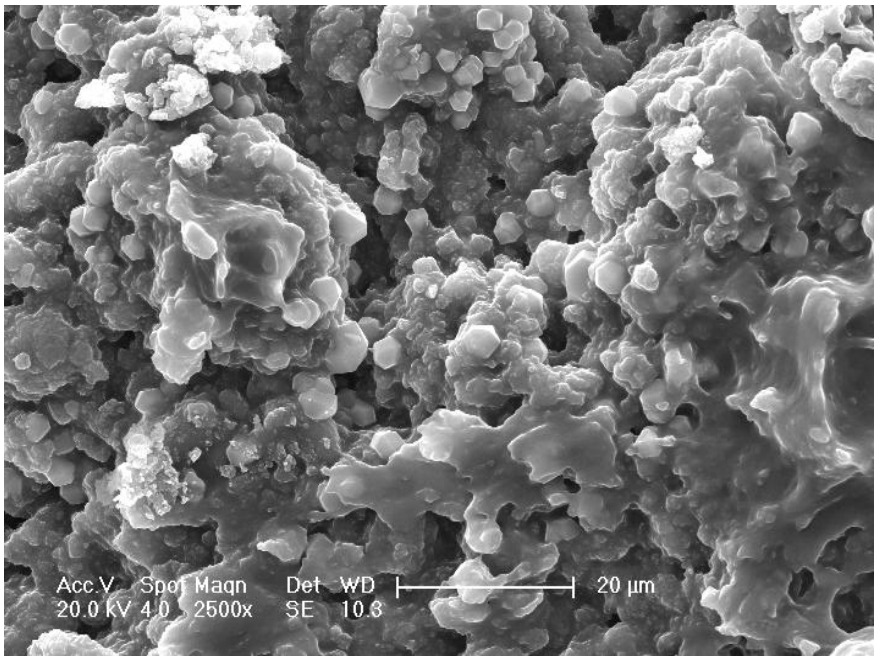


Figure B.23. SEM image of Sample 57 from another part.

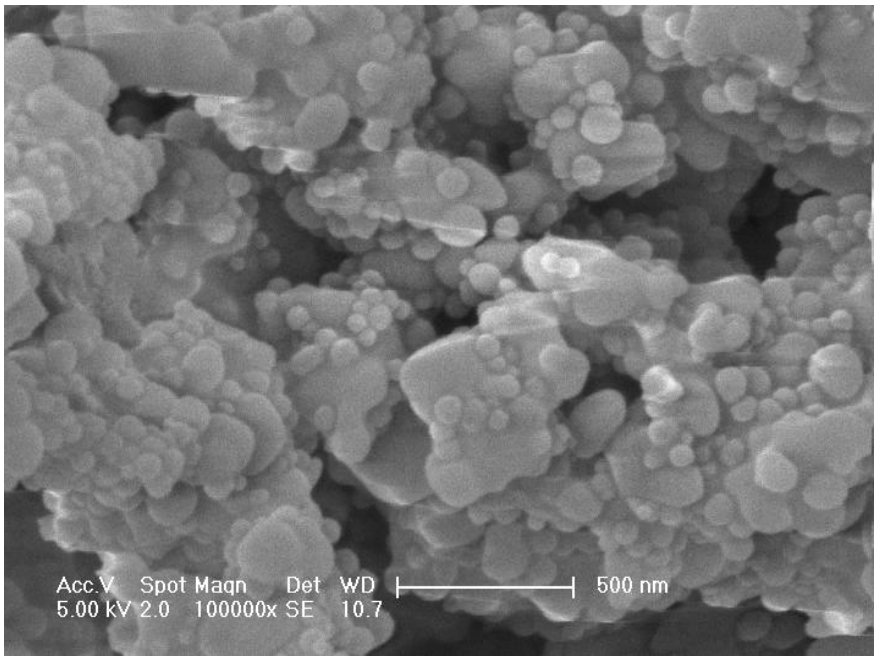


Figure B.24. SEM image of Sample 58.

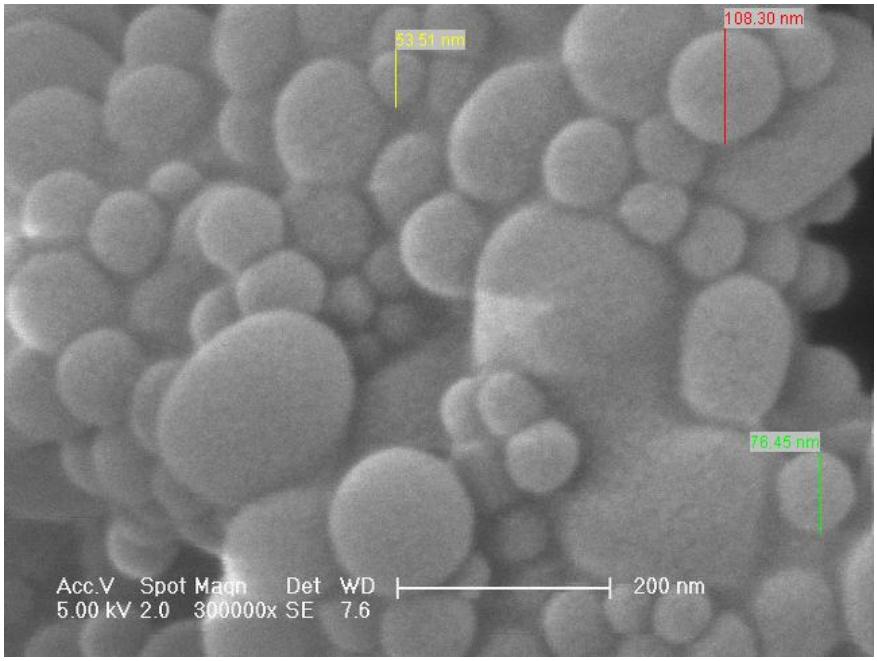


Figure B.25. SEM image of Sample 58 from another part, with measurements.

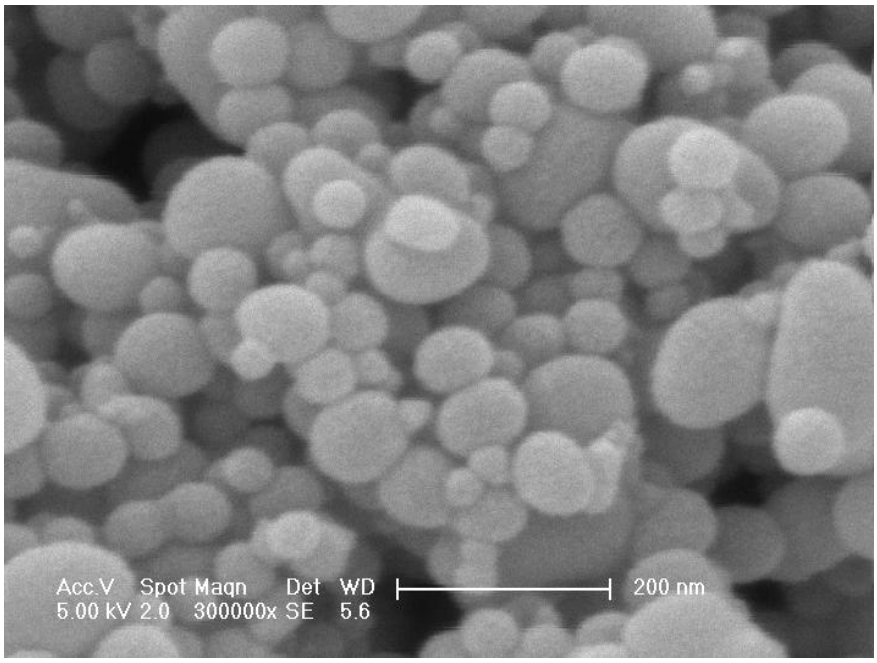


Figure B.26. SEM image of Sample 59.

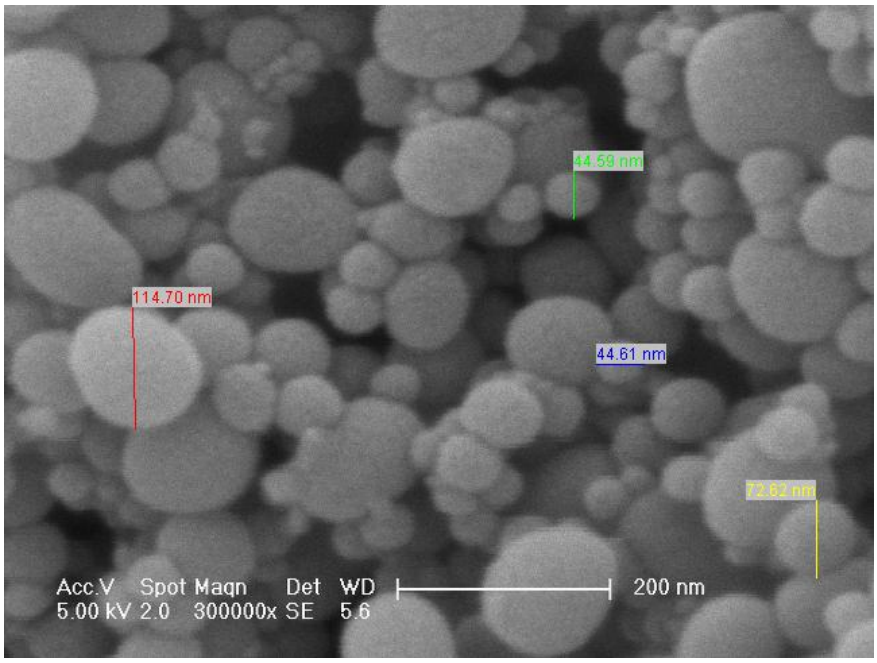


Figure B.27. SEM image of Sample 59 from another part, with measurements.

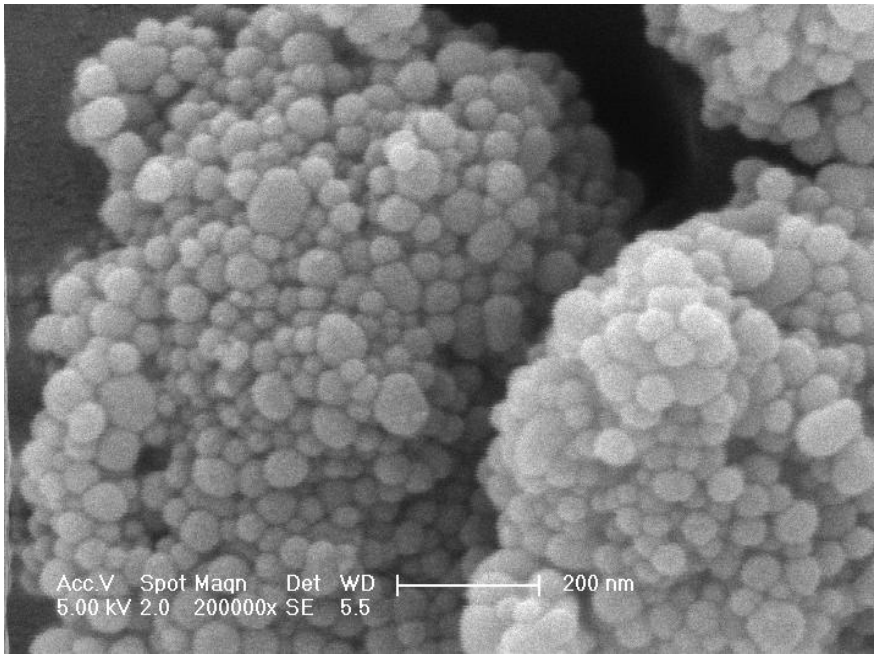


Figure B.28. SEM image of Sample 60.

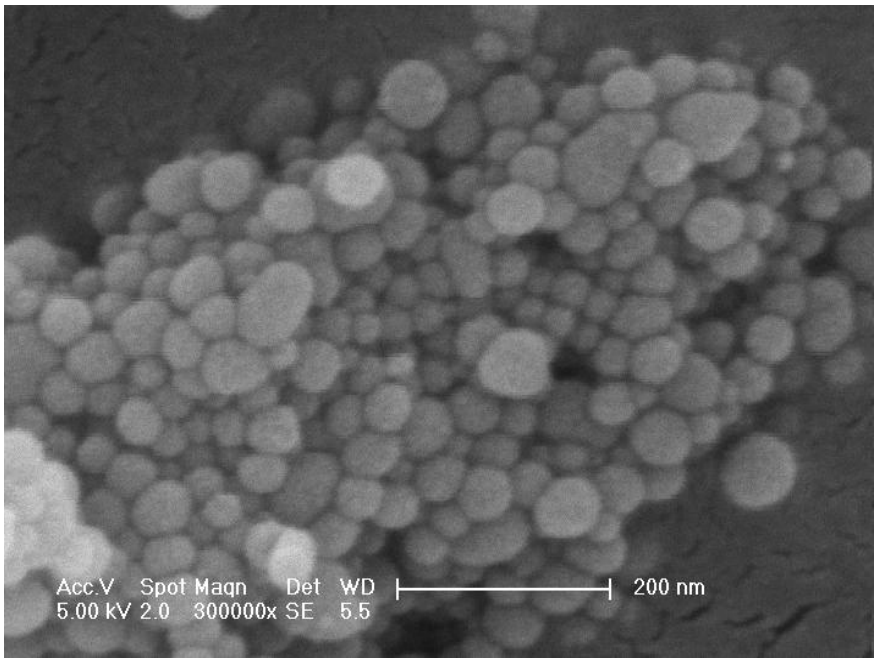


Figure B.29. SEM image of Sample 60 from another part.

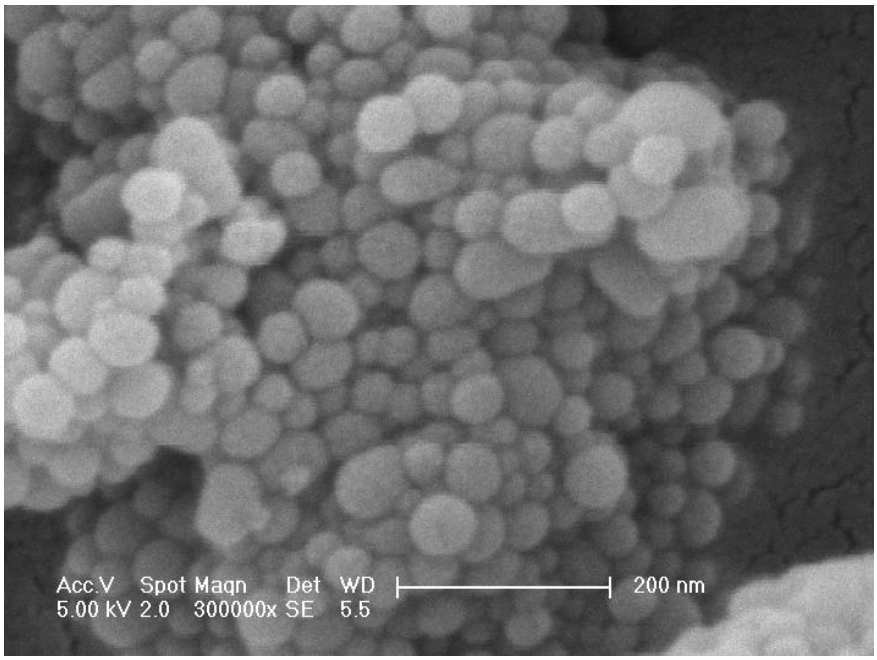


Figure B.30. SEM image of Sample 60 taken from another part.

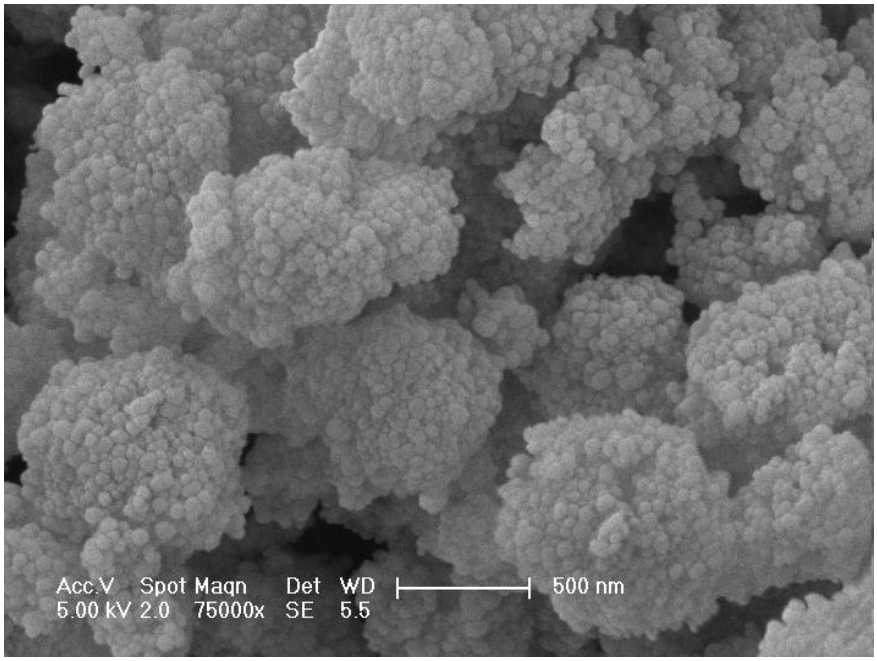


Figure B.31. SEM image of Sample 60 taken from somewhere else within the sample.

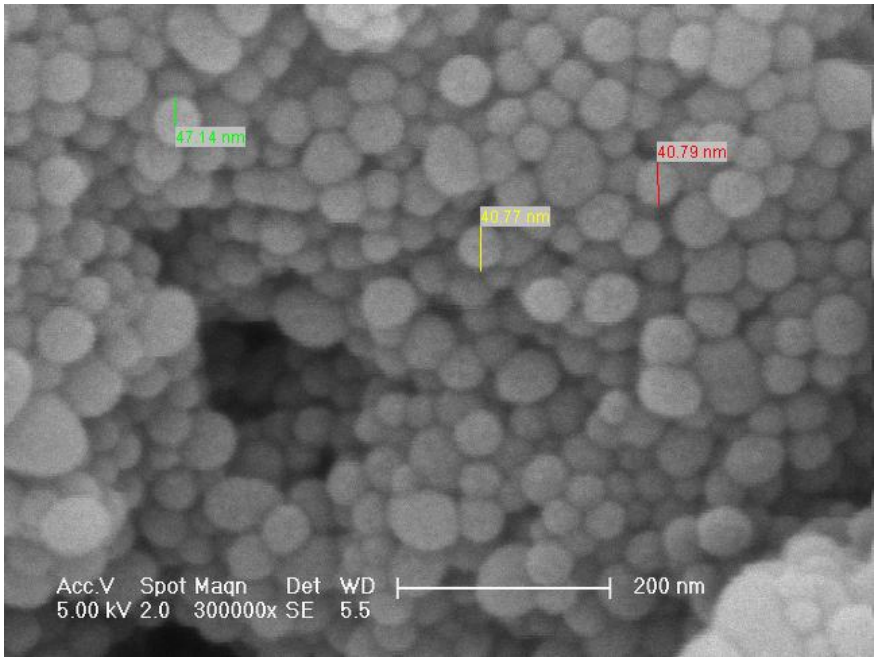


Figure B.32. SEM image of Sample 60 wtih measurements.

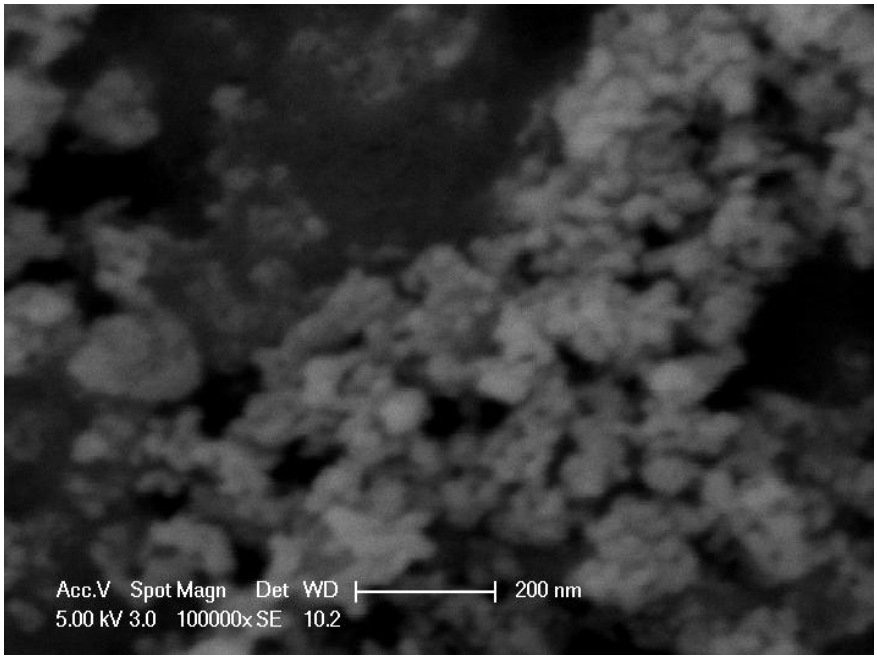


Figure B.33. SEM image of Sample 62.

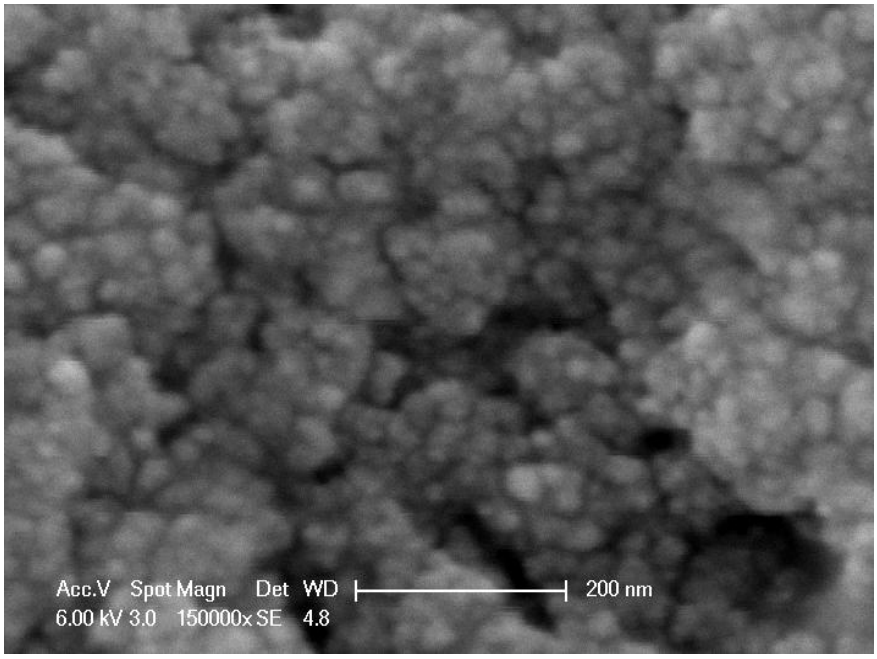


Figure B.34. SEM image of Sample 63.

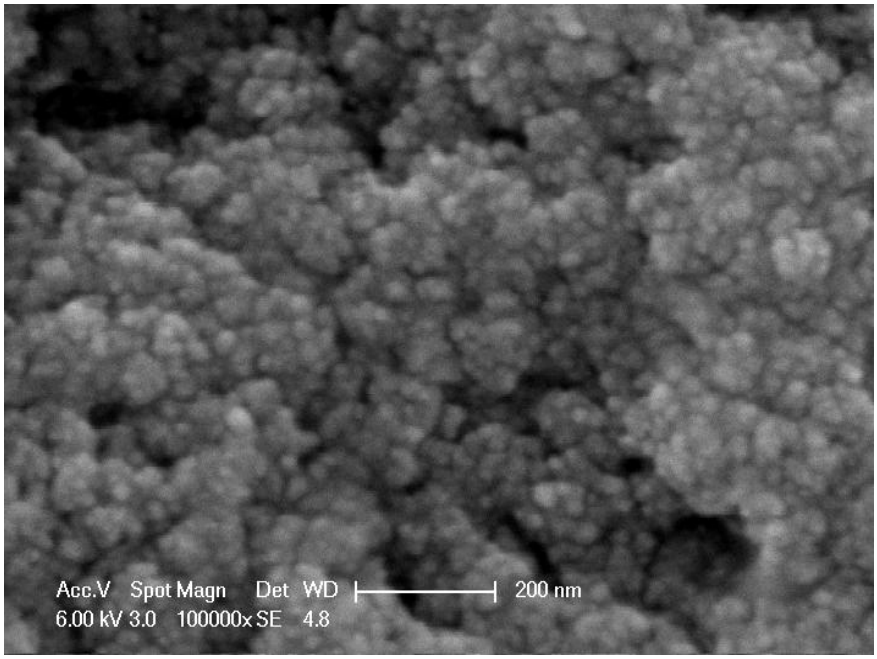


Figure B.35. SEM image of Sample 63 from another part.

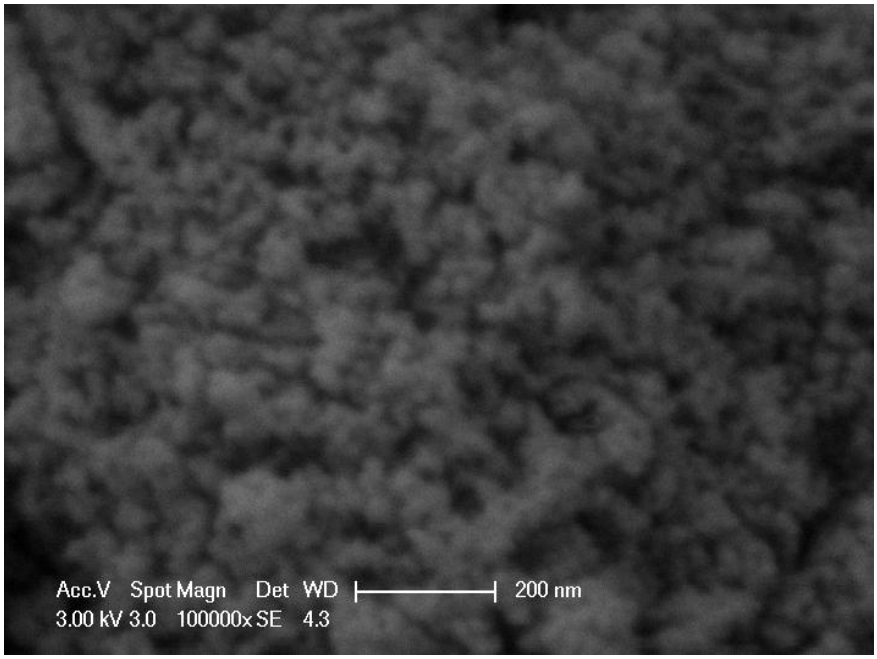


Figure B.36. SEM image of Sample 64.

APPENDIX C: LIST OF SAMPLES

Table C.1. List of all samples and the reaction conditions they were synthesized in.

<table>
<tr><th>Sample No</th><th>The type of reaction it was synthesized in</th><th>Oil</th><th>R</th><th>[AOT] (M)</th></tr>
<tr><td>1</td><td rowspan="24">Silica NP</td><td rowspan="16">n-heptane</td><td rowspan="9">5</td><td rowspan="24">0.1</td></tr>
<tr><td>2</td></tr>
<tr><td>3</td></tr>
<tr><td>4</td></tr>
<tr><td>5</td></tr>
<tr><td>6</td></tr>
<tr><td>8</td></tr>
<tr><td>9</td></tr>
<tr><td>10</td></tr>
<tr><td>16</td><td rowspan="4">7.5</td></tr>
<tr><td>18</td></tr>
<tr><td>19</td></tr>
<tr><td>20</td></tr>
<tr><td>22</td><td rowspan="3">10</td></tr>
<tr><td>23</td></tr>
<tr><td>24</td></tr>
<tr><td>25</td><td rowspan="8">n-decane</td><td rowspan="3">5</td></tr>
<tr><td>26</td></tr>
<tr><td>27</td></tr>
<tr><td>28</td></tr>
<tr><td>29</td><td rowspan="2">7.5</td></tr>
<tr><td>30</td></tr>
<tr><td>31</td><td rowspan="2">10</td></tr>
<tr><td>33</td></tr>
<tr><td>34</td><td rowspan="6">Si-coating of pre-prepared magnetite</td><td rowspan="14">n-heptane</td><td rowspan="14">5</td><td rowspan="4">0.1</td></tr>
<tr><td>35</td></tr>
<tr><td>36</td></tr>
<tr><td>37</td></tr>
<tr><td>38</td></tr>
<tr><td>39</td><td rowspan="2">0.75</td></tr>
<tr><td>40</td></tr>
<tr><td>41</td><td rowspan="4">Magnetite synthesis in ME</td><td rowspan="4">0.75</td></tr>
<tr><td>42</td></tr>
<tr><td>43</td></tr>
<tr><td>44</td></tr>
<tr><td>47</td><td rowspan="2">Si-coating of pre-prepared magnetite</td><td rowspan="2">0.75</td></tr>
<tr><td>48</td></tr>
<tr><td>53</td><td rowspan="2">“ In situ” Si-coating of magnetite</td><td rowspan="2">n-heptane</td><td rowspan="2">5</td><td rowspan="2">0.75</td></tr>
<tr><td>54</td></tr>
</table>

56				
57				
58				
59				
60				1
61				
62	Si-coating of pre-prepared magnetite			0.75
63	Magnetite synthesis in ME			
64	“ In situ” Si-coating of magnetite			

REFERENCES

1. Yang, H., S. Zhang, X. Chen, Z. Zhuang, J. Xu, and X. Wang, "Magnetite-Containing Spherical Silica Nanoparticles for Biocatalysis and Bioseparations", *Analytical Chemistry*, Vol. 76, No. 5, pp. 1316-1321, 2004.

2. Klabunde, K. J., *Nanoscale Materials in Chemistry*, Wiley-Interscience, New York, 2001.

3. Hagura, N., W. Widiyastuti, F. Iskandar, and K. Okuyama, "Characterization of Silica-Coated Silver Nanoparticles Prepared by a Reverse Micelle and Hydrolysis-Condensation Process", *Chemical Engineering Journal*, Vol. 156, pp. 200-205, 2010.

4. Tago, T., T. Hatsuta, K. Miyajima, M. Kishida, S. Tashiro, and K. Wakabayashi, "Novel Synthesis of Silica-Coated Ferrite Nanoparticles Prepared Using Water-in-Oil Microemulsion", *Journal of American Ceramic Society*, Vol. 85, No. 9, pp. 2188-2194, 2002.

5. Lu, Z., J. Dai, X. Song, G. Wang, and W. Yang, "Facile Synthesis of Fe_3O_4/SiO_2 Composite Nanoparticles from Primary Silica Particles", *Colloids and Surfaces A: Physicochemical Engineering Aspects*, Vol. 317, pp. 450-456, 2008.

6. Gupta, A. K. and M. Gupta, "Synthesis and Surface Engineering of Iron Oxide Nanoparticles for Biomedical Applications", *Biomaterials*, Vol. 26, pp. 2995-4021, 2005.

7. Haw, C. Y., C. H. Chia, S. Zakaria, F. Mohamed, S. Radiman, C. H. Teh, P. S. Khiew, W. S. Chiu, and N. M. Huang, "Morphological Studies of Randomized Dispersion Magnetite Nanoclusters Coated with Silica", *Ceramics International*, Vol. 37, pp. 451-464, 2011.

8. Vestal, C. R. and Z. J. Zhang, “Synthesis and Magnetic Characterization of Mn and Co Spinel Ferrite-Silica Nanoparticles with Tunable Magnetic Core”, *Nanoletters*, Vol. 3, No. 12, pp. 1739-1743, 2003.

9. Iida, H., T. Nakanishi, H. Takada, and T. Osaka, “Preparation of Magnetic Iron-Oxide Nanoparticles by Successive Reduction-Oxidation in Reverse Micelles: Effects of Reducing Agent and Atmosphere”, *Electrochimica Acta*, Vol. 52, pp. 292-296, 2006.

10. Lee, H. S. and W. C. Lee, “A Comparison of Coprecipitation with Microemulsion Methods in the Preparation of Magnetite”, *Journal of Applied Physics*, Vol. 85, No. 8, pp. 5231-5233, 1999.

11. Gupta, A. J. and S. Wells, “Surface-Modified Superparamagnetic Nanoparticles for Drug Delivery: Preparation, Characterization, and Cytotoxicity Studies”, *IEEE Transactions on Nanobioscience*, Vol. 3, No. 1, pp. 66-73, 2004.

12. Ozdemir, T., D. Sandal, M. Culha, A. Sanyal, N. Z. Atay and S. Bucak, “Asembly of Magnetic Nanoparticles into Higher Structures on Patterned Magnetic Beads Under the Influence of Magnetic Field”, *Nanotechnology*, Vol. 21, No. 12, pp. 125603-125608, 2010.

13. Cuculayev, R., A. Sanyal, N. Z. Atay, M. Culha and S. Bucak, “The Effect of the Strength and Direction of Magnetic Field on the Assembly of Magnetic Nanoparticles into Higher Structures”, *Journal of Nanoscience and Nanotechnology*, Vol. 12, pp. 2761-2766, 2012.

14. Fornara, A., *Magnetic Nanostructured Materials for Advanced Bio-Applications*, Licentiate, Royal Institute of Technology, 2008.
15. Cornelis, K. and C. S. Hurlburt, *Manual of Mineralogy*, Wiley, New York, 1977.

16. Mixed Valence Chemistry – A Survey and Classification, *Chemexplore*, http://www.chemexplore.net/mixed-valent.htm, December 5, 2012.

17. Si, S., C. Li, X. Wang, D. Yu, Q. Peng, and Y. Li, "Magnetic Monodisperse Fe_3O_4 Nanoparticles", *Crystal Growth & Design*, Vol. 5, No. 2, pp. 391-393, 2005.

18. Watanabe, M. and T. Kadowaki, "Dissociation Reactions of CO Gas on Fe and Fe_3O_4 Surfaces Observed by Raman-Ellipsometry Spectroscopy", *Applied Surface Science*, Vol. 28, No. 2, pp. 147-166, 1987.

19. Babincová, M., P. Babinec, and C. Bergemann, "High-Gradient Magnetic Capture of Ferrofluids: Implications for Drug Targeting and Tumor Embolization", *Zeitschrift für Naturforschung C, Journal of Biosciences*, Vol. 56, pp. 909-911, 2001.

20. Wang, Y. X., S. M. Hussain, and G. P. Krespin, "Superparamagnetic Iron Oxide Contrast Agents: Physiochemical Characteristics and Applications in MR Imaging", *European Journal of Radiology*, Vol. 11, pp. 2319-2331, 2001.

21. Cabuil, V., J. C., Bacri, and R. Perzynski, "Proceedings of the 6th International Conference on Magnetic Fluids", *Journal of Magnetism and Magnetic Materials*, Paris, 20-24 July 1992, Vol. 122, pp. 1-3, 1993.

22. Goya, G. F., T. S. Berquo, and F. C. Fonseca, "Static and Dynamic Magnetic Properties of Spherical Magnetite Nanoparticles", *Journal of Applied Physics*, Vol. 94, No. 5, pp. 3520-3528, 2003.

23. Chen, L., Z. Xu, H. Dai, and S. Zhang, "Facile Synthesis and Magnetic Properties of Monodisperse Fe_3O_4/Silica Nanocomposite Microspheres with Embedded Structures via a Direct Solution-Based Route", *Journal of Alloys and Compounds*, Vol. 497, pp. 221-227, 2010.

24. Narita, A., K. Naka, and Y. Chujo, "Facile Control of Silica Shell Layer Thickness on Hydrophilic Iron Oxide Nanoparticles via Reverse Micelle Method", *Colloids and Surfaces A: Physicochemical and Engineering Aspects*, Vol. 336, pp. 46-56, 2009.

25. Charles, S. W., “Magnetic Fluids (Ferrofluids)”, In: J.L. Dormann, D. Fiorani, editors, North-Holland, Elsevier, 1992.

26. Gupta, A. K. and A. S. G. Curtis, “Lactoferrin and Ceruloplasmin Derivatized Superparamagnetic Iron Oxide Nanoparticles for Targeting Cell Surface Receptors”, *Biomaterials*, Vol. 25, No. 15, pp. 3029-3040, 2004.

27. Fried, T., G. Shemer, and G. Markovich, “Ordered Two-Dimensional Arrays of Ferrite Nanoparticles”, *Advanced Materials*, Vol. 13, pp. 1158-1161, 2001.

28. Sun, S. H. and H. Zeng, “Size-Controlled Synthesis of Magnetite Nanoparticles”, *Journal of the American Chemical Society*, Vol.124, pp. 8204-8205, 2002.

29. Wang, S. Z. and H. W. Xin, “The γ-Irradiation-Induced Chemical Change from β-FeOOH to Fe_3O_4”, *Radiation Physics and Chemistry*, Vol. 56, pp. 567-572, 1999.

30. Itoh, H. and T. Sugimoto, “Systemic Control of Size, Shape, Structure, and Magnetic Properties of Uniform Magnetite and Maghemite Particles”, *Journal of Colloid and Interface Science*, Vol. 265, pp. 283-295, 2003.

31. Reimers, G. W. and S. E. Khalafalla, “Preparing Magnetic Fluids by a Peptizing Method”, *U.S. Bureau of Mines Technical Report*, p. 59, 1972.

32. Hadjipanayis, G. C. and R. W. Siegel, “Nanophase Materials: Synthesis, Properties and Applications”, *NATO ASI Series, Applied Sciences*, Vol. E260, 1993.

33. Sjogren, C. E., K. Briley-Saebo, M. Hanson, and C. Johansson, “Magnetic Characterization of Iron Oxides for Magnetic Resonance Imaging”, *Magnetic Resonance in Medicine*, Vol. 31, No. 3, pp. 268-272, 1994.

34. Liu, Z. L., X. Wang, K. L. Yao, G. H. Du, Q. H. Lu, Z. H. Ding, J. Tao, Q. Ning, X. P. Luo, D. Y. Tian, and D. Xi, "Synhtesis of Magnetite Nanoparticles in W/O Microemulsion", *Journal of Materials Science*, Vol. 39, pp. 2633-2636, 2004.

35. Paul, B. K. and S. P. Moulik, "Microemulsions: An Overview", *Journal of Dispersion Science and Technology*, Vol. 18, No. 4, pp. 301-367, 1997.

36. Degiorgio, V. and M. Corti, *Physics of Amphiphiles: Micelles, Vesicles and Microemulsions*, Elsevier Science Ltd, North-Holland, 1985.

37. Chen, S. H. and R. Rajagopal, *Micelles, Solutions and Microemulsions; Structure, Dynamics and Statistical Thermodynamics*, Springer, New York, 1990.

38. Clayton, W., *The Theory of Emulsions and Their Technical Treatment*, 4th ed., The Blakiston Co., Philedelphia, 1943.

39. Cooke, C. E. and J. H. Schulman, *Surface Chemistry*, Munksgaard, Copenhagen, 1965.

40. Kahlweit, M., "Microemulsions", *Science*, Vol. 240, pp. 617-621, 1988.

41. Spry, D. B., A. Goun, K. Glusac, D. E. Moilanen, and M. D. Fayer, "Proton Transport and the Water Environment in Nafion Fuel Cell Membranes and AOT Reverse Micelles", *Journal of the American Chemical Society*, Vol. 129, pp. 8122-8130, 2007.

42. Cassin, G., S. Illy, and M. P. Pileni, "Chemically Modified Proteins Solubilized in AOT Reverse Micelles. Influence of Proteins Charges on Intermicellar Interactions", *Chemical Physics Letters*, Vol. 221, No. 3-4, pp. 205-212, 1994.

43. Santra, S., R. Tapec, N. Theodoropoulou, J. Dobson, A. Hebard, and W. Tan, "Synthesis and Characterization of Silica-Coated Iron Oxide Nanoparticles in

Microemulsion: The Effect of Nonionic Surfactants", *Langmuir,* Vol. 17, pp. 2900-2906, 2001.

44. Chen, D. H. and S. H. Wu, "Synthesis of Nickel Nanoparticles in Water-in-Oil Microemulsions", *Chemistry of Materials*, Vol.12, pp. 1354-1360, 2000.

45. Chen, D. H. and C. H. Hsieh, "Synthesis of nickel nanoparticles in aqueous cationic surfactant solutions", *Journal of Materials Chemistry*, Vol. 12, pp. 2412-2415, 2002.

46. Yuan, S. L., Z. T. Cai, G. Y. Xu, and Y. S. Jiang, "Mesoscopic Simulation Study on Phase Diagram of the System Oil/Water/Aerosol OT", *Chemical Physics Letters*, Vol. 365, No. 3-4, pp. 347-353, 2002.

47. Wongwailikhit, K. and S. Horwongsakul, "The Preparation of Iron (III) Oxide Nanoparticles Using W/O Microemulsion", *Materials Letters*, Vol. 65, pp. 2820-2822, 2011.

48. Atay, N. Z., *Transport and Interfacial Exchange Kinetics in One- and Two-Phase Disperse Systems*, PhD, University of Kent at Canterbury, 1987.

49. Rahman, I. A. and V. Padavettan, "Synthesis of Silica Nanoparticles by Sol-Gel: Size-Dependent Properties, Surface Modification, and Applications in Silica-Polymer Nanocomposites – A Review", *Journal of Nanomaterials*, Vol. 2012.

50. Vansant, E. F., P. V. D. Voort, and K. C. Vrancken, *Characterization and Chemical Modification of the Silica Surface*, Elsevier Science, New York, 1995.

51. Bagwe, R. P., L. R. Hilliard, and W. Tan, "Surface Modification of Silica Noparticles to Reduce Aggregation and Nonspecific Binding", *Langmuir,* Vol. 22, pp. 4357-4362, 2006.

52. Hilliard, L. R., X. Zhao, and W. Tan, "The Immobilization of Oligonucleotides onto Silica Nanoparticles", *Analytica Chimica Acta*, Vol. 470, pp. 51-56, 2002.

53. Stöber, W., A. Fink, and E. Bohn, "Controlled Growth of Monodisperse Silica Spheres in Micron Size Range", *Journal of Colloid and Interface Science*, Vol.26, No. 1, pp. 62-69, 1968.

54. Ossea-Assare, K. and F. J. Arrigada, "Synthesis of Nanosize Silica in Aerosol OT Reverse Microemulsions", Journal of Colloid and Interface Science, Vol. 170, pp. 8-17, 1995.

55. Bagwe, R. P. and K. C. Khilar, "Effects of the Intermicellar Exchange Rate and Cations on the Size of Silver Chloride Nanoparticles Formed in Reverse Micelles of AOT", Langmuir, Vol. 13, pp. 6432-6438, 1997.

56. Ossea-Assare, K. and F. J. Arrigada, "Growth Kinetics of Nanosized Silica in a Nonionic Water-in-Oil Microemulsion: A Reverse Micellar Pseudophase Reaction Model", Journal of Colloid and Interface Science, Vol. 218, pp. 68-76, 1999.

57. Ossea-Assare, K. and F. J. Arrigada, "Synthesis of Nanosize Silica in a Nonionic Water-in-Oil Microemulsion: Effects of the Water/Surfactant Molar Ratio and Ammonia Concentration", *Journal of Colloid and Interface Science*, Vol. 211, pp. 210-220, 1999.

58. Ossea-Assare, K. and F. J. Arrigada, "Controlled Hydrolysis of Tetraethoxysilane in a
Nonionic Water-in-Oil Microemulsion: A Statistical Model of Silica Nucleation", *Colloids and Surfaces*, Vol. 154, pp. 311-326, 1999.

59. Bagwe, R. P., L. R. Hilliard and W. Tan, "Surface Modification of Silica Nanoparticles to Reduce Aggregation and Nonspecific Binding", *Langmuir*, Vol. 22, pp. 4357-4362, 2006.

60. Chemical Book, *Docusate Sodium*, 2010, http://www.chemicalbook.com/chemicalproductproperty_EN_CB7769467.htm, December 5, 2012.

61. Chemical Book, *Polyoxyethylene(5) Nonylphenyl Ether*, 2010, http://www.chemicalbook.com/chemicalproductproperty_EN_CB3186213.htm, December 5, 2012.

62. Open WetWare, *Triton X-100*, 2009, http://www.openwetware.org/wiki/Triton_X-100, December 5, 2012.

63. Chang, C. L. and H. S. Fogler, "Kinetics of Silica Particle Formation in Nonionic W/O Microemulsions from TEOS", *American Institute of Chemical Engineers Journal*, Vol. 42, pp. 3153-3163, 1996.

64. Li, Y. S., J. S. Church, A. L. Woodhead, and F. Moussa, "Preparation and Characterization of Silica Coated Iron Oxide Magnetic Nano-Particles", *Spectrochimica Acta Part A: Molecular and Biomolecular Spectroscopy*, Vol. 76, pp. 484-489, 2010.

65. Berry, C. C. and A. S. G. Curtis, "Functionalisation of Magnetic Nanoparticles for Applications in Biomedicine", Journal of Physics D: Applied Physics, Vol. 36, pp. 198-206, 2003.

66. Philipse, A. P., M. P. B. van Bruggen, and C. Pathmamanoharan, "Magnetic Silica Dispersions: Preparation and Stability of Surface-Modified Silica Particles with a Magnetic Core", *Langmuir*, Vol. 10, pp. 92-99, 1994.

67. Krauss, P. R. and S. Y. Chou, "Nano-Compact Disks with 400 $Gbit/in^2$ Storage Density Fabricated Using Nanoimprint Lithography and Read with Proximal Probe", *Applied Physics Letters*, Vol. 71, No. 21, pp. 3174-3176, 1997.

68. Qhobosheane, M., S. Santra, P. Zhang, and W. Tan, “Biochemically Functionalized Silica Nanoparticles”, *Analyst*, Vol. 126, pp. 1274-1278, 2001.

69. Gerion, D., F. Pinaud, S. C. Williams, W. J. Parak, D. Zanchet, S. Weiss, and A. P. Alivisatos, “Synthesis and Properties of Biocompatible Water-Soluble Silica-Coated CdSe/ZnS Semiconductor Quantum Dots”, *Journal of Physical Chemistry B*, Vol. 105, No. 37, pp. 8861-8871, 2001.

70. Levy, L., Y. Sahoo, K. S. Kim, E. J. Bergey, and P. N. Prasard, “Nanochemistry: Synthesis and Characterization of Multifunctional Nanoclinics for Biological Applications”, *Chemistry of Materials*, Vol. 14, No. 9, pp. 3715-3721, 2002.

71. Robinson, P. J., P. Dunnill, and M. D. Lilly, “The properties of magnetic supports in relation to immobilized enzyme reactors”, *Biotechnology and Bioengineering*, Vol. 15, No. 3, pp. 603-606, 1973.

72. Bio-Rad, *Bio-Beads® SM Hydrophobic and Polar Interaction Adsorbents Instruction Manual*, 2010, http://www.bio-rad.com/webroot/web/pdf/lsr/literature/9141_Bio-Beads_SM.pdf, September 14, 2012.

73. Lee, K. M., C. M. Sorensen, K. J. Klabunde, and G. C. Hadjipanayis, “Synthesis and Characterization of Stable Colloidal Fe3O4 Particles in Water-in-Oil Microemulsions”, IEEE Transactions on Magnetics, Vol 28, No. 5, 1992.

74. Berne, B. J. and R. Pecora, *Dynamic Light Scattering with Applications to Chemistry, Biology, and Physics*, Wiley-Interscience, United States of America, 1976.

75. Nanowerk, *Multifunctional Nanoparticles Do Double Duty in Fight against Cancer*, 2008, http://www.nanowerk.com/spotlight/spotid=8065.php, December 20, 2012.

76. Waseda, Y., E. Matsubara, and K. Shinoda, *X-Ray Diffraction Crystallography Introduction*, Examples and Solved Problems, Springer, London, New York, 2011.

77. *Diaelectric Constants and Refractive Index*, www.stenutz.eu/chem/solv23.php, January 2, 2013.

78. Dynesonline, *Viscosity, Surface Tension, Specific Density and Molecular Weight of Selected Liquids*, www.dynesonline.com/visc_table.html, January 2, 2013.

79. Malvern Instruments, *Dynamic Light Scattering: An Introduction in 30 Minutes*, http://www.malvern.com/common/downloads/campaign/MRK656-01.pdf, January 8, 2013.

80. Nallathambi, G., T. Ramachandran, V. Rajendran and R. Palaniveru, "Effect of Silica Nanoparticles and BTCA on Physical Properties of Cotton Fabrics", *Materials Research*, Vol. 14, No. 4, pp. 552-559, 2011.

81. Legodi, M. A. and D. de Waal, "The Preparation of Magnetite, Goethite, Hematite and Maghemite of Pigment Quality from Mill Scale Iron Waste", *Dyes and Pigments*, Vol. 74, pp.161-168, 2007.

82. Fletcher, P. D. I., M. F. Galal and B. H. Robinson, *Journal of the Chemical Society, Faraday Transactions I*, Vol. 80, p. 3307, 1984.

83. Nicholson, J. D. and F. J. Clarke, *Surfactants in Solution*, Vol. 3, Plenum Press, 1984.